CRISPR/Cas9-mediated functional screening of novel testis-specific genes in mice

CRISPR/Cas9 による マウスの新規精巣特異的発現遺伝子 の機能的スクリーニング

2022

Cooperative Division of Veterinary Sciences,

Graduate School of Agriculture,

Tokyo University of Agriculture and Technology

MOST SUMONA, Akter

CONTENTS

General Introduction

Mammalian Testis

Testis overview

The testis is responsible for performing two crucial functions-sperm and androgen production, mainly testosterone. The testis is housed in the scrotum and covered with a thick fibrous capsule called tunica albuginea and the rete testis (RT) at the anterior part (Ravindranath et al., 2003). The folding of tunica albuginea forms the mediastinum, and the septum of connective tissue emerges from the mediastinum and subdivides the testis into lobules. The seminiferous tubule (ST) lies within this lobule and is surrounded by interstitial tissue, which is the main structure of the testis. ST is connected to the RT, where the testicular excretory duct contacts the testis to the efferent duct (Hess et al., 2021). The spermatozoa and testicular fluid produced in the ST propel into the efferent duct and epididymis through the RT. The somatic cell in the ST, known as Sertoli cells, support the germ cells during the phages of differentiation (Fig. 1). Adult testis is histologically divided into two compartments- a seminiferous tubular compartment and an interstitial compartment (Ravindranath et al., 2003). The tubular compartment is composed of an outer layer of peritubular myoid cells, and an inner layer of seminiferous epithelium. The interstitial compartment consists of Leydig cells, macrophages, and lymphocytes as immune cells and fibroblasts. These compartments are responsible for performing the function of spermatogenesis and steroidogenesis, respectively.

Male germ cells and spermatogenesis

Mammalian germ cells first harbor from the epiblast cells in post-implantation embryos as primordial germ cells (PGCs) in response to the growth factors secreted from surrounding cells (Extavour and Akam, 2003; Hayashi et al., 2007; Saitou, 2009). In mice, PGCs originate from the subset of cells located in the proximal epiblast of the developing

embryo at embryonic day (E) 7.25 (Kumar and DeFalco, 2017). PGCs are highly specialized precursor cells for both female and male germ cells (Saitou and Yamaji, 2012). The male germ cells undergo three distinct processes: cell fate determination as PGCs, sex determination as male germ cells, and spermatogenesis. PGCs are the transient undifferentiated pioneering precursor cells for both male and female gamete and differentiate- spermatozoa and oocytes. In mice, the male germ cells that had arrested mitotic proliferation at the end of embryonic stages resume proliferation after birth. At this stage, they relocate from the central region to the basement membrane in the seminiferous tubule (Nagano et al., 2000). The male germ cells at these early postnatal stages were termed as gonocytes or prospermatogonia. These gonocytes located near the basement membrane of the seminiferous tubules initiate mitotic proliferation and meiosis to produce functional spermatozoa through spermatogenesis. In mammals, the fusion process of germ cells passes through the harmonized ordered steps (Snell and White, 1996; Wassarman, 1987). Spermatogenesis is a complex process involving meiosis and spermiogenesis, but still, the underlying molecular mechanisms are not fully understood. Human fertility relies on the correct establishment and differentiation of the germline because no other cell type in the body can pass a genome and epigenome from parent to child. Multifactorial pathological condition(s) responsible for male infertility and its genetic causes remain unveiled- it contributes up to 15% to 30% of male infertility cases (Shamsi et al., 2011). Nowadays, the infertility rate has hiked tremendously, approximately 8%–12% of couples are infertile, and a male factor is responsible for almost half of these cases (Devroey et al., 2009; Evers, 2002; Massart et al., 2012). Although various factors could cause infertility in men, the primary cause resides in germ cell development or differentiation processes that lead to the absence of spermatozoa or abnormal spermatozoa (Agarwal et al., 2021; Krausz and Riera-Escamilla, 2018). Mainly, mouse used as a model for performing the cell and molecular events of human germline specification (Chen et al., 2017). Recently several cutting-edge assisted

reproductive techniques (ART) address infertility by manipulating the egg, sperm, or embryo. ARTs such as intracytoplasmic sperm injection or round spermatid injection could partly overcome these problems (Tanaka et al., 2018; Yanagimachi, 2005). Understanding the mechanisms of infertility is essential to develop new technologies to support reproduction. Despite such importance, the dynamic processes of male germ cell development remain elusive.

CRISPR/Cas9

In mammalian reverse genetics, mouse model gene knock-out (KO) plays a magnificent role. Indeed, various KO mouse models have contributed significantly to understanding the molecular mechanisms underlying mammalian male infertility (Extavour and Akam, 2003; Hayashi et al., 2007; Saitou, 2009). For producing KO mice, conventional methods involved targeting vector construction, introducing mutations of embryonic stem cells (ESCs) by homologous recombination, and then injections of the mutant ESCs into the wild-type blastocysts for generating the chimera mice. The total procedure takes around months to find the complete homozygous KO mutations necessary for analyzing the phenotypes (Sommer et al., 2015; Sunagawa et al., 2016). This conventional method requires sufficient time, space, and effort to generate the KO mice. The modern advanced technologies of genome editing facilitated the production of KO mice. For example, zinc-finger nucleases (ZFN) (Urnov et al., 2010), transcription activator-like effector nucleases (TALEN) (Sommer et al., 2015), and clustered regularly interspaced short palindromic repeats (CRISPR)-associated Protein9 (Cas9) (Sander and Joung, 2014) are used to address the limitation arose from the conventional method. These three programmable endonucleases (ZFNs, TALENs, and CRISPR/Cas9 system) are used for programmable changes at the gene of interest by introducing targeted DNA double-strand breaks (DSBs) in eukaryotes. For DNA cleavage, ZFN and TALEN both

contain the Fok I endonuclease domain (Kim et al., 1996), although having different DNA-binding domains for target site recognition. The weak point for ZFN and TALEN is the requirement of multi-step procedures of vector construction for targeting the genome (Miura et al., 2021). Unlike protein-based ZFN and TALEN, CRISPR/Cas9 is an RNA-based DNA recognition system derived from the bacterial adaptive immune system. Cas9 is a multi-functional protein that uses a single guide RNA (sgRNA) molecule to recognize the target DNA sequence, typically about twenty nucleotides (Shamshirgaran et al., 2022). After binding to the target sequence, Cas9 generates a DSB that is quickly repaired by endogenous factors. During this repair process, either insertion or deletion (Indel) is frequently introduced at the target site (Fig. 2). By applying these genome editing technologies, the period of generating KO mice was significantly shortened, which accelerated the identification of causative genes of male infertility (Miura et al., 2021; Susaki et al., 2017).

In this study, I have selected the candidate genes named *Faiml* (*Gm6432*), *Cox8c*, *Cox7b2*, *Tuba3b*, *Tuba3a,* and *Gm773* and performed a genetic screening by modified CRISPR/Cas9-based approach to identify their functions in male germ cell development or spermatogenesis as well as fertilization (In Chapter 1). Later, I continued my research on the roles of germ cell-specific tubulin genes *Tuba3a/3b* and *Tubb4b*, through the successful development of the *Tuba3a/3b* double KO and *Tubb4* KO mice (In Chapter 2). Both chapters focused on novel genes that might have a potential role in mouse spermatogenesis.

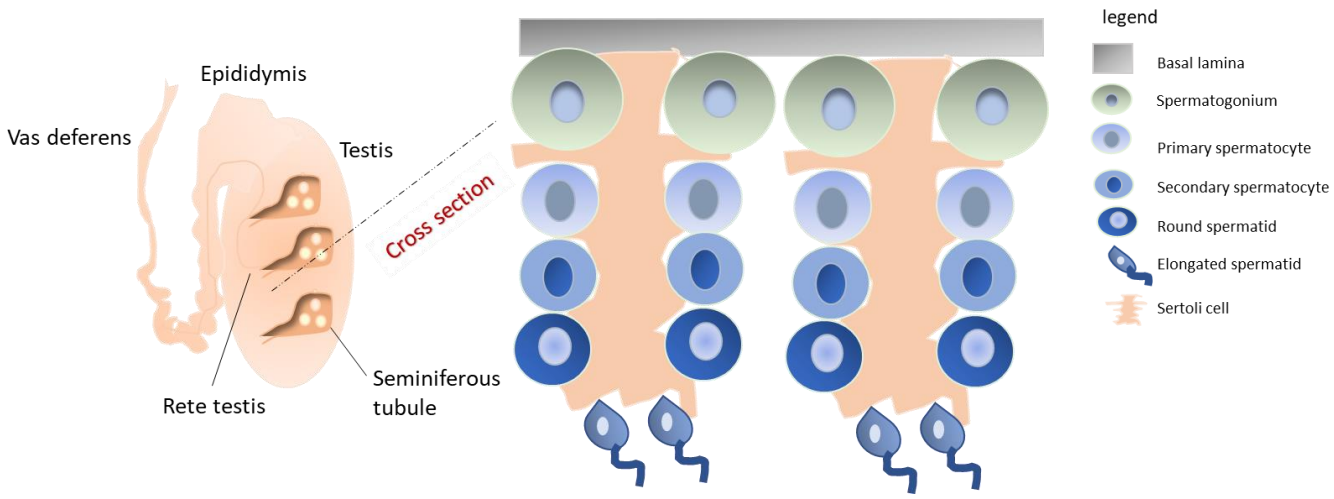

Fig. 1. Representation of the anatomy of mammalian testis

(Left) The mammalian testis is composed of seminiferous tubules connected to the rete testis. Immotile sperm flow from the lumen of the seminiferous tubules into the epididymis via the rete testis. Sperm acquire their motility during the passage through the epididymis to the vas deferens. (Right) Diagrammatic view of cross sections of seminiferous tubules and chronological representation of germ cell and somatic Sertoli cell.

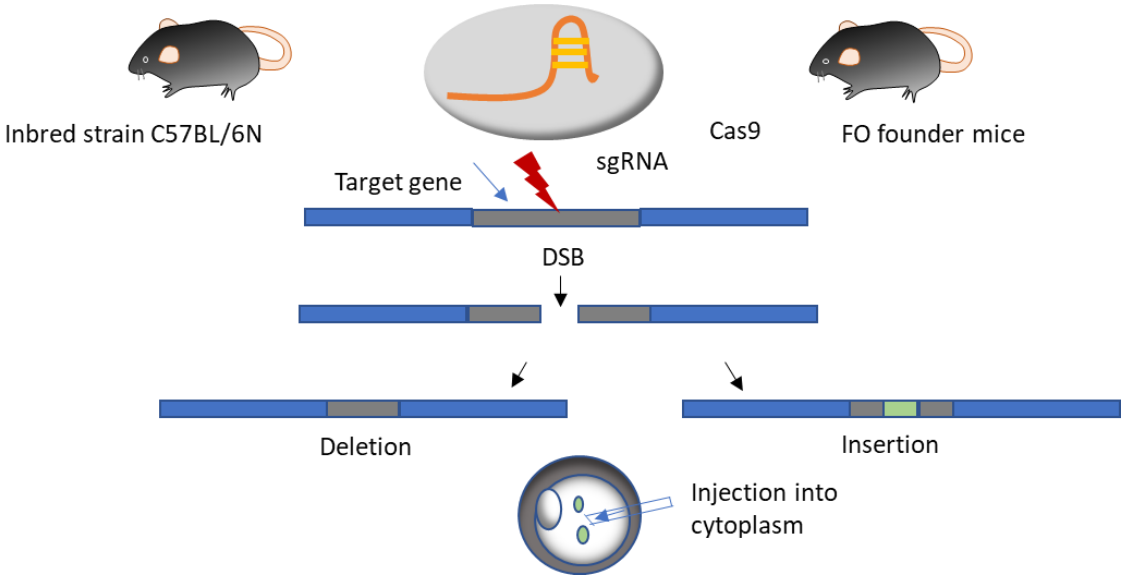

Fig. 2. Outlines of CRISPR/Cas9-mediated genome editing in the mouse zygote

The CRISPR/Cas system recognizes DNA via RNA-DNA interaction between guide RNA, such as single guide RNA (sgRNA), and its target DNA sequence adjacent to the protospacer adjacent motif (PAM). PAM is a short DNA sequence (usually 2-6 base pairs in length) that follows the DNA region targeted for cleavage by the CRISPR/Cas9 method. Cas complexed with guide RNA works as an endonuclease and cleaves the target DNA. A single sgRNA molecule to recognize the target sequence followed by a double-strand break (DSB) either insertion or deletion (Indel) of a reference genome. Wildtype oocytes and sperm were *in vitro* fertilized to generate zygotes. CRISPR mixture (Cas9 mRNA + sgRNAs) was injected into the cytoplasm of the zygotes to produce founder mice that harbor edited alleles.

CHAPTER 1

‘‘Uncover the novel role of SCNT-reprogramming resistant genes in mouse spermatogenesis by CRISPR/Cas9-mediated screening’’

Introduction

Mammals having unique and mysterious fertilization processes undergo the development of new life. The process of fertilization by uniting two types of germ cells, oocytes, and spermatozoa, followed the charismatic pathway by passing through a synchronized cascade of fusion each other. Germ cells are unique and immortal cells that could provide genetic information to offspring. In this process, the somatic chromosome number is restored, followed by the development of new offspring exhibiting characteristics of the individual is initiated (Wassarman, 1999). In all mammals, the male germ cells are organized as a well-defined cell association within the seminiferous epithelium of the testicular tubules. It undergoes unique and complex differentiation processes involving sex determination, epigenetic reprogramming, cell migration, and spermatogenesis, finally generating motile spermatozoa (Griswold, 2016; Kanamori et al., 2019; Stukenborg et al., 2014). In mice, the male germ cells that had arrested mitotic proliferation at the end of embryonic stages resume proliferation after birth. At this stage, they relocate from the central region to the basement membrane in the seminiferous tubule (Nagano et al., 2000). The male germ cells at these early postnatal stages were termed as gonocytes or prospermatogonia. These gonocytes located near the basement membrane of the seminiferous tubules initiate mitotic proliferation and meiosis to produce functional spermatozoa through spermatogenesis. Spermatogenesis is a complex cyclic cascade for developing motile spermatozoa. In this process, diploid spermatogonium goes through the sequential mitotic and meiotic cycles and finally outcome as haploid sperm (Fig. 3). Although researchers have revealed some aspects of spermatogenesis, the molecular mechanisms underlying this complex and dynamic processes largely remain unclear.

A previous in silico survey of gene expression datasets estimated that more than 2,300 genes were predominantly expressed in male germ cells (Schultz et al., 2003). Indeed, dozens

of genes have been identified that play essential roles in male germ cell development or fertility, mainly using mouse genetic models. Lately, the genome-editing technology, CRISPR/Cas9 (Hsu et al., 2014; Wang et al., 2013), has enhanced the speed of genetic screening (Abbasi et al., 2018; Susaki et al., 2017). It is the remarkable feat of genetic engineering for editing the genome that makes precise changes within genes. With this method, researchers can break through rapid screening for a group of genes in mice. For example, the groups of Ikawa and Matzuk have been performing extensive mouse genetic screening using the CRISPR/Cas9 system and have identified many genes that are essential for male fertility or spermatogenesis (Devlin et al., 2020; Fujihara et al., 2014; Larasati et al., 2020; Shimada et al., 2021). However, they and others also found that the great majority of testis-expressed genes are individually dispensable for spermatogenesis or male fertility (Devlin et al., 2020; Khan et al., 2018; Miyata et al., 2016; Park et al., 2020; Sun et al., 2020) which hampers the efficient identification of physiologically critical genes. Therefore, it is ideal to have a unique strategy that efficiently narrows down functionally important candidates before performing the actual genetic screening.

Germ cells separate from somatic cell lineages at the early stage of embryonic development (Hancock et al., 2021). Thus, when the somatic cell genome is transferred to enucleated oocytes by the somatic cell nuclear transfer (SCNT) technique, the reconstructed genome skips the epigenetic reprogramming steps that generally occur during germ cell development (Matoba and Zhang, 2018). Expression of developmental genes is turned through crosstalk between transcription factors and epigenetic regulation. Matoba et al. have previously performed a comprehensive comparison of transcriptome and epigenome between normally fertilized blastocysts and SCNT-generated blastocysts to identify SCNT-reprogramming resistant genes (SRRGs; Fig. 4 and Table 1) (Matoba et al., 2018). Interestingly, this list of SRRGs was highly enriched with the genes known to be essential for spermatogenesis in mouse

KO models such as *Asz1* (Ma et al., 2009), *Tex12* (Hamer et al., 2008), *Slc25a31* (Brower et al., 2007), *Tex101* (Fujihara et al., 2014; Li et al., 2013), *Mael* (Soper et al., 2008), or *Majin* (Shibuya et al., 2015). For example, *Asz1* KO males are sterile due to a block in spermatid development (Ma et al., 2009), *Tex12* KO males exhibit infertility associated with failure of crossover events during meiosis (Hamer et al., 2008), and *Majin* KO males show infertility because of the inability of meiotic telomere tethering (Shibuya et al., 2015). Nonetheless, about half of the SRRGs were not characterized by the KO mouse model. Although these included multiple X-linked genes with a high copy number of family genes (Mage and Xlr family) that are difficult to disrupt using CRISPR/Cas9 simultaneously, some were unique genes, which indicates that the genetic screen by CRISPR/Cas9 targeting is achievable.

In this study, I have selected five candidates from uncharacterized SRRGs and performed a genetic screening using a CRISPR/Cas9-based approach to dissect their functions in male germ cell development or spermatogenesis as well as fertilization. I find that among the five candidates *Faiml* (*Gm6432*), *Cox8c*, *Cox7b2*, *Tuba3b* (and *Tuba3a*), and *Gm773*, three (*Cox7b2*, *Tuba3a/3b*, and *Gm773*) were indeed critical for male germ cell development or spermatogenesis in mice. This study provides a new list of genes required for male germ cell development and the concept that an SCNT-reprogramming-resistant feature can be used as an efficient selection method to identify the list of germline essential genes.

Materials and methods

Mice

C57BL/6N (B6N) and ICR mice were purchased from SLC, Inc. (Shizuoka, Japan) for my research. Feed and water were provided *ad libitum* and checked almost every day. Mice were housed under controlled lighting conditions (daily light from 07:00 to 21:00). All experimental protocols were approved by the Institutional Animal Care and Use Committee of RIKEN Tsukuba Institute and conducted by the Principles of Laboratory Animal Care. Animal care and use were conducted in compliance with the ARRIVE guidelines.

RT-qPCR

Total RNA was purified from adult mouse tissues using RNeasy Mini Kits (#74104; Qiagen). After that, cDNAs were synthesized from the purified RNAs using the SuperScript IV First-Strand Synthesis System (#18091050; Thermo Fisher Scientific). RT-qPCR was then performed using PowerUp SYBR Green Master Mix (#A25742; Thermo Fisher Scientific) with the QuantStudio 7 system (Thermo Fisher Scientific). The Ct values were normalized to that of glyceraldehyde 3-phosphate dehydrogenase (*Gapdh*). The expression level of each gene was further normalized for testis as 1. The primers used for RT-qPCR are shown in Table 2.

Single-cell RNA-seq analysis

Read count matrix and clustering list of single-cell RNA-seq data of mouse adult testis were obtained from Green et al., 2018 (GSE112393). Read counts were transferred to counts per million (CPM), and the mean CPM of each cluster was computed using R (version 3.6.1) (R Core Team, 2015).

KO mouse production by the CRISPR/Cas9 system

I used a CRISPR-based approach, termed Triple CRISPR, to generate KO mice (Fig. 5A) (Matoba et al., 2019; Susaki et al., 2017). Briefly, two or three sgRNAs targeting distinct exons of each target gene were designed using the MIT CRISPR Designer (currently closed) or CRISPOR (http://crispor.tefor.net/) (Fig. 5B). Sequences complementary to sgRNAs were cloned into the px330 vector by oligo annealing. The T7 promoter was added to sgRNA templates using PCR, and sgRNAs were synthesized via *in vitro* transcription from the PCR products as templates using MEGAshortscript T7 Transcription Kit (#AM1354, Thermo Fisher Scientific). Some sgRNAs were synthesized using the GeneArt Precision gRNA Synthesis Kit (#A29377, Thermo Fisher Scientific). The CRISPR target sequences and primers to generate sgRNAs are enlisted in Table 3. *Cas9* mRNA was synthesized from pcDNA3-T7-NLS hCas9-pA vector (RIKEN, RDB13130) using mMESSAGE mMACHINET7 ULTRA Transcription Kit (#AM1345, Thermo Fisher Scientific). Synthesized sgRNAs and Cas9 mRNA were adjusted to 500 ng/μL, and aliquots were frozen at –80 °C until use. The mixture of two or three distinct sgRNAs (50 ng/μL each) targeting coding exons and Cas9 mRNA (100 ng/μL) were injected into zygotes using a piezo-driven micromanipulator at 5–6 h post-insemination. (Fig. 5C).

***In vitro* fertilization (IVF), embryo transfer (ET), and caesarian section (C-section)**

Adult (over 10 weeks of age) wild-type B6N or CRISPR founder mice were used for IVF. Briefly, spermatozoa were collected from the epididymis of adult males and incubated in Human Tubal Fluid medium (HTF) drops for 1 h before insemination for their activation. Cumulus-oocyte complexes (COCs) were collected from the oviducts of B6N females that were superovulated by injecting 7.5 IU of pregnant mare serum gonadotropin (PMSG; #367222, Merck Millipore) plus anti-inhibin serum and 7.5 IU of human chorionic

gonadotropin (hCG; #230734, Millipore). At 15–17 h after the hCG injection, the isolated COCs were incubated in HTF containing 1.25 mM reduced glutathione (GSH; #G6013-5G, Merck Millipore) for 1 h before insemination. After preincubation, the activated spermatozoa were introduced to the COC-containing HTF drops to initiate insemination. In some experiments, the zona pellucida was removed by treatment with the acid Tyrode. At 5–6 h after insemination, the fertilized zygotes were washed in potassium simplex optimized medium (KSOM) drops. Two-cell stage embryos were transferred to the oviducts of pseudo-pregnant (E0.5: the day when the vaginal plug was observed was considered as E0.5) ICR females. The pups were recovered by C-section on the day of delivery (E19.5) (Fig. 6).

Immunohistochemistry

All specimens (neonatal and adult testes) (Fig. 7) were fixed overnight in 4% paraformaldehyde in phosphate-buffered saline (PBS) solution and then embedded in paraffin wax after dehydration. Embedded samples were sectioned as 4 μm. After deparaffinization and rehydration, antigen retrieval was performed using sodium citrate buffer (pH 6.0) pretreated in a microwave for 10 min to maintain a sub-boiling temperature. Incubation in 3% hydrogen peroxide was carried out to block endogenous peroxidase. Nonspecific staining was blocked by 1% bovine serum albumin for 1 h at room temperature. Then, the sections were incubated overnight with primary antibodies at 4 °C (Table 4). Negative controls were carried out in the absence of a primary antibody. After that, the sections were washed three times in PBS with 0.05% Tween-20. The sections were then exposed to the biotin-labeled second antibodies for 1 h and then Vectastain Elite ABC Kit (#PK-6100, Vector Laboratories) for 30 min at room temperature. Positive staining was visualized by adding 3,3′-diaminobenzidine for 1–2 min. The tissues were then counterstained with hematoxylin and dehydrated before mounting. At least two sections of each specimen were examined under light microscopy.

TUNEL staining

For checking the apoptosis, sections of postnatal P3 and P7 testis were subjected to the Terminal deoxynucleotidyl transferase dUTP nick end labeling (TUNEL) staining by using *in situ* Apoptosis Detection Kit (#CAG-3397, Fujifilm wako) according to the manufacturer's protocol. The wild-type adult testis was used as a control sample. Consistent with the previous report (Jeyaraj et al., 2003), TUNEL-positive signals were found in the seminiferous tubules at a relatively low frequency, confirming the validity of my staining method.

Genotyping PCR

Genomic DNA was purified from the tail tip using the Wizard Genomic DNA Purification Kit (#A1120, Promega). Genotyping PCR was performed using Tks Gflex DNA Polymerase (#R060A, Takara Bio Inc.) The primers were listed in Table 5. Putative off-target sites for each sgRNA were identified by CRISPOR (http://crispor.tefor.net/).

Sperm staining

Spermatozoa were stained with Hoechst 33342 (for DNA) and Rhodamine 123 (for mitochondria) to evaluate the morphology of the sperm head and midpiece. The sperm mass was collected from the cauda epididymis and incubated in 200 μL HTF medium for sperm swim-up. A 10 μL aliquot of sperm suspension was collected at 5–10 min and stained with 5 μg/mL of Hoechst 33342 and 5 μg/mL of Rhodamine 123 for 15 min at 37 °C. After washing twice with PBS, the stained sperm suspension was placed on a glass slide and covered with a cover glass. The samples were observed using Nikon C2 confocal microscopy (Nikon). The plasma membrane integrity and acrosome status of spermatozoa were evaluated by using PI (2.4 mM, LIVE/DEAD Sperm Viability Kit; #L7011, Thermo Fisher Scientific) and PNA conjugated with Alexa Fluor 488 (1 mg/mL, Thermo Fisher Scientific) (Liu et al., 2018). The

sperm mass was collected from the cauda epididymis and incubated in 200 μL HTF medium for sperm swim-up. A 20 μL aliquot of sperm suspension was collected at 5–10 min, 1 h, and 2 h of incubation and stained with PNA and PI for 15 min in a dark box. After incubation with dyes, 5 μL of suspension was put on a glass slide and covered with a cover glass. The samples were then observed with fluorescent microscopy (BX53, Olympus) (Fig. 8).

Sperm kinetics analysis

Computer-assisted sperm analysis (CASA) was performed using a Hamilton Thorn IVOS (ver. 12.01) CASA analyzer (Hamilton Thorn Research). Spermatozoa were collected from the cauda epididymis of adult B6N or CRISPR founder mice (12–15 weeks) and preincubated in 200 μL HTF medium for 1 h in a humidified atmosphere at 37 °C in 5% CO_2. After 50 min of sperm preincubation, the CASA machine was set up and equilibrated to 37 °C. After 1 h of preincubation, the spermatozoa suspension was loaded into a prewarmed rectangular boro tubing (0.10 mm × 2.30 mm) and inserted in the CASA machine to record quantitative parameters of sperm movement.

Results

Testicular germ cell-specific expression of SRRGs

Twenty-nine SRRGs were identified by the comparison of DNA methylome and transcriptome between fertilized blastocysts and SCNT blastocysts (DNA hypermethylated at the promoter [absolute methylation level > 5%] and transcriptionally repressed in SCNT blastocysts [Fold change > 2]; (Fig. 4 and Table 1; original datasets were obtained from Matoba et al., 2018). I selected five SRRGs not characterized in KO mouse studies; *Faiml (Gm6432)*, *Cox8c*, *Cox7b2*, *Tuba3b*, and *Gm773* as my screening targets. As a positive control, I also included *Majin*, one of the well-characterized SRRGs required for meiosis in mice (Shibuya et al., 2015), for all the following gene expression analyses as screening procedures. First, I analyzed the expression patterns of the six selected genes in different adult mouse tissues using RT-qPCR. I found that all these genes were predominantly expressed in the testis (Fig. 9A). To understand the cell type-specific expression patterns of these genes in the testis, I analyzed single-cell RNA-seq datasets of adult mouse testis published by Green et al. (Green et al., 2018). I found that all six genes are highly expressed in germ cells but are very low in somatic cells of the adult testis (Fig. 9B-C). Moreover, while *Majin* and *Gm773* are highly expressed in premeiotic spermatogonia, *Cox8c*, *Cox7b2*, and *Tuba3b* showed the highest expression in spermatocytes. *Faiml* showed the highest expression in post-meiotic round or elongated spermatids. These results indicate that the six SRRGs, including *Majin*, are highly expressed in testicular germ cells.

Generation of SRRG KO founder mice by using CRISPR

To determine the biological roles of SRRGs, I generated KO mice of each SRRG using the Triple CRISPR-based method (Matoba et al., 2019; Susaki et al., 2017). This method

efficiently disrupts the function of target genes biallelically by targeting multiple sites of protein-coding exons and enables direct analysis of founder mice. Thus, I injected *Cas9* mRNA together with multiple sgRNAs targeting protein-coding exons of SRRGs into the zygotes of the C57BL/6N (B6N) strain. The CRISPR-injected embryos were transferred to pseudo-pregnant females of ICR and delivered at E19.5 by the C-section. Founder mice, grown to adult (12–15 weeks), were subjected to the spermatogenesis screening pipeline for the following parameters: body weight, testis weight, testis histology, *in vitro* fertilization (IVF), computer-assisted sperm analysis (CASA), and sperm morphology. To speed up the screening, I did not apply a natural mating-based fertility test involving up to several months of mating with females. Instead, I performed IVF to evaluate the fertility of spermatozoa quickly. First, I questioned whether two or three sgRNAs could disrupt the function of target genes by targeting *Majin*. *Majin* KO mice have been shown to display meiotic arrest during spermatogenesis, but no other phenotype including aberrations of embryonic development or postnatal growth, in male mice (Shibuya et al., 2015). Consistent with that KO report from Shibuya and his colleagues (Shibuya et al., 2015), embryos injected with three sgRNAs against *Majin* (sgMajin-3) showed no growth defects in body size (Fig. 10A), but a severe reduction in testis size (Fig. 10B-C). Importantly, founders generated by two sgRNAs against *Majin* (sgMajin-2) also showed a similar phenotype with sgMajin-3 founders at a consistent efficiency (Fig. 10A-C). I next asked if the germ cells are present in these *Majin* KO mice by immunostaining against mouse VASA homolog (MVH, also known as DEAD-Box Helicase 4 [DDX4]), which is widely expressed in testicular germ cells (Toyooka et al., 2000). I then found that DDX4-positive germ cells were present but arrested during meiosis in all sgMajin-2 and sgMajin-3 mice (Fig. 11A). I further confirmed such phenotype by a marker for meiosis, synaptonemal complex protein 3 (SCP3), and a post-meiotic cell-specific haploid marker, Protamine-1 (Fig.

11B-C). Because it was impossible to design three sgRNAs with high specificity for some target SRRGs, I applied the two sgRNAs approach to screening other SRRGs.

Spermatozoa of sgCox7b2 mice failed to fertilize under IVF due to their poor motility

Knockout mice of the five target SRRGs developed normally and grew into adults (Table 6). Consistent with their testis-specific expression (Fig. 9A), these SRRG KO female mice showed normal fertility by IVF and produced pups after embryo transfer (Table 7). By contrast, sgMajin-2 and sgMajin-3 females did not ovulate due to the absence of oocytes, as reported (Shibuya et al., 2015), validating the reliability of my approach (Table 7). Genotyping PCR confirmed that insert/deletions (indels) were highly efficiently induced at the target sites of sgRNAs in each founder, while no apparent indel was observed at the off-target sites (Fig. 12). During measurements of testis size or histology analyses, I did not detect any significant defects in the five SRRG KO males (Fig. 10B-C, 11). Therefore, I next examined the ability of spermatozoa to fertilize oocytes. The sperm clot was isolated from the epididymis and suspended in a drop of HTF medium to allow sperm to swim up and capacitate. After 1 h of incubation, the control sperm actively swam to distribute evenly within the drop (Fig. 13A). Because spermatogenesis was completely arrested at meiotic stages in sgMajin-2 and sgMajin-3 mice (Fig. 11B-C), I could not obtain spermatozoa from the epididymis of these mice. Spermatozoa isolated from other SRRG KO mice actively swam up and evenly distributed in the drop, except for those of sgCox7b2 mice. The spermatozoa of sgCox7b2 mice remained aggregated in the HTF drop even after 1 h of incubation and showed very poor motility (Fig. 13B). Indeed, CASA analysis revealed that sperm motility was severely reduced in sgCox7b2 sperm (Fig. 13B). Consistent with such severely reduced motility, spermatozoa of sgCox7b2 mice failed to fertilize with oocytes under IVF (Fig. 13C). I further analyzed the morphology of spermatozoa by DNA/mitochondria (Hoechst 33342/Rhodamine 123) staining. I found that

most sperm of sgCox7b2 mice displayed abnormal morphology in their head (58%) and midpiece (92%) (Fig. 13D, E). Mitochondria that aligned at the midpiece appeared to be severely disorganized or reduced in these sgCox7b2 spermatozoa (Fig. 13E).

Gm773 KO mice spermatozoa showed reduced fertility due to the poor capability to penetrate the zona pellucida

Although spermatozoa of all SRRG KO mice, except for sgCox7b2, showed normal motility (Fig. 13B), sgGm773 spermatozoa showed significantly reduced fertility to less than 10% by IVF (Fig. 13C). Careful examination of oocytes after IVF revealed that, while many spermatozoa of control mice could penetrate through the zona pellucida (Fig. 14A; blue arrows), the great majority of sgGm773 spermatozoa failed to penetrate and stacked up at the surface of the zona pellucida (Fig. 14A; red arrows). Therefore, I examined whether the sgGm773 spermatozoa can efficiently fertilize with oocytes when the zona pellucida is removed. After zona removal by acid Tyrode treatment, sgGm773 spermatozoa fertilized with the nude oocytes at 100% efficiency (Fig. 14B). I next examined the integrity of the sperm plasma membrane and acrosome by staining with propidium iodide (PI) and peanut agglutinin (PNA), respectively (Fig. 14C) (Liu et al., 2018). PI staining allow me to distinguish between membrane-damaged (PI (+)) and intact (PI (−)) spermatozoa. Because PNA stains the acrosome, the PI (–)/PNA (+) sperm represents those alive and ready for the acrosome reaction. I observed similar levels of PI (+) and PI (−)/PNA (+) population ratio in the control. I found that significantly more of the sgGm773 sperm was PI (+) compared with control sperm at all time points analyzed (Fig. 14C). Furthermore, the PI (−)/PNA (+) population ratio gradually decreased during the preincubation period of spermatozoa (Fig. 14D).

Germ cells are completely lost at the early postnatal stages in *Tuba3a/3b* double KO founder mice

Although sgTuba3b mice did not show any defects on screening, I found that *Tuba3b* has a paralogue gene, *Tuba3a*, which encodes a protein TUBA3A having the same amino acid sequence as TUBA3B that is coded by *Tuba3b*. *Tuba3a* is expressed exclusively in testicular germ cells, like *Tuba3b* (Fig. 9A, C), suggesting that *Tuba3a* may compensate for the function of *Tuba3b* in sgTuba3b testis. Moreover, among seven Tubulin alpha (*Tuba*) genes present in the mouse genome, *Tuba3a* and *Tuba3b* are the only ones expressed in adult male germ cells (Fig. 15). Thus, I generated *Tuba3a* KO mice and *Tuba3a/3b* double KO mice by injecting *Cas9* mRNA together with two sgRNAs against *Tuba3a* (sgTuba3a) or both *Tuba3a* and *Tuba3b* (sgTuba3a/3b), respectively. Both sgTuba3a and sgTuba3a/3b founder mice grew normally to adulthood, and females had normal fertility (Fig. 10A, Tables 6 and 7). The sgTuba3a male did not show any defects in all screening steps, like sgTuba3b males. However, the testes of adult sgTuba3a/3b founder mice were tiny (Fig. 10B-C). Histological examination revealed that sgTuba3a/3b testes completely lack DDX4-positive germ cells at 12 weeks of age (Fig. 11A). I next asked at what stage germ cells disappear in sgTuba3a/3b testes during development. The DDX4-positive gonocytes were usually present in the sgTuba3a/3b testis at E16.5 (Fig. 16A). However, the number of gonocytes was slightly reduced at the newborn stage. Thereafter, gonocytes of sgTuba3a/3b mice were gradually depleted during the postnatal growth period between P3 and P7 and entirely lost by 3 weeks after birth (Fig. 16A, B). During these stages, I did not find any Terminal deoxynucleotidyl transferase dUTP nick end labeling (TUNEL) signals, which represent apoptosis, in sgTuba3a/3b gonocytes (Fig. 16C).

Discussion

In this study, I focused on a unique list of SRRGs that are predominantly expressed in male germ cells and performed a CRISPR-based genetic screen to examine their physiological functions in mice. Although there are more than 2,300 genes that show predominant expression in male germ cells, this list of SRRGs appears to be enriched for physiologically important genes based on the available KO reports (germline defects are observed in 10 out of the 13 SRRGs for which KO mice have been reported (Fig. 4 and Table 1). Indeed, I demonstrated that among five screened SRRGs three were essential for the male germ cell development and maturation at different time points. Specifically, *Tuba3a* and *Tuba3b* are required for the survival of gonocytes during postnatal growth, *Cox7b2* is necessary for the completion of spermiogenesis to mature into motile sperm, and *Gm773* plays a critical role in the acquisition of zona pellucida-penetration capacity (Fig. 14).

The strategy of directly analyzing founder mice generated by CRISPR-targeting to the protein-coding exons can promptly and efficiently reveal the function of candidate genes (Susaki et al., 2017). In a conventional Triple CRISPR method, three sgRNAs targeting protein-coding exons were simultaneously introduced to the zygote to efficiently generate complete KO mice (Susaki et al., 2017). However, in this study, I found that two sgRNAs could efficiently induce a KO phenotype like three sgRNAs as shown in the case of sgMajin (Fig. 10 and 11). This strategy is particularly powerful when multiple genes complement each other because it allows these genes to be knocked out simultaneously. Using this strategy, I successfully generated a double KO for *Tuba3a* and *Tuba3b* in founder mice that showed highly consistent phenotypes among different founders. Thus, my approach to disrupting multiple genes simultaneously using CRISPR may help dissect the roles of redundant genes.

The initial list of SRRGs included two cytochrome c oxidase (COX) genes, *Cox8c* and *Cox7b2*. COX, or Complex IV, is a large transmembrane protein complex responsible for the terminal step in the mitochondrial electron transport chain that drives oxidative phosphorylation (Rak et al., 2016). COX has been thought to be composed of 13 subunits, three encoded by mitochondrial DNA, while the other 10 are from nuclear DNA. Recently NUDFA4 was added as the 14th member of this group which previously belonged to the group of complexes I (Brischigliaro and Zeviani, 2021). Among these 14 subunits, COX7B2 forms subunit VIIb, which could be made from either of two nuclear genes, *Cox7b* or *Cox7b2*, in mammals. Based on the single-cell RNA-seq data of adult testis, testicular germ cells express *Cox7b2* but not *Cox7b* (Fig. 17A). Similarly, among three *Cox8* family genes (*Cox8a*, *Cox8b*, and *Cox8c*), only *Cox8c* is expressed in testicular germ cells (Fig. 17B). Therefore, in testicular germ cells, COX subunits VIIb and VIII are likely composed of COX7B2/*Cox7b2* and COX8C/*Cox8c*, respectively. From my screening result, sgCox7b2 spermatozoa were morphologically abnormal, and their motility was severely reduced, which led to complete infertility by IVF, whereas sgCox8c mice did not show any defects. These results suggest that *Cox7b2* plays essential roles in spermatogenesis at the last step of spermiogenesis to mature into functional spermatozoa. Interestingly, the COXVIII subunit is dispensable, while the VIIb subunit is critically vital for spermatozoa. Nuclear-coded COX subunits, including *Cox8c* and *Cox7b2*, are generally thought to regulate the assembly of mitochondria-coded core subunits of COX. Thus, *Cox7b2*/COX7B2 might play a unique role in COX assembly during spermatogenesis. It is also interesting how abnormal COX assembly affected the morphogenesis of sperm heads, as observed in sgCox7b2 spermatozoa. Further detailed examination of *Cox7b2* KO sperm, focusing on mitochondrial COX assembly, may reveal the relationship between Cox genes and sperm mitochondrial organization as well as sperm head morphogenesis.

The sgGm773 spermatozoa showed poor zona penetration activity leading to reduced fertility, likely because of the poor integrity of their plasma membrane as well as a reduced acrosome reaction. The GM773 protein possesses a Cor1/Xlr/Xmr/Slx conserved domain in meiosis-related XLR proteins (Li et al., 2015). Thus, *Gm773* was expected to play a critical role during meiosis. However, sgGm773 mice did not show any apparent defects in meiosis. Instead, the spermatozoa of sgGm773 showed poor zona penetration activity, likely because of defects in the integrity of the cytoplasmic membrane or acrosome. This indicates that *Gm773* may play a unique role during spermatogenesis other than meiosis. Indeed, gene expression of *Gm773* was not observed in meiotic spermatocytes, but rather, was specific to spermatogonia (Fig. 9C). How GM773 expressed in spermatogonia safeguards the integrity of spermatozoa membrane/acrosome would be of interest for future study. Detailed localization analysis of GM773 proteins in spermatocytes as well as spermatozoa using GM773-specific antibodies would give an insight into the molecular function of GM773.

Germ cells were lost entirely in sgTuba3a/3b mice at the early postnatal stages, while sgTuba3a and sgTuba3b showed no apparent phenotype. *Tuba3a* and *Tuba3b* encode Tubulin alpha proteins. The *Tuba* gene family in mice consists of seven members: *Tuba1a*, *Tuba1b*, *Tuba1c*, *Tuba3a*, *Tuba3b*, *Tuba4a*, and *Tuba8* (Fig. 15). Although each TUBA protein has several unique residues in its amino acid sequence, those of TUBA3A and TUBA3B are the same (they are paralogue genes). Thus, each gene appears to compensate for the function of another gene in individual KO mice. Given that microtubules play critical roles in fundamental cellular processes, including cell division, such loss of alpha-tubulin in sgTuba3a/3b gonocytes may have induced collapse of essential cellular homeostasis leading to germ cell elimination, independent of apoptosis around P3 to P7. Indeed, such loss of critical factors for cellular homeostasis has been suggested to induce accidental cell death, or necrosis, instead of regulated cell death, or apoptosis (Galluzzi et al., 2018). Also, mitotic catastrophe, another type of cell

death regulated by Caspase-2, could be induced by the aberration of microtubule dynamics (Dominguez-Brauer et al., 2015). Further detailed analysis of molecular markers for each type of cell death would reveal the mechanism of how the germ cells were eliminated in postnatal sgTuba3a/3b testis.

Conclusion

In summary, I have provided genetic evidence that among the five SRRGs that I screened, three (*Cox7b2*, *Gm773*, and *Tuba3a/3b*) are required for normal male germ cell development and maturation in mice (Fig. 18). Although knockout of the other two genes (*Faiml* and *Cox8c*) did not show any apparent phenotype in my screening criteria, I cannot exclude the possibility that these genes still play critical roles in male fertility because my screen did not include natural mating-based fertility tests. Indeed, several genes are reported to be required for the steps present in natural mating processes but circumvented in IVF procedures such as entry into the oviduct (Fagerberg et al., 2014; Fujihara et al., 2018; Li et al., 2013). Also, there remains a possibility that the founder mice I generated might still have functional proteins, as I did not confirm a complete lack of functional proteins in each founder. However, this possibility is very low considering the highly efficient induction of indels at target sites (Fig. 12). Although *Gm773* appears to be conserved only among rodents (mouse and rat), *Cox7b2* is widely conserved in mammals, including humans (National Center for Biotechnology Information [NCBI] Gene database). Importantly, the human homolog *COX7B2* shows testis-specific expression patterns in humans like that in mice (Fig. 17C), suggesting that human *COX7B2* might also play critical roles in the formation of functional spermatozoa in humans. Further analyses of KO mice may reveal detailed molecular mechanisms underlying each defective process that would provide important insights into human reproductive medicine and mammalian reproduction.

Table 1. A list of SCNT-reprogramming resistant genes (SRRGs)

Gene	Chromosome	Gene expression levels at the blastocyst stage			DNA methylation levels at promoter		
		IVF	SCNT	Fold change (log2)	IVF	SCNT	Methylation difference
Asz1	Chr6	5.59	0.74	-2.75	0.01	0.34	0.33
Ezhip	ChrX	7.12	1.81	-1.92	0.03	0.33	0.30
Tex12	Chr9	15.91	4.57	-1.78	0.02	0.27	0.25
**Tuba3b*	Chr6	14.51	2.25	-2.64	0.08	0.26	0.18
**Cox8c*	Chr12	5.95	0.67	-2.98	0.05	0.22	0.17
Slc25a31	Chr3	4.01	0.67	-2.42	0.04	0.21	0.17
**Cox7b2*	Chr5	3.63	0.17	-3.80	0.10	0.26	0.16
**Faiml*	Chr9	13.75	4.47	-1.60	0.02	0.17	0.15
Tex101	Chr7	6.29	1.97	-1.63	0.06	0.21	0.15
Fabp9	Chr3	10.10	1.11	-3.08	0.05	0.15	0.10
Mael	Chr1	6.76	2.01	-1.70	0.05	0.14	0.09
#*Majin*	Chr19	3.44	0.93	-1.78	0.03	0.11	0.08
**Gm773*	ChrX	7.50	0.85	-3.01	0.17	0.23	0.06

(Data obtained from Matoba et al., 2018)

IVF: *in vitro* fertilization, SCNT: somatic cell nuclear transfer, *Asz1*: ankyrin repeat, SAM and basic leucine zipper domain containing 1, *Ezhip*: EZH inhibitory protein, *Tex12*: testis expressed 12, *Tuba3b*: tubulin alfa 3B, *Cox8c*: cytochrome c oxidase subunit 8C, *Slc25a31*: solute carrier family 25 (mitochondrial carrier; adenine nucleotide translocator), *Cox7b2*: cytochrome c oxidase subunit 7B2, *Faiml*: Fas apoptotic inhibitory molecule like, *Tex101*: testis expressed 101, *Fabp9*: fatty acid binding protein 9, *Mael*: maelstrom spermatogenic transposon silencer, *Majin*: membrane anchored junction protein, *Gm*773: predicted gene 773

Used as control along with candidate genes

* The selected candidate genes

Table 2. RT-qPCR primers used in this study

Primer name	Sequence
Majin-RT-F1	CTCTGCAGAAACTTACGCCC
Majin-RT-R1	GTGCACATACATGGAGGCTG
Faiml-RT-F1	AATAGTAGAGTCGGTGGGCG
Faiml-RT-R1	CCTTCTCTCTTCTTCCCGCT
Cox8c-RT-F1	GCTGTTGGGATTGTCGTGTT
Cox8c-RT-R1	TTTAAAGGAGCCATGCCGTG
Cox7b2-RT-F1	ACTTCTGAGGAGAGCGTCTG
Cox7b2-RT-R1	TGCATATCTGGCCAAGGGAA
Gm773-RT-F1	TTGAGGAAATCGTGAAGCCG
Gm773-RT-R1	TCAACAGGAATAGGGGTGCC
Tuba3b-RT-F1	ATGCCAAGCGACAAAACCAT
Tuba3b-RT-R1	GTTCCGGTGCGTACTTCATC
Tuba3a-RT-F1	GCGGCTTTCAGTGGACTATG
Tuba3a-RT-R1	GGAATGCTCTAGGGTGGTGT

Table 3. Sequence information of the primers used for the synthesis of sgRNAs

sgRNA name	Target exon	sgRNA synthesis approach*	Primer/sequence names	Sequence
Majin-sg1#	Exon 3	GeneArt	Target+PAM	GGATAAGGAAGTCATCGTCC+AGG
			Majin-sg1-F	TAATACGACTCACTATAGgataaggaagtcatcgtcc
			Majin-sg1-R	TTCTAGCTCTAAAACggacgatgacttccttatcc
Majin-sg2#	Exon 5	GeneArt	Target+PAM	AAACAAACGGGTAGGGCGTC+AGG
			Majin-sg2-F	TAATACGACTCACTATAGaaacaaacgggtagggcgtc
			Majin-sg2-R	TTCTAGCTCTAAAACgacgccctacccgtttgttt
Majin-sg3	Exon 10	GeneArt	Target+PAM	CGTTGGGGCATGGCCTGCAA+GGG
			Majin-sg3-F	TAATACGACTCACTATAGcgttggggcatggcctgcaa
			Majin-sg3-R	TTCTAGCTCTAAAACttgcaggccatgccccaacg
Faiml-sg1	Exon 2	Cloning-IVT	Target+PAM	AAACGAGTTGTGTACGTGGA+TGG
			Faiml-sg1-F	CACCGaaacgagttgtgtacgtgga
			Faiml-sg1-R	AAACtccacgtacacaactcgtttC
			Faiml-sg1-IVT	TTAATACGACTCACTATAGaaacgagttgtgtacgtgga
Faiml-sg2	Exon 3	Cloning-IVT	Target+PAM	GTCATCCAAGTGCAATACCC+AGG
			Faiml-sg2-F	CACCgtcatccaagtgcaataccc
			Faiml-sg2-R	AAACgggtattgcacttggatgac
			Faiml-sg2-IVT	TTAATACGACTCACTATAgtcatccaagtgcaataccc
Cox8c-sg1	Exon 1	Cloning-IVT	Target+PAM	TCGAGAACAGGACTGCACGG+TGG
			Cox8c-sg1-F	CACCGtcgagaacaggactgcacgg
			Cox8c-sg1-R	AAACccgtgcagtcctgttctcgaC
			Cox8c-sg1-IVT	TTAATACGACTCACTATAGtcgagaacaggactgcacgg
Cox8c-sg2	Exon 1	Cloning-IVT	Target+PAM	AGCAGCAGGCGAGACATCGC+AGG
			Cox8c-sg2-F	CACCGagcagcaggcgagacatcgc
			Cox8c-sg2-R	AAACgcgatgtctcgcctgctgctC
			Cox8c-sg2-IVT	TTAATACGACTCACTATAGagcagcaggcgagacatcgc
Cox7b2-sg1	Exon 3	Cloning-IVT	Target+PAM	TGGGGGGTAACTCTGCCAAT+AGG
			Cox7b2-sg1-F	CACCGtgggggggtaactctgccaat
			Cox7b2-sg1-R	AAACattggcagagttacccccccaC
			Cox7b2-sg1-IVT	TTAATACGACTCACTATAGtgggggggtaactctgccaat
Cox7b2-sg2	Exon 3	Cloning-IVT	Target+PAM	GAGATAGTTTAGTGCATATC+TGG
			Cox7b2-sg2-F	CACCgagatagtttagtgcatatc
			Cox7b2-sg2-R	AAACgatatgcactaaactatctcC

			Cox7b2-sg2-IVT	TTAATACGACTCACTATAgagatagtttagtgcatatc
Gm773-sg1	Exon 3	GeneArt	Target+PAM	GCATTGGTTCCTACAAGAAT+GGG
			Gm773-sg1-F	TAATACGACTCACTATAGgcattggttcctacaagaat
			Gm773-sg1-R	TTCTAGCTCTAAAACattcttgtaggaaccaatgc
Gm773-sg2	Exon 7	GeneArt	Target+PAM	GCTGTGGACCTGCCGTGATG TGG
			Gm773-sg2-F	TAATACGACTCACTATAGgctgtggacctgccgtgatg
			Gm773-sg2-R	TTCTAGCTCTAAAACcatcacggcaggtccacagc
Tuba3b-sg1	Exon 3	Cloning-IVT	Target+PAM	AAGTACGCACCGGAACCTAC+CGG
			Tuba3b-sg1-F	CACCGaagtacgcaccggaacctac
			Tuba3b-sg1-R	AAACtgccgtactggacctggcggC
			Tuba3b-sg1-IVT	TTAATACGACTCACTATAGaagtacgcaccggaacctac
Tuba3b-sg2	Exon 4	Cloning-IVT	Target+PAM	CAGGGCGCCATCGAACCTTA+GGG
			Tuba3b-sg2-F	CACCGcagggcgccatcgaacctta
			Tuba3b-sg2-R	AAACtaaggttcgatggcgccctgC
			Tuba3b-sg2-IVT	TTAATACGACTCACTATAGcagggcgccatcgaacctta
Tuba3a-sg1	Exon 3	GeneArt	Target+PAM	GTCGACAATCTCTTTGCCGA+TGG
			Tuba3a-sg1-F	TAATACGACTCACTATAGgtcgacaatctctttgccga
			Tuba3a-sg1-R	TTCTAGCTCTAAAACtcggcaaagagattgtcgac
Tuba3a-sg2	Exon 4	GeneArt	Target+PAM	CCCACTGGCAACCTACGCCC+CGG
			Tuba3a-sg2-F	TAATACGACTCACTATAGcccactggcaacctacgccc
			Tuba3a-sg2-R	TTCTAGCTCTAAAACgggcgtaggttgccagtggg

* GeneArt: GeneArt Precision gRNA synthesis kit, Cloning-IVT: Cloned into px330 and in vitro transcription by MEGAshortscript.

These two sgRNAs were used to produce sgMajin-2 mice.

Table 4. List of primary antibodies used in this study

Primary Antibody	Host species	Dilution	Source	Product ID
MVH/DDX4	Rabbit	1:500	Abcam	ab13840
SCP3	Mouse	1:500	Abcam	ab97672
Protamine P1	Mouse	1:500	BRIAR PATCH BIOSCIENCES	HUP1N

MVH: Mouse Vasa Homolog, DDX4: DEAD-Box Helicase 4, SCP3: Synaptonemal Complex Protein 3

Table 5. Genotyping PCR primers used in this study

Primer name	Sequence
Majin-1-GT-F1	TGGTACTTCTCTGTTTCCCTTCT
Majin-2-GT-F1	GGAGAGAGTTTCCCACCTGA
Majin-3-GT-F1	GCCCTGTGGTCTCCTCTTAG
Faiml-1-GT-F1	GCAAGCACTTCTCTGTAGCA
Faiml-2-GT-F1	TCCACAGGTACAGTCCCAAC
Cox8c-1-GT-F1	CCCTTTTCTGACCTGCGATG
Cox8c-2-GT-F1	CACACTTTACCAACGGCCTT
Cox7b2-1-GT-F1	GGCGGGTTAAAACTGGTCAG
Cox7b2-2-GT-F1	GAGACAGGTTCCACTCCACA
Gm773-1-GT-F1	ACGTAGCTGAGAATGTCACTGA
Gm773-2-GT-F1	AAGAGCGTGTCATTTGCCTG
Tuba3A-1-GT-F1	GGAATTGAACAGTCCTTGCCT
Tuba3A-2-GT-F1	ACCAACCTCAACCGTCTGAT
Tuba3B-1-GT-F1	ACAGCCACCATCTAAAGCCT
Tuba3B-2-GT-F1	GACAGCTGCTCATGGTATGC
Majin-1-GT-R1	GGTGTGATTCATCCTTGACTTCA
Majin-2-GT-R1	CCCGTCAACTCCCTCTTTCT
Majin-1-GT-R1	GTGGTGGACTGCTATGTTGC
Faiml-1-GT-R1	TGAATTTGAACATGGGACCACA
Faiml-2-GT-R1	ACACTCTGGAAATTGATGGGAA
Cox8c-1-GT-R1	TTTGTGGGCTTTCTGAGTGG
Cox8c-2-GT-R1	AGGCTTCGAGAACAGGACTG
Cox7b2-1-GT-R1	AGATGGGTGTGGAGTGGAAC

Cox7b2-2-GT-R1	TGCTCCAGGAGATCTAGGGT
Gm773-1-GT-R1	ACTGAGAAGGCATTGGTTCC
Gm773-2-GT-R1	CCCAGCATCAAGAGCAACAA
Tuba3B-1-GT-R1	TCCTTCCCAGTGATGAGCTG
Tuba3B-2-GT-R1	GGAAGTGGATGCGAGGGTAT
Tuba3A-1-GT-R1	CTGGAAAGGAAGATGCAGCC
Tuba3A-2-GT-R1	TGTGTCGTCCATTACAGCCT
Majin-1-OT-F1	GCGAGCAACCTTGTACCAAT
Majin-2-OT-F1	ACCTACCCAGCTTCAGAACT
Majin-3-OT-F1	AGTCGGGCAGGGTTTTCTTA
Faiml-1-OT-F1	AGAGGCCATGGATTTGACAG
Faiml-2-OT-F1	CGACATTAGCAAGCCAACGT
Cox8c-1-OT-F1	TAGGGAACAGGACTGAACGG
Cox8c-2-OT-F1	TCCTGTGACCCTATTGATACCA
Cox7b2-1-OT-F1	CTGGGAAGAGATGAGAGAAGGT
Cox7b2-2-OT-F1	TCACGTCTTAACCTCTGATGACT
Gm773-1-OT-F1	TCTCATCAAGAATCACAGGGG
Gm773-2-OT-F1	GGAGTGCCTTTTGTCAGCA
Tuba3A-1-OT-F1	CTGGGGAGGAAAGGGTTGAT
Tuba3A-2-OT-F1	CCGTGGTTAAAGTGTGGCTC
Tuba3B-1-OT-F1	TGCTGAGTCTAGTGGCACA
Tuba3B-2-OT-F1	CCCCAAATGACGATGCCTTC
Majin-1-OT-R1	TCCATGTTTGCCAAGACTGC
Majin-2-OT-R1	CTGTGTGCCTTTCCTCTTGG
Majin-3-OT-R1	AGCCTCTATAGTTCCCTCAGG

Faiml-1-OT-R1	TCAAGCCCTCTTATTCCTACCC
Faiml-2-OT-R1	CCAACCCTTTGCCCTAATCC
Cox8c-1-OT-R1	TGTTAGACATGCCACCACCA
Cox8c-2-OT-R1	ACAGGCAAGACATAGCTGGG
Cox7b2-1-OT-R1	GTCACATGATGTTCTCTGCCC
Cox7b2-2-OT-R1	TAGAATGCGGTTATGTCCCC
Gm773-1-OT-R1	GACTCTGACATTCATTCTCCTGA
Gm773-2-OT-R1	TGCCTGCTTAAGTGCTTTCA
Tuba3B-1-OT-R1	TAGCACTACTCCATGGCCTC
Tuba3B-2-OT-R1	GAGAGGGAGCCATCAAACCT
Tuba3A-1-OT-R1	GGTCCTGAGTTCATATCCTAGCA
Tuba3A-2-OT-R1	CCTGCACAGACACAAAACCT

Table 6. Embryonic and postnatal development of CRISPR founder mice

Group name	CRISPR target gene(s)	Injected RNA		No. of ET	Term (C-section at E19.5)			Adult (12-15 weeks old)	
		Cas9 mRNA	No. of sgRNAs		No. of implanted (% per ET)	No. of pups (% per ET)	No. of males (% per total)	No. of survived (% per born)	No. of survived males (% per total)
Control	-	-	0	105	59 (56.2)	27 (25.7)	14 (51.9)	17 (63.0)	6 (35.3)
sgControl	-	+	0	65	42 (64.6)	19 (29.2)	8 (42.1)	13 (68.4)	6 (46.2)
sgFaiml	*Faiml*	+	2	104	51 (49.0)	14 (13.5)	8 (57.1)	9 (64.3)	6 (66.7)
sgCox7b2	*Cox7b2*	+	2	91	53 (58.2)	24 (26.4)	12 (50.0)	15 (62.5)	7 (46.7)
sgCox8c	*Cox8c*	+	2	60	34 (56.7)	14 (23.3)	4 (28.6)	11 (78.6)	3 (27.3)
sgTuba3a	*Tuba3a*	+	2	35	18 (51.4)	6 (17.1)	2 (33.3)	5 (83.3)	2 (40.0)
sgTuba3b	*Tuba3b*	+	2	61	38 (62.3)	17 (27.9)	10 (58.8)	11 (64.7)	6 (54.5)
sgTuba3a/ 3b	*Tuba3a, Tuba3b*	+	2 + 2	101	56 (55.4)	14 (13.9)	12 (85.7)	10 (71.4)	9 (90.0)
sgGm773	*Gm773*	+	2	181	102 (56.4)	46 (25.4)	19 (41.3)	23 (50.0)	9 (39.1)
sgMajin-2	*Majin*	+	2	67	37 (55.2)	12 (17.9)	9 (75.0)	11 (91.7)	8 (72.7)
sgMajin-3	*Majin*	+	3	84	41 (48.8)	6 (7.1)	5 (83.3)	4 (66.7)	3 (75.0)

ET: Embryo transfer

Table 7. Development of embryos derived from CRISPR founder female mice

Female name	CRISPR targeted gene(s)	Embryo transfer at the 2-cell stage		C-section at E19.5	
		No. of transferred embryos	No. of recipients for ET	No. of implanted (% per ET)	No. of pups (% per ET)
Control	-	90	4	60 (66.7)	43 (47.8)
sgControl	-	80	4	54 (67.5)	35 (43.8)
sgFaiml	*Faiml*	48	3	34 (70.8)	15 (31.3)
sgCox7b2	*Cox7b2*	95	5	57 (60.0)	30 (31.6)
sgCox8c	*Cox8c*	71	4	52 (73.2)	29 (40.8)
sgTuba3a	*Tuba3a*	84	4	53 (63.1)	22 (26.2)
sgTuba3b	*Tuba3b*	83	4	49 (59.0)	24 (28.9)
sgTuba3a/3b	*Tuba3a, Tuba3b*	115	6	57 (50.0)	17 (14.8)
sgGm773	*Gm773*	104	5	67 (64.4)	29 (27.9)
sgMajin-2#	*Majin*	-	-	-	-
sgMajin-3#	*Majin*	-	-	-	-

ET: Embryo Transfer

#These mice did not produce oocytes upon superovulation.

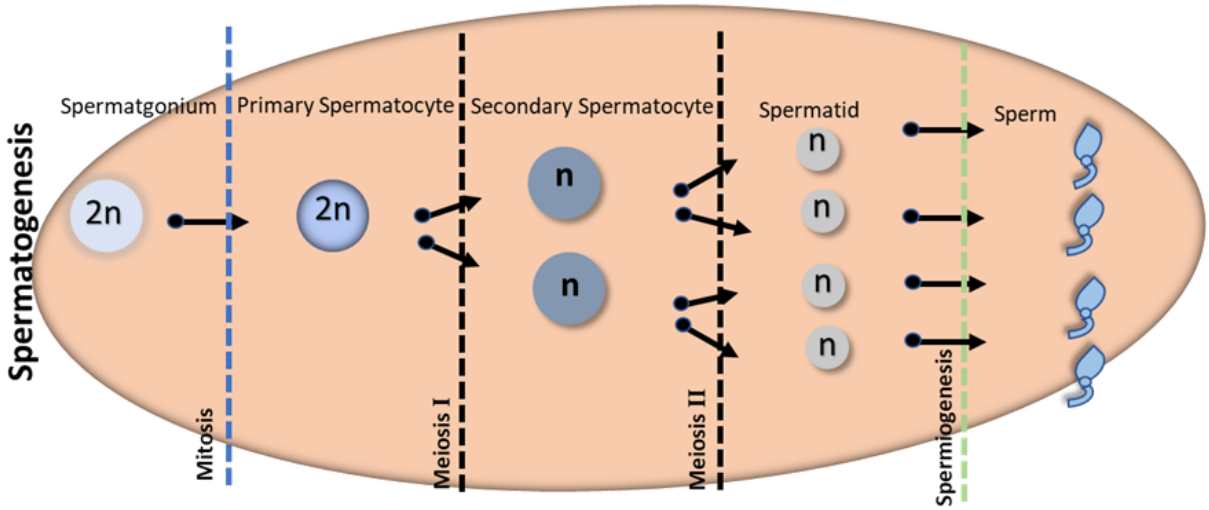

Fig. 3. Stages of spermatogenesis

Schematic illustration of continuous phases of spermatogenesis from spermatogonium to spermatozoa. The subsequent conversion of differentiated spermatogonia to primary spermatocyte goes through mitosis and then further differentiation to secondary spermatocyte by meiosis I. In the second meiosis division, the two new daughter cells further divide themselves into four spermatids. By the process of spermiogenesis, (round to elongated) spermatids spermatid finally converts to spermatozoa.

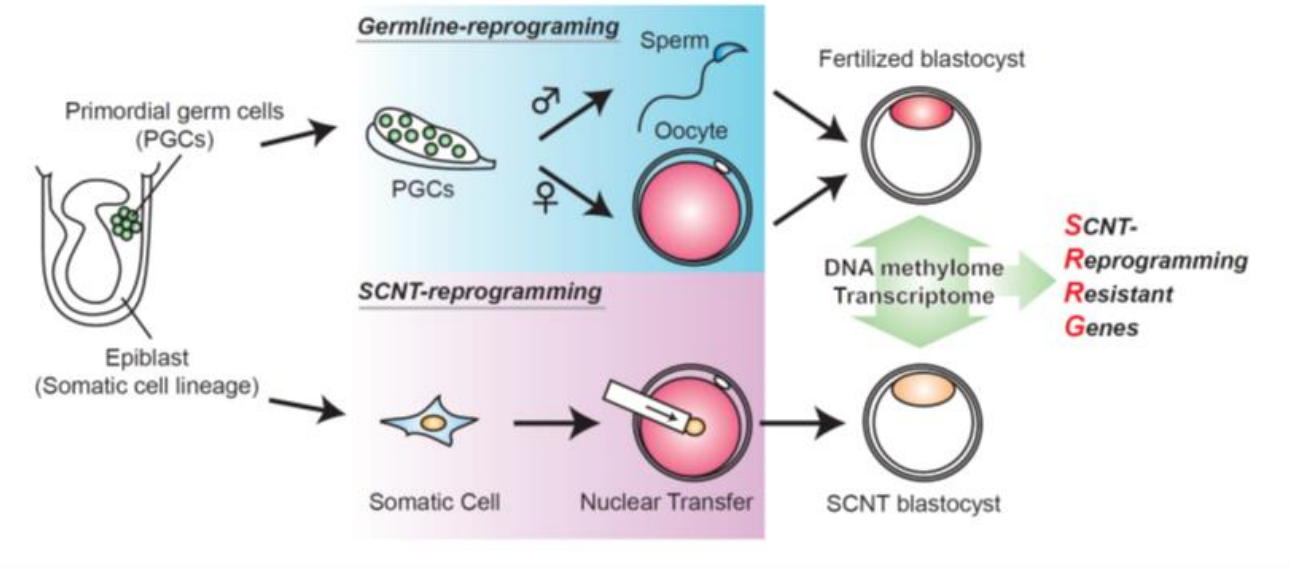

Fig. 4. Schematic illustration comparing germline reprogramming and SCNT-reprogramming and the strategy to identify SCNT reprogramming resistant genes (SRRGs).

Germ cells that are differentiated from epiblast as primordial germ cells undergo germline-specific epigenetic reprogramming through either spermatogenesis or oogenesis and produced the mature sperm or oocyte. On the other hand, in the SCNT, the somatic cell genome skips germline reprogramming, instead undergoing SCNT reprogramming in the ooplasm. Therefore, it is assumed that SCNT embryos possess epigenetic abnormalities that are resistant to SCNT reprogramming but are successfully reprogrammed only in the germline.

A

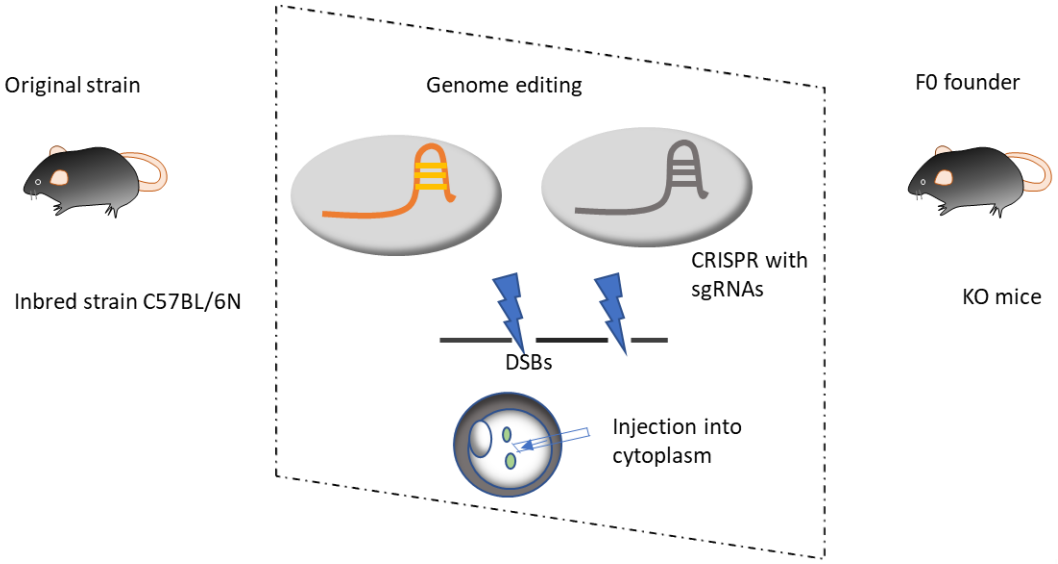
Original strain
Genome editing
F0 founder
Inbred strain C57BL/6N
CRISPR with sgRNAs
KO mice
DSBs
Injection into cytoplasm

B

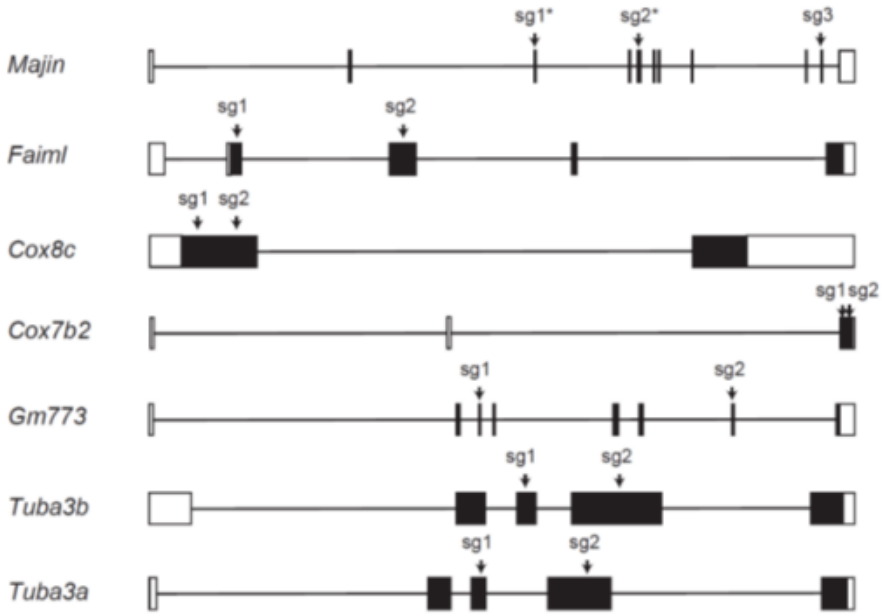
Majin
Faiml
Cox8c
Cox7b2
Gm773
Tuba3b
Tuba3a
sg1*
sg2*
sg3
sg1
sg2
sg1 sg2

C

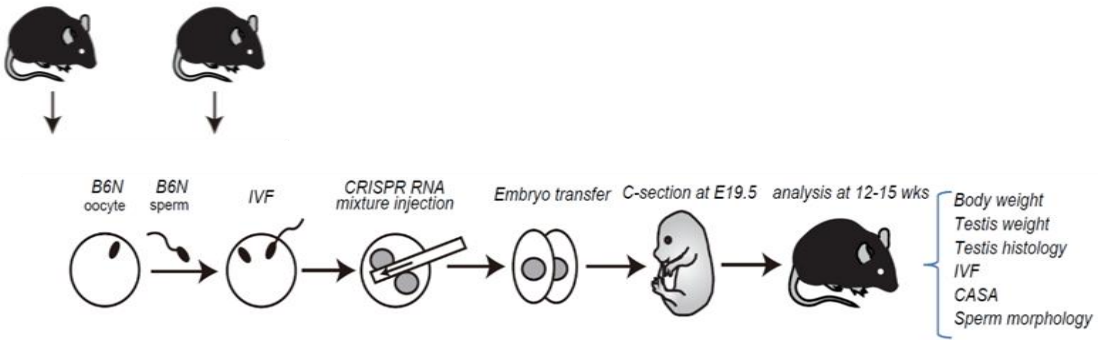
B6N oocyte
B6N sperm
IVF
CRISPR RNA mixture injection
Embryo transfer
C-section at E19.5
analysis at 12-15 wks
Body weight
Testis weight
Testis histology
IVF
CASA
Sperm morphology

Fig. 5. Representative method to generate KO mice by the modified Triple CRISPR/Cas9 system and screening procedures for founders

(A) The mixture of two or three distinct sgRNAs (50 ng/μL each) targeting coding exons and *Cas9* mRNA (100 ng/μL) were injected into B6N inbred zygotes to produce KO founder mice. The individual *Cas9*/sgRNA complexes generate DSBs in the target region. (B) Two or three guide RNAs were designed for distinct protein-coding regions of target gene exons. Targeted regions for designed sgRNAs; *Majin*: exon 3, exon 5, exon 10 (for two sgRNA methods, sgRNAs with asterisks were used); *Faiml*: exon 2, exon 3; *Cox8c*: exon 1; *Cox7b2*: exon 3. *Gm773*: exon 3, exon 7; *Tuba3b*: exon 3, exon 4; *Tuba3a*: exon 3, exon 4. (C) C57BL/6N (B6N) oocytes and sperm were *in vitro* fertilized to generate B6N inbred zygotes. CRISPR mixture (Cas9 mRNA + sgRNAs) was injected into the cytoplasm of the zygotes by using a piezo-driven micromanipulator at 6 hours post insemination (hpi). Embryos developed to the 2-cell stage were transferred to the oviduct of pseudo-pregnant females. The caesarian section (C-section) was performed at E19.5 to obtain the pups. The pups were ablactated at three weeks and observed up-to the adulthood. The phenotypes of founder mice were screened for the prescribed parameters at 12-15 weeks old respectively.

sgRNA: single guide RNA, KO: knock-out, DSB: double-strand break, IVF: *in vitro* fertilization, CASA: computer-assisted sperm analysis.

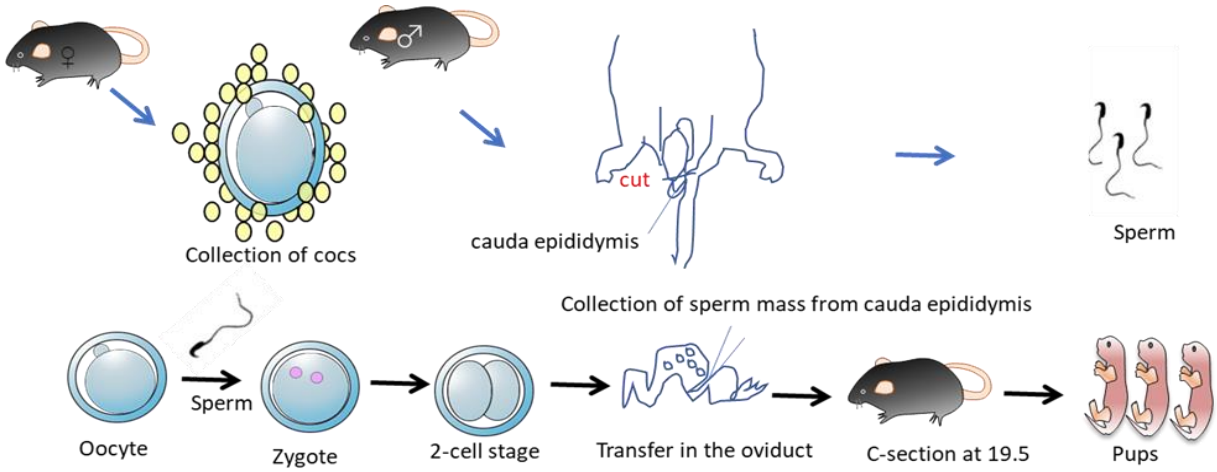

Fig. 6. Schematic presentation of IVF, ET, and C-section of getting pups

After the collection of Cumulus-oocyte complexes (COCs), introduced sperm collected from the cauda epididymis, followed by in vitro fertilization to develop to the one-cell stage zygote. Embryos were transferred into the oviduct of pseudo-pregnant females at the 2-cell stage and finally recovered the pups by C-section at E19.5.

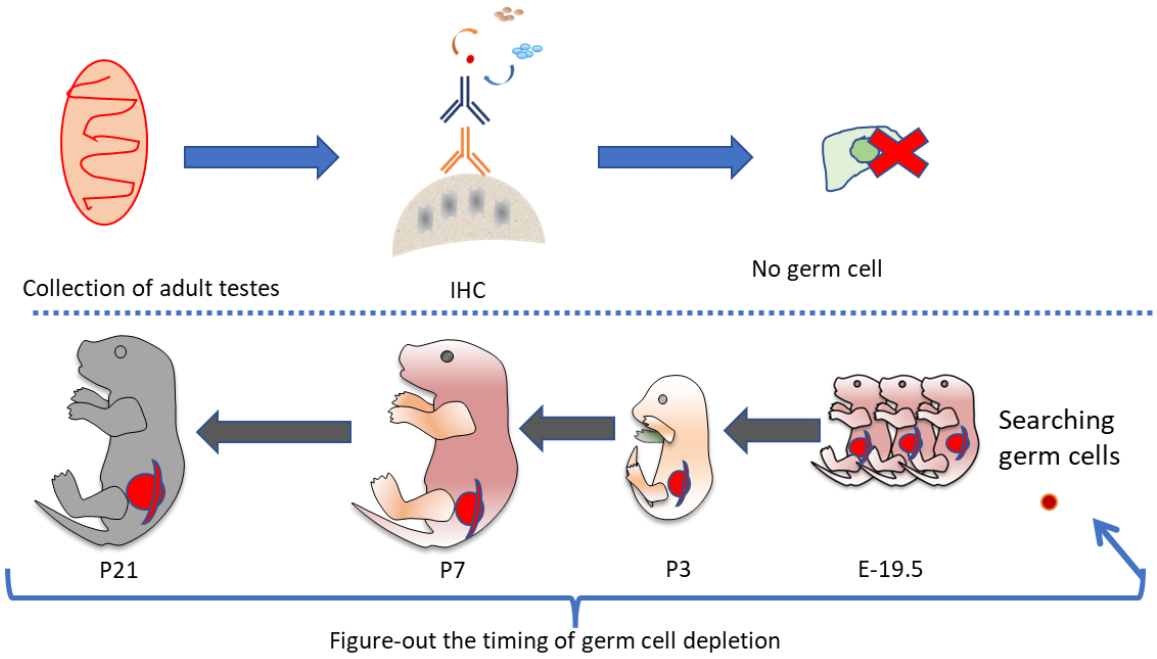

Fig. 7. Timing of testis collection for germ cell analysis of *Tuba3a/3b* DKO mice

A representative scenario of testis collection for sgTuba3a/3b mice from E19.5-P21 pups. Collected testes were examined by immunohistochemistry (IHC) against germ cell markers.

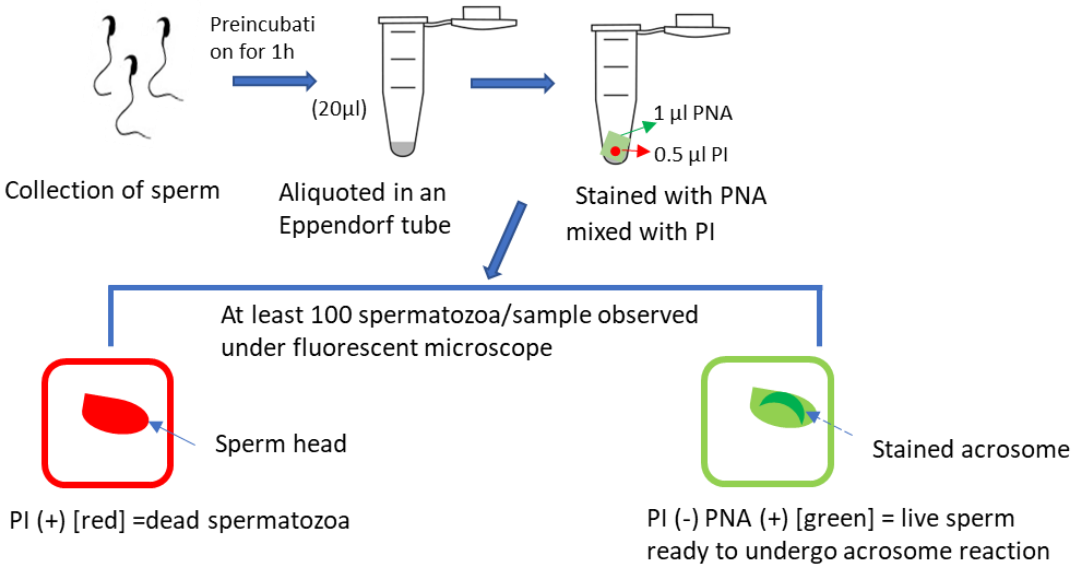

Fig. 8. Sperm staining for the assessment of plasma membrane integrity and the acrosome status

The procedure of sperm staining and counting of stained sperm. Sperm was collected and preincubated for an hour and aliquoted in an Eppendorf tube. Then the sperm suspension was stained with peanut agglutinin (PNA) mixed with propidium iodide (PI), and the tube was incubated at 37°C for 15 min. Finally, at least 100 spermatozoa were observed under a fluorescent microscope for each sample at three different time points. I counted the dead sperm (lost plasma membrane integrity) [red] and the live one (stained acrosomal bending) [green] ready to undergo acrosome reaction.

A

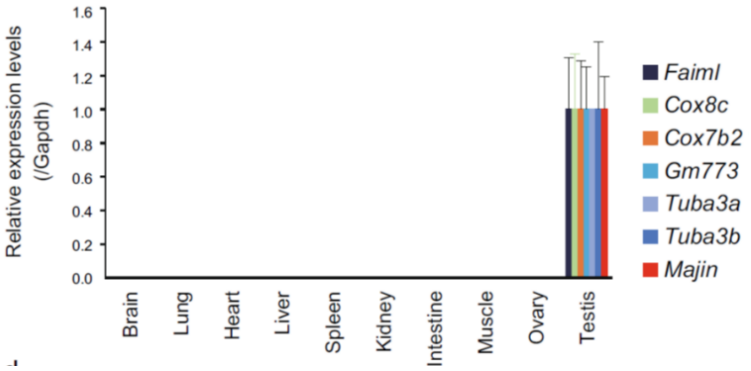
Relative expression levels (/Gapdh)
1.6
1.4
1.2
1.0
0.8
0.6
0.4
0.2
0.0
Brain
Lung
Heart
Liver
Spleen
Kidney
Intestine
Muscle
Ovary
Testis
Faiml
Cox8c
Cox7b2
Gm773
Tuba3a
Tuba3b
Majin

B

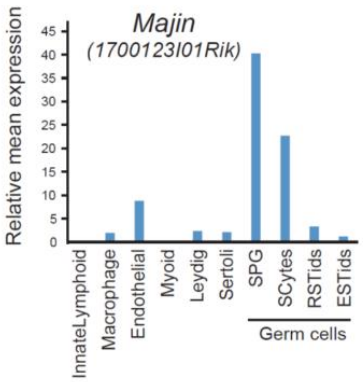
Majin
(1700123I01Rik)
Relative mean expression
45
40
35
30
25
20
15
10
5
0
InnateLymphoid
Macrophage
Endothelial
Myoid
Leydig
Sertoli
SPG
SCytes
RSTids
ESTids
Germ cells

C

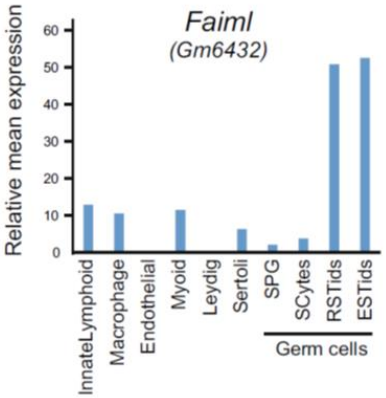
Faiml
(Gm6432)
Relative mean expression
60
50
40
30
20
10
0
InnateLymphoid
Macrophage
Endothelial
Myoid
Leydig
Sertoli
SPG
SCytes
RSTids
ESTids
Germ cells

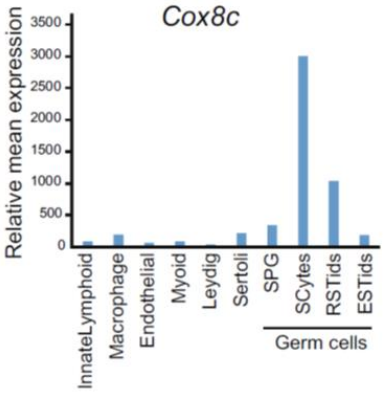
Cox8c
Relative mean expression
3500
3000
2500
2000
1500
1000
500
0
InnateLymphoid
Macrophage
Endothelial
Myoid
Leydig
Sertoli
SPG
SCytes
RSTids
ESTids
Germ cells

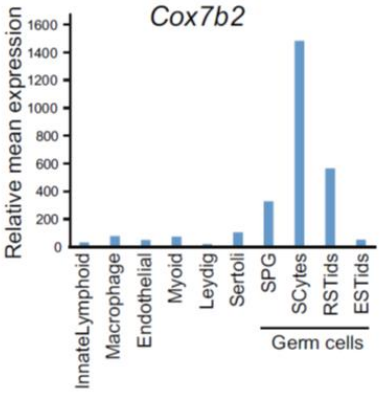
Cox7b2
Relative mean expression
1600
1400
1200
1000
800
600
400
200
0
InnateLymphoid
Macrophage
Endothelial
Myoid
Leydig
Sertoli
SPG
SCytes
RSTids
ESTids
Germ cells

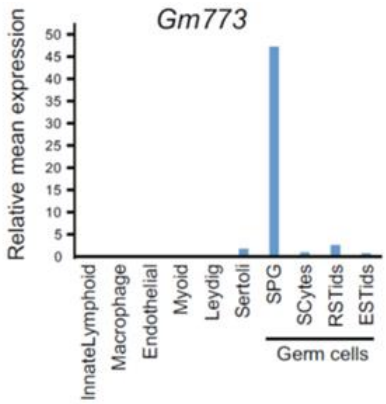
Gm773
Relative mean expression
50
45
40
35
30
25
20
15
10
5
0
InnateLymphoid
Macrophage
Endothelial
Myoid
Leydig
Sertoli
SPG
SCytes
RSTids
ESTids
Germ cells

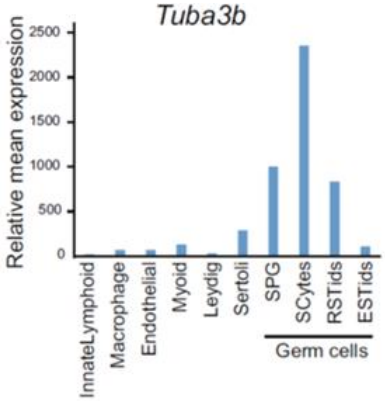
Tuba3b
Relative mean expression
2500
2000
1500
1000
500
0
InnateLymphoid
Macrophage
Endothelial
Myoid
Leydig
Sertoli
SPG
SCytes
RSTids
ESTids
Germ cells

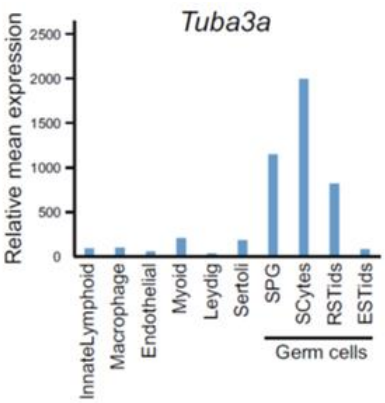
Tuba3a
Relative mean expression
2500
2000
1500
1000
500
0
InnateLymphoid
Macrophage
Endothelial
Myoid
Leydig
Sertoli
SPG
SCytes
RSTids
ESTids
Germ cells

Fig. 9. Testicular germ cell-specific expression of target SRRGs

(A) RT-qPCR analysis of gene expression levels of target SRRGs and *Majin* in adult mouse tissues and found that all the candidates exclusively expressed in the testis. Data shown are mean expression values relative to *Gapdh*. The expression level of each gene was normalized for testis as 1.

(B) and (C) Bar graphs showing the gene expression levels of *Majin* (B) and target SRRGs (C) in multiple cell types of the adult testis. Single-cell RNA-seq data were obtained from Green et al., 2018 (GSE112393). SPG; spermatogonia. SCytes; spermatocytes. RSTids; round spermatids. ESTids; elongated spermatids.

A

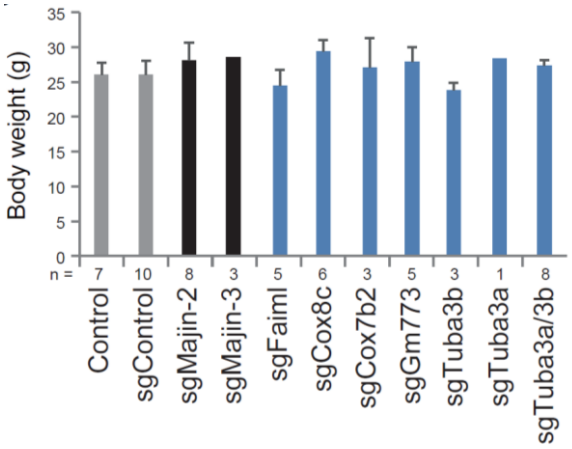
Body weight (g)
35
30
25
20
15
10
5
0
n =
7
10
8
3
5
6
3
5
3
1
8
Control
sgControl
sgMajin-2
sgMajin-3
sgFaiml
sgCox8c
sgCox7b2
sgGm773
sgTuba3b
sgTuba3a
sgTuba3a/3b

B

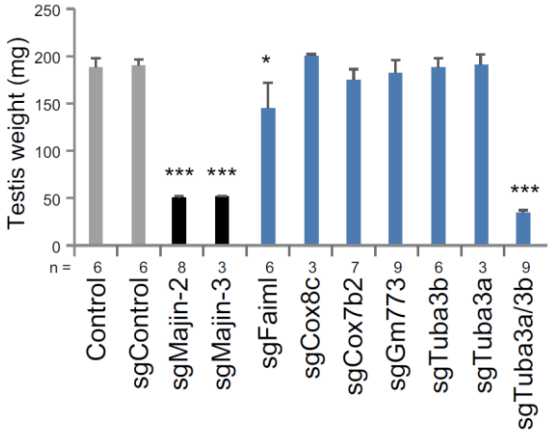
Testis weight (mg)
250
200
150
100
50
0
n =
6
6
8
3
6
3
7
9
6
3
9
***
***
*
***
Control
sgControl
sgMajin-2
sgMajin-3
sgFaiml
sgCox8c
sgCox7b2
sgGm773
sgTuba3b
sgTuba3a
sgTuba3a/3b

C

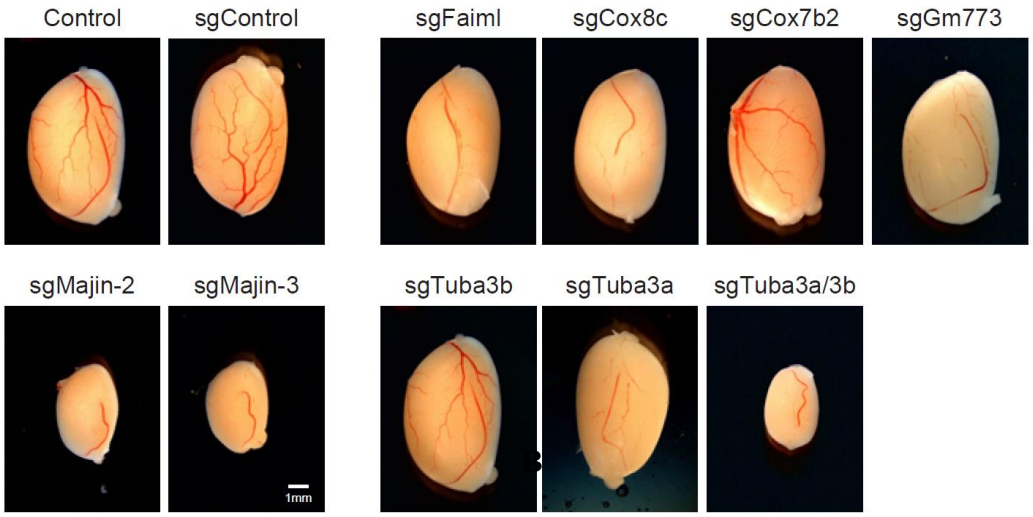
Control
sgControl
sgFaiml
sgCox8c
sgCox7b2
sgGm773
sgMajin-2
sgMajin-3
sgTuba3b
sgTuba3a
sgTuba3a/3b
1mm

Fig. 10. CRISPR-based genetic screening of 5 SRRGs

(A) and (B) Bar graphs showing the body weight (A) and testis weight (B) of adult founder mice. No significant change was observed in the body weight of adult candidate mice. The testis weight was greatly reduced in sgMajin-2, sgMajin-3, and sgTuba3a/3b mice, while it was slightly reduced in sgFaiml mice. * $p < 0.05$, *** $p < 0.001$.

(C) Gross morphology of founder testis. Note that sgMajin-2, sgMajin-3 and sgTuba3a/3b mice had significantly smaller testis compared to the control. Scale bar, 1 mm.

A

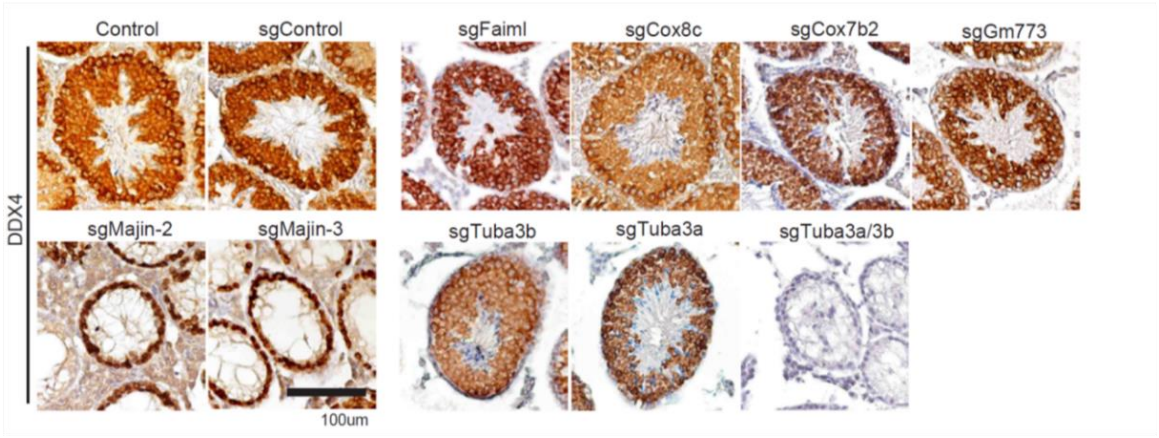
Control
sgControl
sgFaiml
sgCox8c
sgCox7b2
sgGm773
DDX4
sgMajin-2
sgMajin-3
sgTuba3b
sgTuba3a
sgTuba3a/3b
100um

B

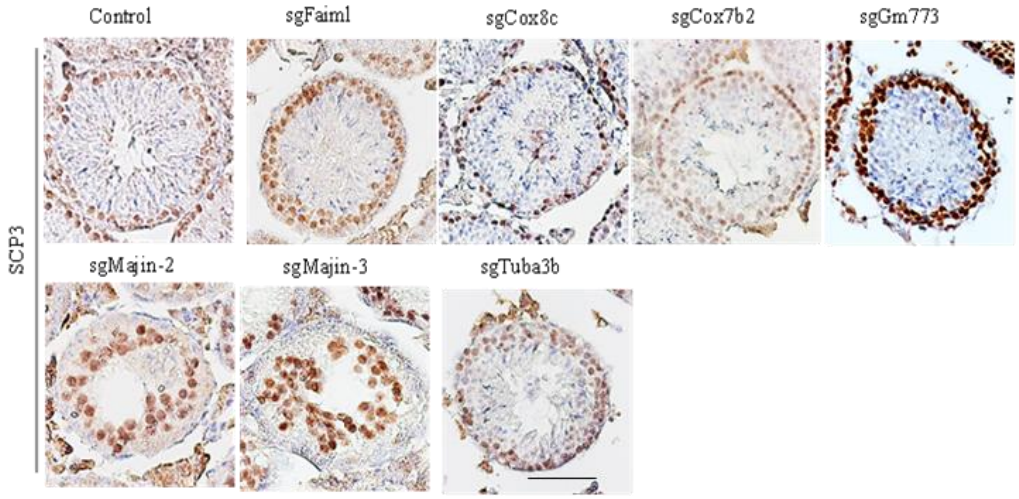
Control
sgFaiml
sgCox8c
sgCox7b2
sgGm773
SCP3
sgMajin-2
sgMajin-3
sgTuba3b

C

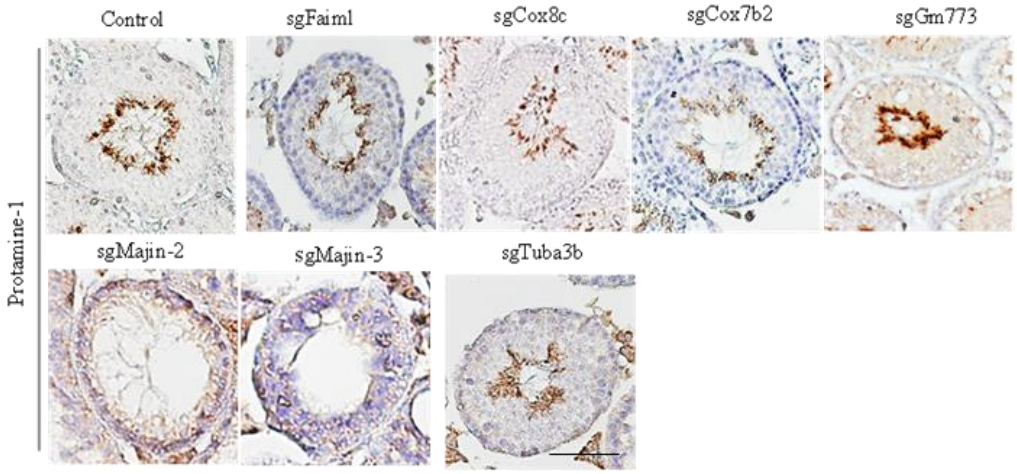
Control
sgFaiml
sgCox8c
sgCox7b2
sgGm773
Protamine-1
sgMajin-2
sgMajin-3
sgTuba3b

Fig. 11. Histology of the CRISPR-generated founder testes

(A) Representative immunostaining images of testis sections stained against a germ cell-specific marker, DDX4. Note that, while germ cells are depleted in sgMajin-2 and sgMajin-3 testis, they are completely absent in sgTuba3a/3b testis. Scale bar, 100 μm.

(B**)** Representative immunostaining images of testis sections stained against synaptonemal complex protein 3 (SCP3), a spermatocyte marker. Scale bar, 100 μm.

(C) Representative immunostaining images of testis sections stained against Protamine-1, a postmeiotic spermatid marker. Scale bar, 100 μm.

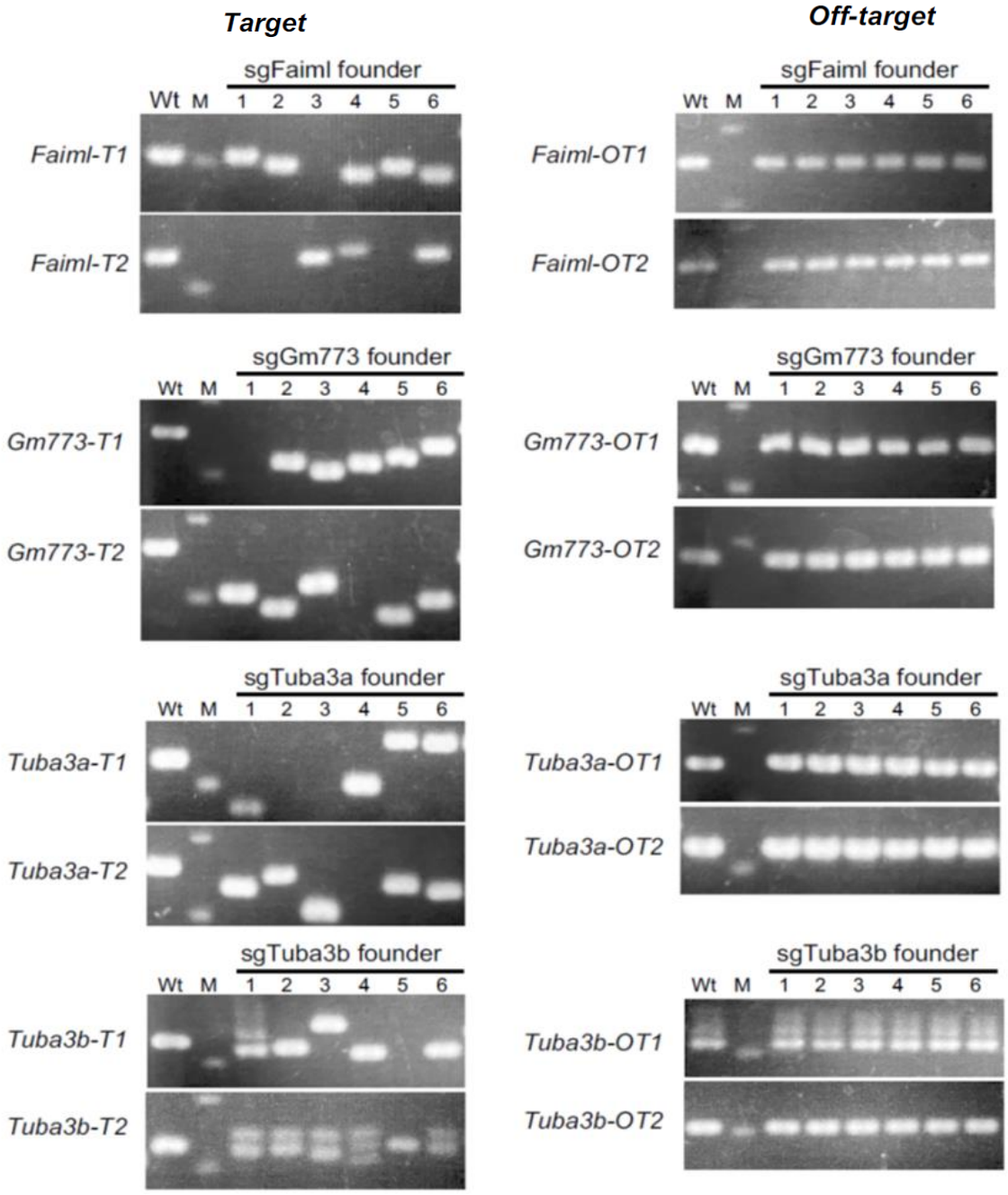
Target
Off-target
sgFaiml founder
Wt M 1 2 3 4 5 6
Faiml-T1
Faiml-T2
Faiml-OT1
Faiml-OT2
sgGm773 founder
Gm773-T1
Gm773-T2
Gm773-OT1
Gm773-OT2
sgTuba3a founder
Tuba3a-T1
Tuba3a-T2
Tuba3a-OT1
Tuba3a-OT2
sgTuba3b founder
Tuba3b-T1
Tuba3b-T2
Tuba3b-OT1
Tuba3b-OT2

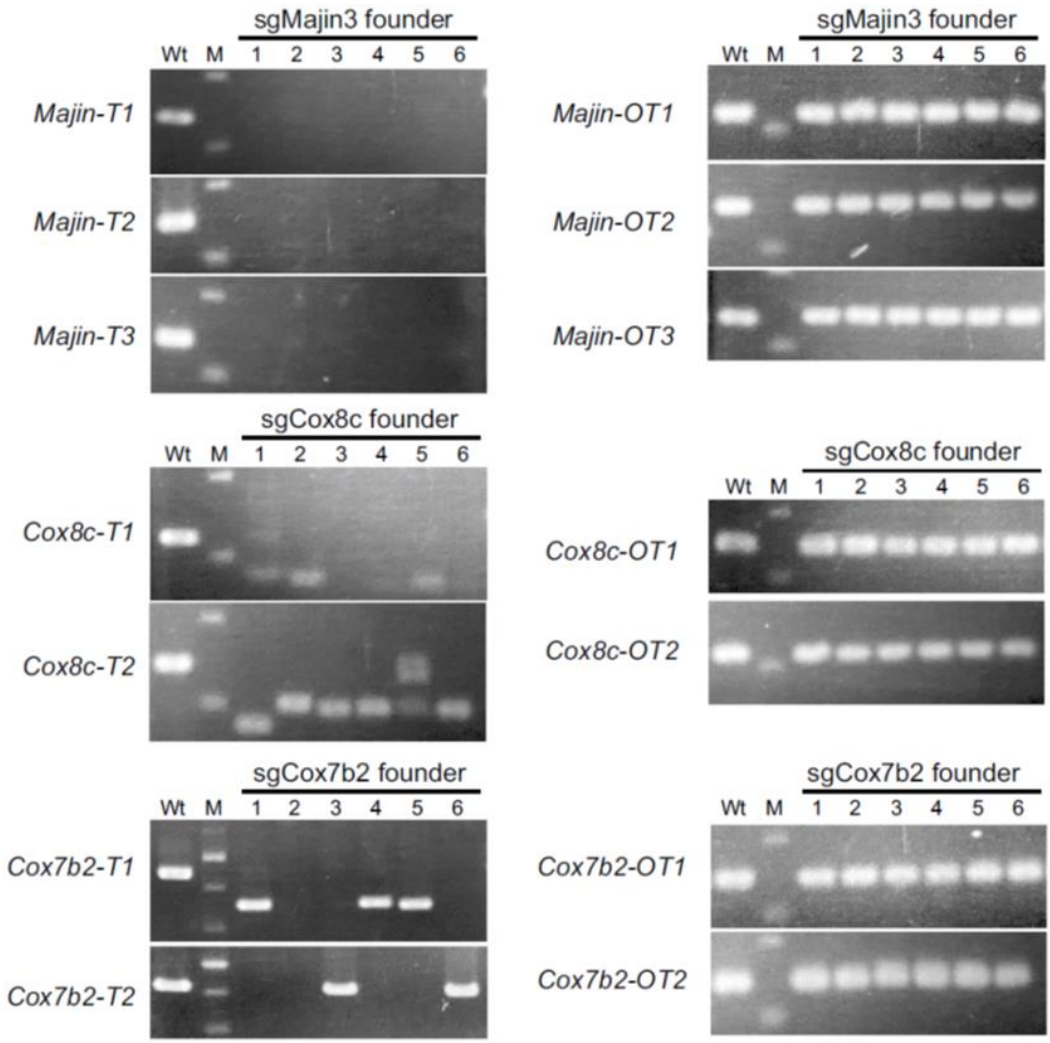

Fig. 12. Highly efficient induction of indels at the target sites of the founder mice

(Left) Electrophoresis images of genotyping PCR using pairs of primers that surrounded target sites of each sgRNA. Note that essentially all founders analyzed appeared to have biallelic indels at the target SRRGs. (Right) Electrophoresis images of genotyping PCR using pairs of primers that surrounded the top-ranked putative off-target site of each sgRNA. No apparent mutation was found at these off-target sites. M: marker (100 bp ladder), Wt: wild type.

A

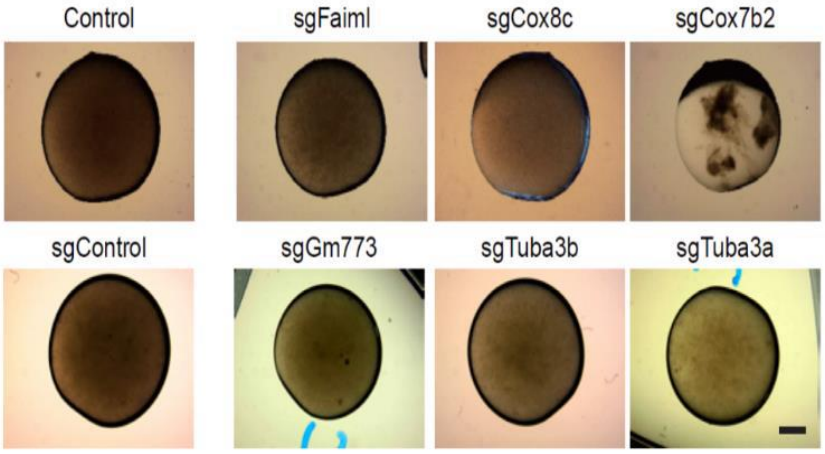
Control
sgFaiml
sgCox8c
sgCox7b2
sgControl
sgGm773
sgTuba3b
sgTuba3a

B

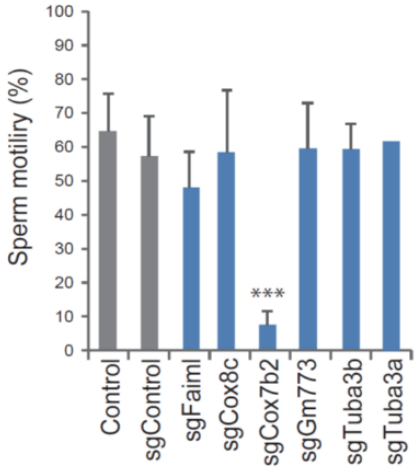
Sperm motiliry (%)
100
90
80
70
60
50
40
30
20
10
0
***
Control
sgControl
sgFaiml
sgCox8c
sgCox7b2
sgGm773
sgTuba3b
sgTuba3a

C

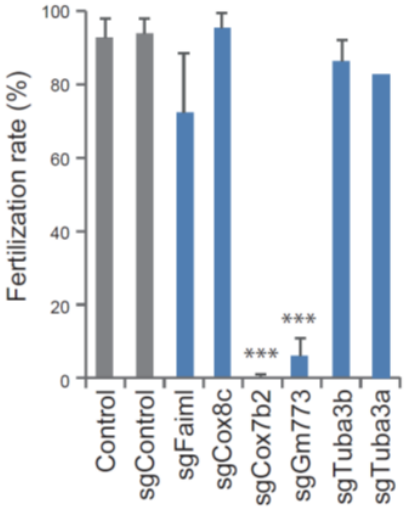
Fertilization rate (%)
100
80
60
40
20
0
***
***
Control
sgControl
sgFaiml
sgCox8c
sgCox7b2
sgGm773
sgTuba3b
sgTuba3a

D

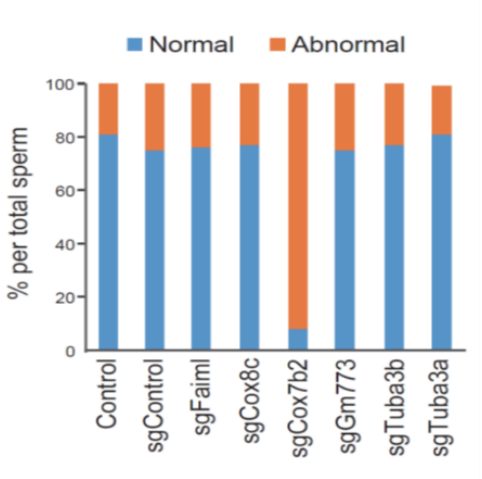
Normal
Abnormal
% per total sperm
100
80
60
40
20
0
Control
sgControl
sgFaiml
sgCox8c
sgCox7b2
sgGm773
sgTuba3b
sgTuba3a

E

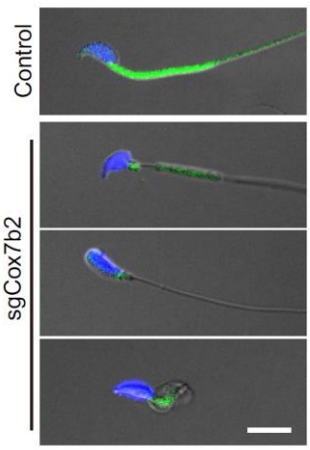
Control
sgCox7b2

Fig. 13. Sperm fertility, motility, and morphology analyses of SRRG KO mice

(A) Representative images of HTF drops suspended with epididymis-isolated spermatozoa at 1 hour of culture. Scale bar, 1 mm. Note that sperm clots of sgCox7b2 failed to spread throughout the drop and remained aggregated.

(B) Bar graphs showing the sperm motility examined by CASA at 1 hour after preincubation. The motility was severely reduced in sgCox7b2 spermatozoa. *** $p < 0.001$.

(C) Bar graphs showing the fertilization rate of spermatozoa of founder males with B6N oocytes by IVF. Fertilized zygotes were identified by the presence of two pronuclei at 5 to 6 hours after insemination. *** $p < 0.001$.

(D) Bar graphs showing the ratio of sperm with normal or abnormal morphology. Note that the great majority of spermatozoa showed abnormal morphology in the sgCox7b2 testis.

(E) Representative images of spermatozoa of control and sgCox7b2 mice. sgCox7b2 spermatozoa displayed abnormality in the head and midpiece. Residual cytoplasm was frequently observed in sgCox7b2 spermatozoa. Scale bar, 10 μm.

A

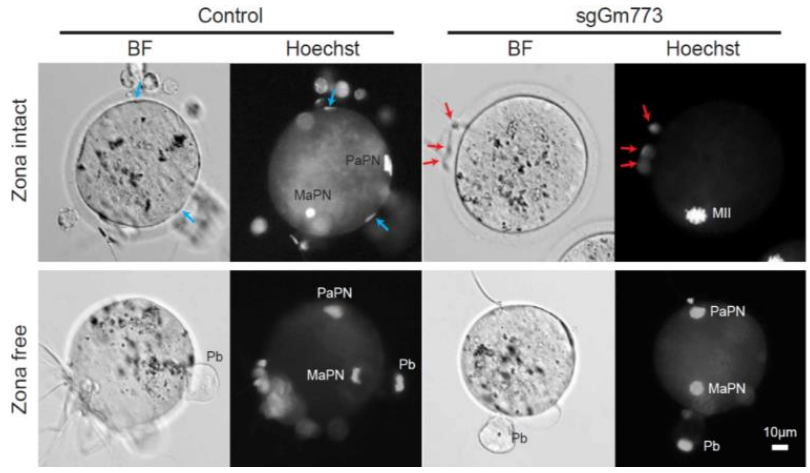
Control
sgGm773
BF
Hoechst
BF
Hoechst
Zona intact
Zona free
PaPN
MaPN
MII
PaPN
MaPN
Pb
Pb
PaPN
MaPN
Pb
10μm

B

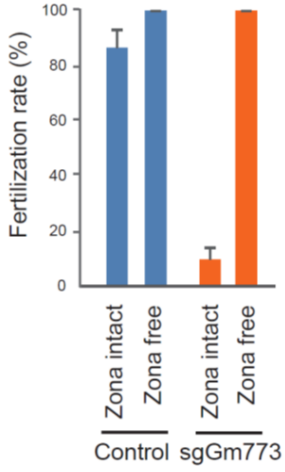
Fertilization rate (%)
100
80
60
40
20
0
Zona intact
Zona free
Zona intact
Zona free
Control
sgGm773

C

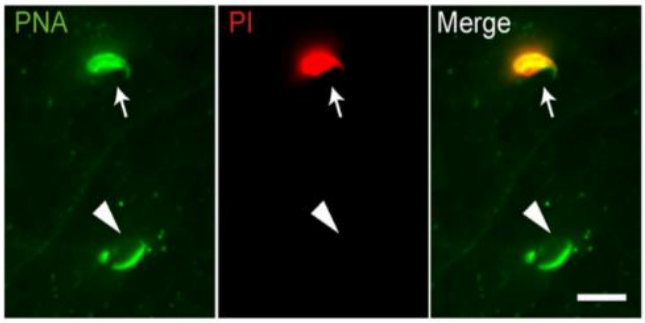
PNA
PI
Merge

D

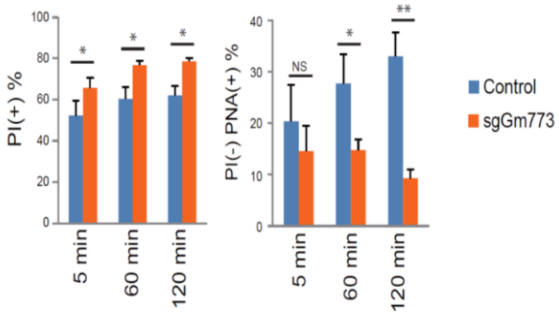
PI(+) %
100
80
60
40
20
0
*
*
*
5 min
60 min
120 min
PI(-) PNA(+) %
40
30
20
10
0
NS
*
**
5 min
60 min
120 min
Control
sgGm773

Fig. 14. Defects of sgGm773 spermatozoa related to their poor fertility

(A) Representative images of oocytes and spermatozoa at 1 hour after insemination by IVF. Zona-free oocytes were prepared by brief treatment with acid Tyrode. DNA was stained with Hoechst 33258. Blue arrows: sperm heads penetrated the perivitelline space. Red arrows: spermatozoa stacked on the surface of zona pellucida. BF: bright field. PaPN: paternal pronucleus. MaPN: maternal pronucleus. MII: MII stage spindle. Pb: polar body. Scale bar, 10 μm.

(B) Bar graphs showing the fertilization rate of control and sgGm773 spermatozoa inseminated with zona-intact or zona-free oocytes. While the fertilization rate remained only less than 10% when sgGm773 spermatozoa were inseminated with zona intact oocytes, that increased to 100% when zona pellucida was removed.

(C) Representative images of sperm head stained with propidium iodide (PI) or peanut agglutinin (PNA). Arrows indicate PI (+) spermatozoon. Arrowheads indicate PI (−)/PNA (+) spermatozoon. Scale bar, 10 μm.

(D) Bar graphs showing the percentage of PI (+) and PI (-)/PNA (+) spermatozoa at the indicated time points of preincubation.

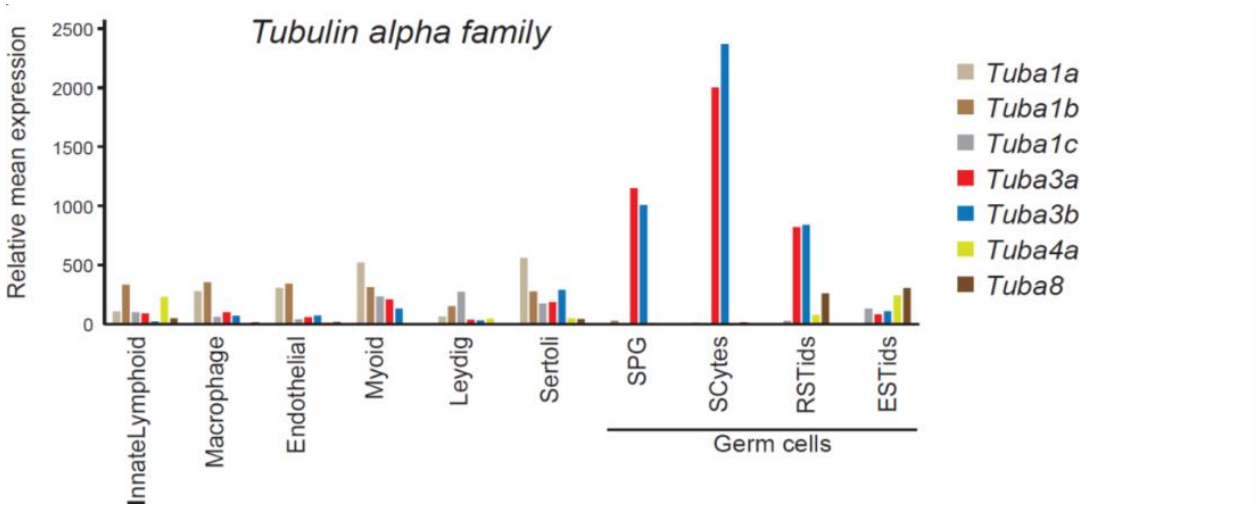

Fig. 15. Gene expression of Tubulin alpha family genes in the male germ line

Bar graphs showing the expression levels of Tubulin alpha family genes in multiple cell types of adult mouse testis. Single-cell RNA-seq data were obtained from Green et al., 2018 (GSE112393). SPG; spermatogonia. SCytes; spermatocytes. RSTids; round spermatids. ESTids; elongated spermatids. Among seven *Tuba* genes, *Tuba3a* and *Tuba3b* were exclusively expressed in germ cells, especially in spermatogonia and spermatocytes.

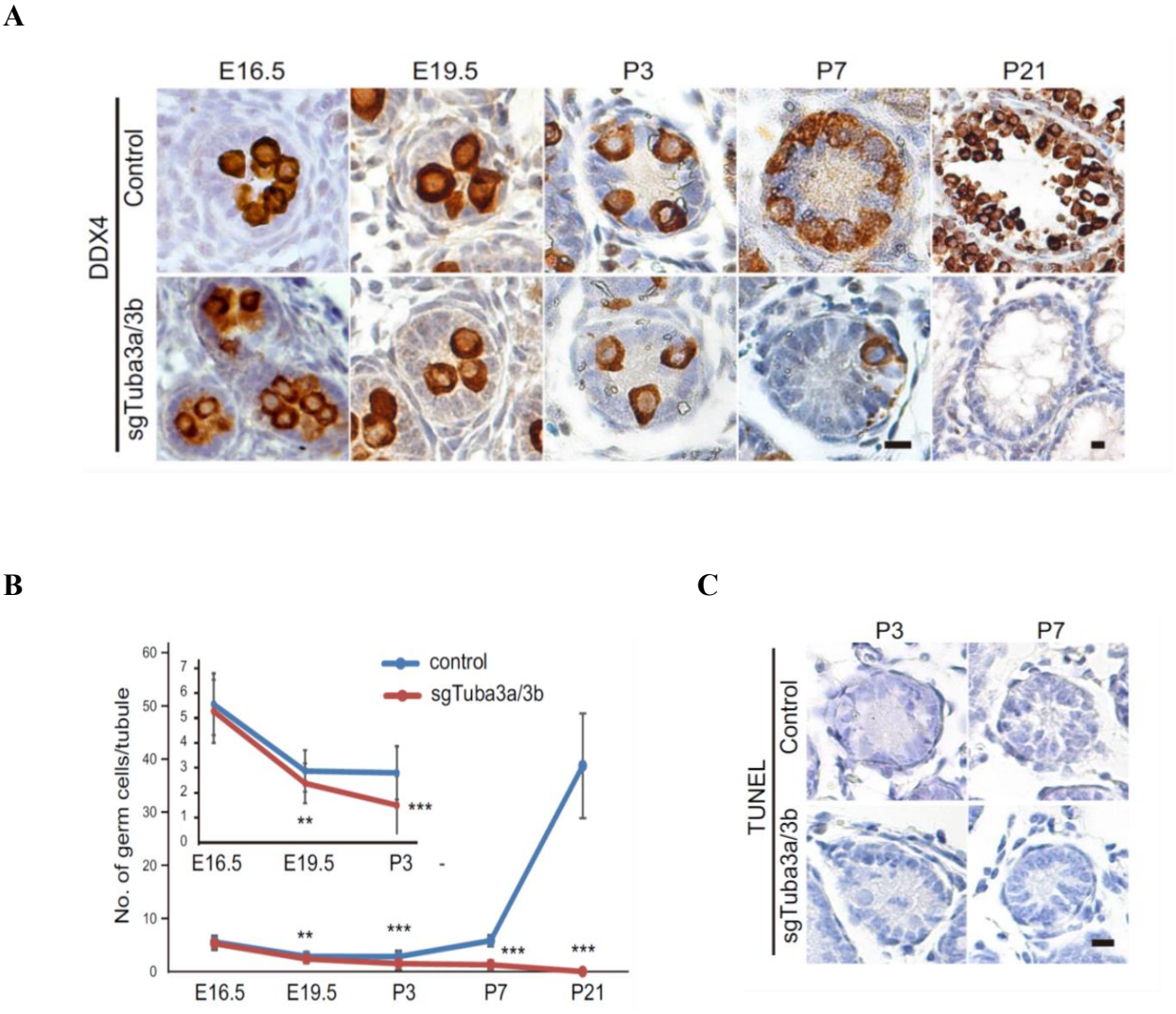

Fig. 16. Complete depletion of gonocytes at the early postnatal stages in sgTuba3a/3b mice

(A) Representative images of embryonic and postnatal testis sections of E16.5, E19.5, P3, P7, and P21 immunostained against DDX4 (germ cell marker). Note that the germ cells were absent in the sgTuba3a/3b testis at P21. (B) Bar graphs showing the average number of DDX4-positive germ cells that survived in each seminiferous tubule. Note that the DDX-positive germ cells were progressively lost by P21. (C) Representative images of TUNEL-stained postnatal testis sections. Scale bar, 10 μm. TUNEL: Terminal deoxynucleotidyl transferase dUTP nick end labeling.

A **B**

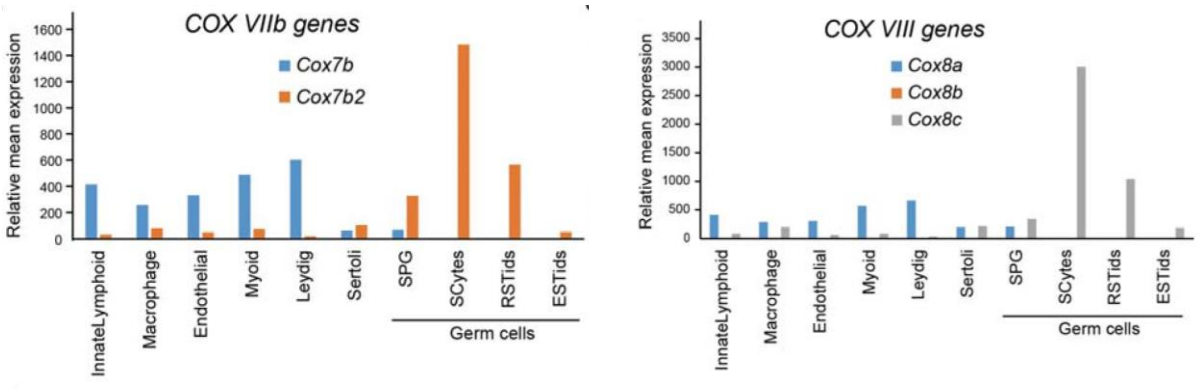

C

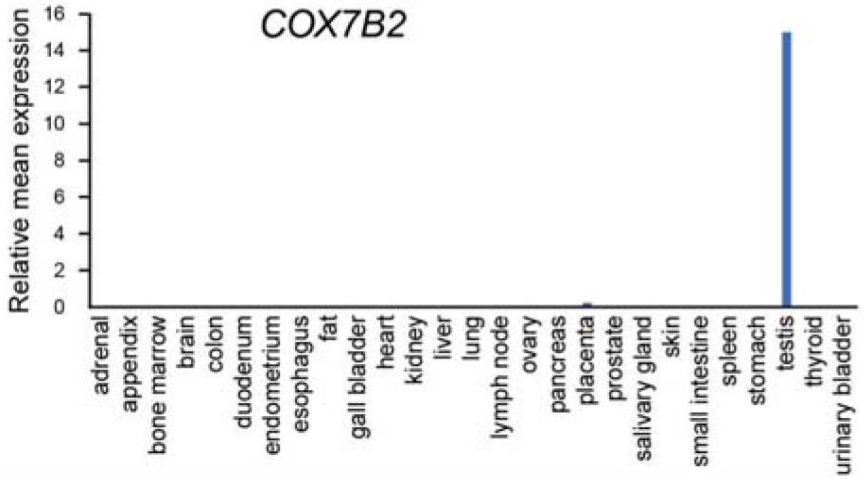

Fig. 17. Gene expression of *COX* genes

(A) and (B) Bar graphs showing the expression levels of COX VIIb (A) and COX VIII (B) family genes in multiple cell types of adult mouse testis.

(C) Bar graphs showing the expression levels of *COX7B2* in human tissues. (RNA-seq data were obtained from Fagerberg et al., 2014 (PRJEB4337).

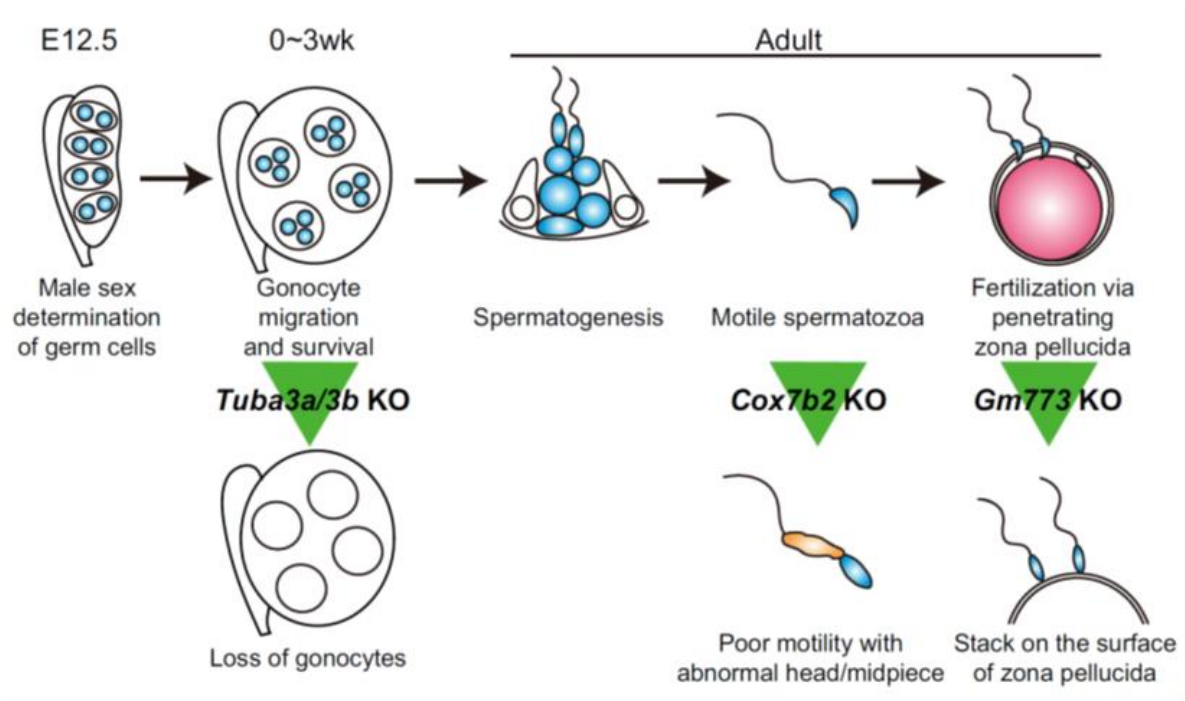

Fig. 18. SRRG KO caused variable defects during male germ cell development

Schematic illustration of male germ cell development and the phenotypes observed in the SRRG KO mice in this study. *Tuba3a/3b* KO caused complete depletion of gonocytes at the early postnatal stages. *Cox7b2* KO caused poor motility of spermatozoa, likely because of the abnormal morphology in the midpiece of spermatozoa. *Gm773* KO caused a significant reduction of sperm fertility, likely because of the poor penetration capacity through zona pellucida.

CHAPTER 2

"Functional screening of male germ line- specific tubulins: *Tuba3a/3b* and *Tubb4b*"

Introduction

The cell cytoskeleton is composed of microfilaments, intermediate filaments, and microtubules (MT). MT modulates the morphology and functions of all eukaryotic cells (Ti, 2022). MTs are polarized, ubiquitous, small hollow tube-like structures and are responsible for various movements in eukaryotic cells (Fig. 19A). It plays essential and diverse functions in cellular transport, intracellular organization, organelle trafficking, structural support, cell division, and chromosome segregation (Brouhard and Rice, 2018; Desai and Mitchison, 1997) (Fig. 19B). During mitosis, MTs participate in spindle formation. Tubulin, a globular protein, is the structural building block of microtubules; the dimer of each polypeptide is known as αβ -tubulin, and the molecular weight of each subunit is 55 KDa. The genes of the tubulin superfamily encode tubulin proteins. In eukaryotes, there are six types of tubulins: alfa-tubulin, beta-tubulin, gamma-tubulin, delta-tubulin, epsilon-tubulin, and zeta-tubulin (α-tubulin, β -tubulin, γ-tubulin, δ-tubulin, ε-tubulin, and ζ-tubulin respectively). At least eight α-tubulin and eight β-tubulin isotypes exist in mammals, each encoded by separate, highly conserved genes (Fertuzinhos et al., 2022).

The germ cell lineage begins with the specification of primordial germ cells (PGCs and the PGCs must complete a complex and dynamic developmental process during embryogenesis to establish the germline that involves migration, survival, sex differentiation, and extensive epigenetic reprogramming (Nguyen et al., 2019). PGCs proliferate during migration and reach the developing gonad at (embryonic day) E 11 and become residents then termed to as gonocytes (Culty, 2009; McLaren, 2003). Gonocytes then goes through proliferation and enter mitotic arrest from E 13.5 and prior to birth at E 18.5 start to relocate from periphery to basal membrane of seminiferous cords (Nagano et al., 2000).

Interestingly, I found in Chapter 1 that male germ cells express their specific alpha tubulin genes *Tuba3a* and *Tuba3b*. From the initial genetic screening by generating single KO mice for each gene *Tuba3a* or *Tuba3b*, I found these single KO mice showed no phenotypes and normaly proceeded spermatogenesis. On the other hand, simultaneous double KO of *Tuba3a and Tuba3b* induced critical effects on germ cell status; progressive loss of germ cells in the proliferative stages from P3 to P7, and the germ cells were entirely lost by P21. These results suggest that *Tuba3a* and *Tuba3b* has an overlapping function in germ cell survival. Indeed, *Tuba3a* and *Tuba3b* genes encode the same protein (paralogs), meaning the mouse genome has 4 copies of *Tuba3* genes. Some genes are known to be sensitive to the gene dosage, and disruption of a single allele (heterozygous) induces a significant phenotype called haploinsufficiency (Johnson et al., 2019; Morrill and Amon, 2019). Given that the *Tuba3* gene was duplicated in the mouse genome, the *Tuba3* gene product might have dosage-sensitive functions in the male germ cells. To address these questions, I performed my 2nd research study to decipher the dosage-sensitive roles of germ cell-specific tubulin on the critical point of spermatogenesis. I categorized it into five separate models: *Tuba3a/3b*- 100%, 75%, 50%, 25%, and 0%, and try to dig out the dosage effect of *Tuba3* of these distinct groups on germ cell status at different age points.

The α and β subunits share more than 40% sequence homology (Little and Seehaus, 1988), but they eventually turned out to have similar structures (Hill et al., 2018; Knossow et al., 2020; Nogales et al., 1998). The α-tubulin and β-tubulin form a heterodimer that polymerizes into MT. This heterodimer formed a beaded structure known as protofilaments, and thirteen protofilaments laterally began a lumen of MTs (Fig. 19A). As the heterodimer of αβ-tubulin polymerizes into MT, I also asked which β-tubulin is the partner of *Tuba3a/3b* gene in the male germ cells. Among 8 members of the β-tubulin family genes, I focused on one of the members known as Tubulin Beta 4B class IVb shortly as *Tubb4b* gene, since the expression

pattern of *Tubb4b* was similar to that of *Tuba3a/3b.* I generated sgTubb4b founder mice using the Triple CRISPR method to uncover the phenotype and its critical role in spermatogenesis. This study provides evidence that disruption of germ cell-specific tubulin genes causes specific phenotypes in spermatogenesis based on testicular germ cell status and could be a hallmark for the diagnosis or treatment of mammalian reproductive diseases.

Materials and methods

Mice

C57BL/6 N (B6N) and ICR mice were purchased from SLC, Inc. (Shizuoka, Japan). Feed and water were provided *ad libitum* and checked every day. Mice were housed under controlled lighting conditions (daily light from 07:00 to 21:00). All experimental protocols were approved by the Institutional Animal Care and Use Committee of RIKEN Tsukuba Institute and conducted by the Principles of Laboratory Animal Care. Animal care and use were conducted in compliance with the ARRIVE guidelines.

In vitro fertilization (IVF), embryo transfer (ET), and cesarian section (C-section)

I used wild-type B6N or *Tuba3a/3b* mutant (as described below) adults over 10 weeks of age for IVF. Briefly, I collected spermatozoa from the epididymis of adult males and incubated them in the HTF drops for 1 h before insemination for their activation. Then I collected cumulus-oocyte complexes (COCs) from the oviducts of B6N females that were superovulated by injecting 7.5 IU of pregnant mare serum gonadotropin (#367222, Merck Millipore) plus anti-inhibin serum and 7.5 IU of human chorionic gonadotropin (hCG; #230734, Millipore). At 15–17 h after the hCG injection, I incubated the isolated COCs in HTF drops containing 1.25 mM reduced glutathione (GSH; #G6013-5G, Merck Millipore) for 1h before insemination. Then, after preincubation, I introduced the activated spermatozoa to the COC-containing HTF drops to initiate insemination. At 5–6 h after insemination, the fertilized zygotes were washed in potassium simplex optimized medium (KSOM) drops. After that, two-cell stage embryos were transferred to the oviducts of pseudo-pregnant (E0.5) ICR females.

Generation of *Tuba3a/3b* KO mouse line

I aimed to generate *Tuba3a* and *Tuba3b* deletion lines to confirm the phenotype screened by the Triple CRISPR (Chapter 1) and examine the dosage effect of TUBA3 proteins on germ cell status. Although I have successfully established multiple deletion lines for *Tuba3a* and *Tuba3b* separately, obtaining double deleted mutants from the mating of these individual KO mice was expected to be very inefficient since *Tuba3a* and *Tuba3b* are located on the same chromosome 6 within 20 Mbp distance on the mouse genome. Therefore, I chose an approach to generate a double KO line by newly generating a deletion of one gene by CRISPR in another gene mutant background (Fig. 20A). First, I selected a *Tuba3a* deleted male line (Line#3, Fig. 20B) and then performed IVF with control B6N female oocytes, followed by zygote injection of sgTuba3b targeting introns surrounding exon 2 through exon 4 (Fig. 20C). The target sequence and sgRNA sequences were listed in Table 8. Afterward, the injected embryos were transferred to pseudo-pregnant females of ICR and delivered at E19.5 by C-section (Fig. 20A). Among 15 founder pups, 2 possessed deleted alleles for both *Tuba3a* and *Tuba3b* (Fig. 20D, the genotyping primers were listed in Table 9). I successfully established a double deletion line from founder #12 (Table 10). The established *Tuba3a* and *Tuba3b* double KO mice were intercrossed to generate a variety of wild-type (wt) *Tuba3* allele numbers. I categorized the double mutant mice into five distinct groups according to *Tuba3* allele numbers or gene dosages as follows: *Tuba3a*+/+ (wt), *Tuba3b*+/+ (wt) [100% *Tuba3*]; *Tuba3a*+/+ (wt), *Tuba3b*+/- (heterozygous [het]) and *Tuba3a*+/- (het), *Tuba3b*+/+ (wt) [75% *Tuba3*]; *Tuba3a*+/- (het), *Tuba3b*+/- (het) and *Tuba3a*+/+ (wt), *Tuba3b*-/- (null) and *Tuba3a*-/- (null), *Tuba3b*+/+ (wt) [50% *Tuba3*]; *Tuba3a*+/- (het), *Tuba3b*-/- (null) and *Tuba3a*-/- (null), *Tuba3b*+/- (het) [25% *Tuba3*]; *Tuba3a*-/- (null), *Tuba3b*-/- (null) [0% *Tuba3*] (Table 11). Each group of mice at 3 weeks and 12-15 weeks were subjected to the experimental pipelines to measure the body and testis weight, followed by histological analysis.

Sperm status analysis

Sperm clots were collected from the cauda epididymis of five groups of *Tuba3a/3b* KO mice (12–15 weeks) and preincubated in 200 μL drop of human tubal fluid medium (HTF) for 1 h in a humidified atmosphere at 37 °C in 5% $C0_2$. After 1 h of preincubation, I checked the sperm suspension under dissecting microscopy to confirm the presence or absence and motility of sperm in the adult mouse of each group (Table 12).

Single-cell RNA-seq analysis

Read count matrix and clustering list of single-cell RNA-seq data of mouse adult testis were obtained from Green et al., 2018 (GSE112393). Read counts were transferred to counts per million (CPM), and the mean CPM of each cluster was computed using R (version 3.6.1) (R Core Team, 2015).

***Tubb4b* KO mouse generation by the CRISPR/Cas9 system**

I utilized the Triple CRISPR method to generate *Tubb4b* KO mice (Fig. 21A) as described in Chapter 1 (Matoba et al., 2019; Susaki et al., 2017). Briefly, three sgRNAs targeting distinct exons (one for exon 1 and two for exon 4) (Fig. 21B) were designed by using the CRISPOR (http://crispor.tefor.net/), and designed sgRNAs were synthesized by GeneArt Precision gRNA synthesis kit (#A29377, Thermo Fisher Scientific). Primers used for the synthesis of sgRNAs were listed in Table 8. Synthesized sgRNAs and Cas9 mRNA were adjusted to 500 ng/μL, and aliquots were frozen at –80 °C until use. The mixture of three distinct sgRNAs (50 ng/μL each) targeting coding exons and Cas9 mRNA (100 ng/μL) were injected into the cytoplasm of B6N zygotes using a piezo-driven micromanipulator at 5–6 h post-insemination. Following ET and C-section, the pups were examined by multiple

screening parameters, including body weight, survival rate, testis weight, and germ cell status (Fig. 21C).

Genotyping PCR

Genomic DNA was purified from the tail tip using the Wizard Genomic DNA Purification Kit (#A1120, Promega). Genotyping PCR was performed using Tks Gflex DNA Polymerase (#R060A, Takara Bio Inc.). The primers used for genotyping were listed in Table 9.

Immunohistochemistry

All specimens (E19.5, P7, 3 weeks, and 12-15 weeks testes) were fixed overnight in 4% paraformaldehyde in phosphate-buffered saline (PBS) solution and then embedded in paraffin wax after dehydration (Fig. 22). Then sections were made from the embedded samples at four μm. After deparaffinization and rehydration, I performed antigen retrieval using sodium citrate buffer (pH 6.0) pretreated in a microwave for 10 min to maintain a sub-boiling temperature. The sections were incubated in 3% hydrogen peroxide to block endogenous peroxidase for 20 min and 1% bovine serum albumin in PBS for 1 h at room temperature to block the nonspecific staining. Afterward, the sections were incubated overnight with the primary antibody at 4°C (Table 13). Also, negative controls were prepared in the absence of a primary antibody. After that, the sections were washed three times in PBS with 0.05% Tween-20 and incubated with the biotin-labeled secondary antibodies for 1 h at room temperature. The signals were amplified by Vectastain Elite ABC Kit (#PK-6100, Vector Laboratories) and visualized with 3,3′-diaminobenzidine (DAB). The stained sections were counterstained for nuclear signals by hematoxylin. Later, the sections were dehydrated with a series of alcohol and mounted with cover glasses. The mounted sections were examined under a light

microscope (Fig. 22). For the Cleaved caspase-3 staining, the wild-type adult testis was used as a control sample. Consistent with the previous report (Jeyaraj et al., 2003), apoptotic cells were found in the seminiferous tubules at a relatively low frequency, confirming the validity of my staining method. I also confirmed the presence of the Cleaved caspase-3 positive signals in the age-matched control testis sample at 3 weeks of age.

Results

Testicular germ cell-specific expression of tubulins: α-tubulin family members

To understand the expression patterns of the candidate genes of the α-tubulin family-*Tuba3a* and *Tuba3b*, I first performed RT-qPCR in different adult mouse tissues and observed that both genes were predominantly expressed in testis (Chapter 1; Fig. 9A). I also analyzed the expression pattern of *Tuba3a/b* homolog genes, *TUBA3C*, *TUBA3D*, and *TUBA3E*, in human tissues (Fig. 23). The RNA-seq datasets of human tissues were obtained from NCBI database (originally from Fagerberg et al., 2014 [BioProject accession number: PRJEB4337]). I found that these three *TUBA3* genes show testis-specific expression patterns in humans similar to the counterpart genes in mice (Fig. 23).

Next, I analyzed the cell type-specific expression patterns of *Tuba3a* and *Tuba3b* genes in the testis by analyzing the published single-cell RNA-seq datasets of adult mouse testis (Green et al., 2018). The α-tubulin family consists of seven members of *Tuba* genes; among them, *Tuba3a* and *Tuba3b* were exclusively expressed in testicular germ cells, predominantly in spermatogonia and spermatocytes and round spermatids (Fig. 24A). On the contrary, the other five members of this group were absent in testicular germ cells (Fig. 24A). To further understand the dynamic expression patterns of *Tuba* family genes during male gonadal development, I analyzed RNA-seq datasets of testicular germ cells at embryonic (Hill et al., 2018) and postnatal stages (Kuroki et al., 2020). These analyses revealed that the expression dynamics of *Tuba3a* and *Tuba3b* are synchronized, initiated from the middle embryonic stages (from E12.5 to E14.5), and become predominant among the *Tuba* family after birth (Fig. 24B-C).

Dosage-dependent effects of *Tuba3* on testicular development

To confirm the phenotype screened by the Triple CRISPR (Chapter 1) and examine the dosage effect of *Tuba3* genes on testicular development and germ cell status, I generated *Tuba3a* and *Tuba3b* double KO mouse lines (see method for details). By intercrossing males and females that simultaneously possess *Tuba3a* heterozygous (het) and *Tuba3b* het alleles, a variety of mouse groups with different *Tuba3* allele numbers (0 to 4 wild-type alleles) were generated. I categorized the mice based on dosage distinctions of five models as *Tuba3a/3b*: *Tuba3a*+/+ (wild-type [wt]), *Tuba3b*+/+ (wt) [4/4 wt alleles; 100% *Tuba3*]; *Tuba3a*+/+ (wt), *Tuba3b*+/- (heterozygous [het]) and *Tuba3a*+/- (het), *Tuba3b*+/+ (wt) [3/4 wt alleles; 75% *Tuba3*]; *Tuba3a*+/- (het), *Tuba3b*+/- (het) and *Tuba3a*+/+ (wt), *Tuba3b*-/- (null) and *Tuba3a*-/- (null), *Tuba3b*+/+ (wt) [2/4 wt alleles; 50% *Tuba3*]; *Tuba3a*+/- (het), *Tuba3b*-/- (null) and *Tuba3a*-/- (null), *Tuba3b*+/- (het) [1/4 wt alleles; 25% *Tuba3*]; *Tuba3a*-/- (null), *Tuba3b*-/- (null) [0/4 wt alleles; 0% *Tuba3*] (Table 11). All the mice of these groups went to adulthood without any remarkable gross physical changes compared to the control (100% *Tuba3*). Also, I did not observe any change in body weight in adult (12-15 weeks of age) mice (Fig. 25A). Next, I examined the testis weight of each group of adult mice and found that the testis weight was significantly reduced in *Tuba3* 25% and *Tuba3* 0% mice groups (Fig. 25B). Consistently, the gross morphology of adult testis was noted as tiny testis in *Tuba3* 25% and *Tuba3* 0% model compared to the control (Fig. 25C). Next, I also collected the sperm clot from the cauda epididymis of the adult mice and suspended it in a drop of human tubal fluid (HTF) medium to allow sperm to swim up. After 1 h of incubation, I checked the presence/ absence of sperm state in this drop in distinguished five grouped mice (Table 12). I found that the HTF drops of 0% and 25% *Tuba3* groups did not contain any matured sperm (Table 12).

Dosage-dependent effects of *Tuba3* on germ cell development

The above results suggested that 25% of the *Tuba3* expression level cannot support complete spermatogenesis in mice. However, whether the 0% *Tuba3* and 25% *Tuba3* models exhibit the same phenotype in germ cell survival remained unclear. For this, I performed the immunohistochemical analyses on the five groups of *Tuba3* mice models using several germ cell markers. First, I used the antibody against DEAD-box helicase 4 (DDX4; also known as mouse VASA homolog [MVH]) as a pan-germ cell marker (Fayomi and Orwig, 2018) to observe the presence or absence of testicular germ cells in these five distinguished groups. I found that germ cells are present in 75% *Tuba3* and 50% *Tuba3* models, similar to the control (100% model) (Fig. 26A). Consistent with the data of sgTuba3a/3b mice (Chapter 1, Akter et al., 2021), the testis of the 0% *Tuba3* model did not contain any DDX4-positive germ cells. Interestingly, the 25% *Tuba3* model did not lose germ cells but possessed few germ cells near the basement membrane of seminiferous tubules where typically spermatogonia reside (Fig. 26A). I counted the number of DDX4-positive germ cells in each tubule and found that the average number of DDX4-positive germ cells was significantly reduced in the 25% *Tuba3* model compared to control testis: control (102 ± 16.43) and 25% *Tuba3* (4 ± 2.07) in adult testis (Fig. 26B). To determine the stage of germ cells present in the 25% model, I examined the expression of promyelocytic leukemia zinc finger protein (PLZF), a marker for spermatogonia (Koonin, 2005), and synaptonemal complex protein 3 (SCP3), a spermatocyte marker, by immunohistochemistry. I found that all the germ cells in the 25% *Tuba3* model were positive for PLZF but negative for SCP3 (Fig. 26A). I also performed immunohistochemistry with an antibody against Sry-box containing transcription factor 9 (SOX9), a Sertoli cell marker, in adult testis and found that Sertoli cells were present in all groups of the *Tuba3* model (Fig. 26A).

To determine the dynamic phenotype of germ cells in *Tuba3* mutants, I also analyzed the testes of these mice at 3 weeks of age (Fig. 27). Consistent with the data in adults (Fig. 26), all *Tuba3* mutant groups normally grew up to adult (Fig. 27A). While the testes of 75% *Tuba3* and 50% *Tuba3* models appeared normal, those of 25% *Tuba3* and 0% *Tuba3* were small even at 3 weeks of age (Fig. 27B). Immunohistochemical analyses revealed that DDX4-positive germ cells were completely lost in *Tuba3* 0% model at 3 weeks of age (Fig. 28A), but some DDX4-positive cells remain in *Tuba3* 25% testis (Fig 28A). The number of DDX4-positive cells in 25% *Tuba3* (8 ± 2.35) was significantly lower than that in the control (39 ± 9.83) at 3 weeks (Fig. 28B). These residual germ cells were positive for PLZF but negative for SCP3 (Fig. 28A).

Testicular germ cell-specific expression of tubulins: β-tubulin family members

As microtubules assembly α-tubulin and β-tubulin as a heterodimer (Fig. 19A), I next asked which β-tubulin family member is possibly the partner of *Tuba3a* and *Tuba3b* in the male germ cells. In mice, the β-tubulin family consists of eight members: *Tubb1*, *Tubb2a*, *Tubb2b*, *Tubb3*, *Tubb4a*, *Tubb4b*, *Tubb5*, and *Tubb6*. I analyzed the expression pattern of these *Tubb* family genes in the testicular cells using a single-cell RNA-seq dataset of the adult testis (Fig. 29; Green et al., 2018). I found that, among the 8 members, *Tubb4b* is exclusively expressed in testicular germ cells, predominantly in spermatogonia, spermatocytes, and round spermatids, but the other seven members of this *Tubb* group were absent in testicular germ cells (Fig. 29A), a similar expression pattern to *Tuba3a* and *Tuba3b* (Fig. 24A). Nonetheless, it should be noted that *Tubb5* and *Tubb6b* were slightly expressed in the spermatogonia and round spermatids, respectively alongside *Tubb4b* (Fig. 29A). I also analyzed the dynamic expression of *Tubb*

genes in the postnatal stages and found that the differentiating spermatogonia at P3-P7 expressed both *Tubb4b* and *Tubb5* (Fig. 29B).

To determine if the expression of *Tubb4b* is testicular germ cell-specific or not, I also examined the expression of *Tubb4b* in a variety of mouse tissues (Fig. 30A). The result indicated that, although *Tubb4b* is highly expressed in testis, its expression is not limited to the testis, rather broadly expressed in every tissue examined with a relatively lower expression levels (Fig. 30A). I also examined the expression pattern of the human homolog of *Tubb4b* gene, *TUBB4B* (Fig. 30B). The RNA-seq data was obtained from NCBI Gene database (Gene ID: 10383). Interestingly, human *TUBB4B* showed a testis-enriched expression pattern, a very similar expression pattern to mouse counterpart *Tubb4b* (Fig. 30B).

sgTubb4b founder mice showed high mortality and growth retardation

To examine the function of *Tubb4b* in mice, I generated the sgTubb4b KO mice using the Triple CRISPR method (Fig. 21). Initially, I observed the implantation rate and pup rate for sgTubb4b KO founder pups and found no notable changes compared to the B6N control (Fig. 31A-B). However, I noticed that the sgTubb4b pups grow slowly compared to the control (Fig. 31C-D) and gradually died after birth regardless of their sex. Eventually, only less than 10% of the sgTubb4b pups survived over 5 weeks of age (Fig. 31E). Also, I analysed the body weight every 7 days interval at P0, P7, P14, and P21 of survived sgTubb4b pups and found that the body weight of sgTubb4b pups was significantly lower than control from birth and continuously stagnant growth from the first week (Fig. 31D) up-to the three weeks in comparison to age-matched control pups (Fig. 31C).

Arrested differentiation of spermatogonia in the survived sgTubb4b founder mice

To ask if *Tubb4b* plays an essential role in male germ cell development, I analyzed the phenotypes of testis in the survived sgTubb4b male pups. First, I found that the gross testis morphology was smaller than the control (Fig. 32A). Then, I examined the testis weight and noted that the testis weight of the sgTubb4b KO pup was lower than that of the control pup at the 3 weeks of age (Fig. 32B). To examine the germ cell status in the testes of survived sgTubb4 pups, I collected sgTubb4b and control testes at P0 (E19.5), P7, and P21 and performed immunohistochemistry using DDX4 antibody. I found that DDX4-positive germ cells are present in sgTubb4b newborn pups (E19.5), but the number of DDX4-positive germ cells per seminiferous tubule was slightly but significantly reduced at this stage (control 2.87 ± 0.83 vs sgTubb4b 1.85 ± 0.69; Fig 32C). The number of germ cells per tubule did not increase in sgTubb4b testis during the postnatal growth period, while that of the control testis continuously increased till P21 (control 38.73 ± 9.84 vs sgTubb4b 3.54 ± 1.87, Fig. 32D). To determine the differentiating stages of germ cells in the sgTubb4b testis at 3 weeks, I analyzed the expression of PLZF and SCP3 by immunohistochemistry. As a result, I found that the surviving germ cells in sgTubb4 testis were positive for PLZF but negative for SCP3 (Fig. 32E). I also examined the Cleaved caspase-3, a marker for apoptosis, but no signal was observed in sgTubb4b testis while a few signals were observed in the control (Fig. 32F).

Discussion

In Chapter 1, I demonstrated that, amongst 7 members of alpha-tubulin genes (*Tuba*), *Tuba3a* and *Tuba3b* encode the same protein TUBA3, are exclusively expressed in the developing mouse male germ cells after birth, and such expression was essential for the survival of spermatogonia. These data are consistent with the previous result shown in Chapter 1, that germ cells were gradually lost after birth and became completely absent at P21 in the sgTuba3a/3b testis. Although these results identified *Tuba3a* and *Tuba3b* as the sole genes that produce alpha tubulin proteins in the male germ cells, it remained unclear whether the gene dosage of *Tuba* affects the processes of male germ cell development and which of the beta-tubulin family proteins are the partner of TUBA3 in these cells.

In this Chapter 2, I examined the effects of gene dosage of *Tuba3a* and *Tuba3b* in male germ cell development by using newly established *Tuba3a/Tuba3b* double KO mouse lines. I found that the male germ cells were lost at the postnatal stages when all 4 alleles of *Tuba3* genes (2 alleles of *Tuba3a* and 2 alleles of *Tuba3b*) were knocked out, but they can survive as spermatogonia until adulthood if 1 copy of *Tuba3* remains intact. In other words, amongst 4 alleles of *Tuba3* genes, at least 1 allele (25%) of *Tuba3* is required for the survival of spermatogonia, while 2 alleles are essential to complete spermatogenesis. These results indicate that male germ cells have two different thresholds of *Tuba3* expression levels to achieve complete spermatogenesis in mice (Fig. 33). Although I was not able to assess the TUBA3 protein levels in these different dosages of *Tuba3* KO groups due to the lack of antibodies that specifically recognize TUBA3 and technical difficulties, genetic evidence that one copy of either *Tuba3a* or *Tuba3b* was sufficient to support spermatogonia survival suggests that the expression levels of *Tuba3a* and *Tuba3b* from each allele are at a similar level. Given that the

expression dynamics appeared almost identical between these two genes (Fig. 24A), it is speculated that these genes are under the regulation of the same transcriptional machinery. The reason spermatogonia only require 1 allele of *Tuba3* but initiation of meiosis to differentiate spermatocytes requires 2 alleles of *Tuba3* remains unclear. It is well known that some phenotypes of diploid organisms are sensitive to gene dosage. Loss-of-function of a single allele as heterozygous (50% dosage) causes significant effects on the phenotype, termed haploinsufficiency (Morrill and Amon, 2019). However, in the case of *Tuba3* KO mouse models, 50% of the dosage did not cause any obvious phenotype, but 25% caused severe defects in spermatogenesis. Although diploid organisms, including mammals, possess essentially 2 alleles for each gene, some genes have duplicated additional alleles as paralogs. It has been suggested that two copies of paralogue genes produce a higher amount of proteins, which may be advantageous for evolutional selection (Koonin, 2005). The human genome has at least 3 copies of *TUBA3* genes (*TUBA3C*, *TUBA3D*, and *TUBA3E*), and all of them show testis-specific expression patterns (Fig. 23), suggesting that the acquisition of multiple copies of TUBA3 proteins are advantageous even for human species.

In the search for beta-tubulin that forms a heterodimer with TUBA3 proteins in male germ cells, I identified *Tubb4b* as a promising candidate. *Tubb4b* was highly expressed in the mouse testis compared to other tissues (Fig. 30A). Moreover, scRNA-seq analysis of adult testicular cells revealed that *Tubb4b* shows a mostly exclusive expression pattern among 8 members of the *Tubb* family genes in the spermatogenic cells (Fig. 29). These results suggest that *Tubb4b* might play a critical role in the male germ cells. Consistent with such exclusive expression in the male germ cells, I found severe defects in testis size as well as spermatogonial differentiation in the sgTubb4b testis during the growth period. However, unlike sgTuba3a/3b (Chapter 1) or *Tuba3a/3b* double KO mice (0% model; Chapter 2) both of which showed complete loss of germ cells after birth, the sgTubb4b testis contained PLZF positive

spermatogonia at least until 3 weeks of age. Such phenotype appeared similar to the one observed in *Tuba3* 25% model (Fig. 28A, 32E, and 33). I speculate that *Tubb5* slightly expressed in spermatogonia compensated the function of *Tubb4*b in spermatogonia. The phenotype became severe at the spermatocyte, where *Tubb4b* expression became completely exclusive among the *Tubb* family due to the silencing of *Tubb5* at this stage. Since most sgTubb4 male mice died before 3 weeks of age, I could not analyze the later stages of the sgTubb4b testis. Although the cause of death of sgTubb4b mice was unclear, they appeared to show growth defects and representative phenotypes of neural defects. Since *Tubb4b* is widely expressed in various tissues, though its expression levels were much lower than that in the testis (Fig. 30), *Tubb4b* might play essential roles in multiple tissues. Indeed, it has recently been reported that *TUBB4B* gene mutation is responsible for Leber congenital amaurosis (LCA) in humans (Luscan et al., 2017; Maasz et al., 2022). LCA is a neurodegenerative disease of photoreceptor cells associated with the early onset of deafness and pigmentation of the eye that leads to blindness in humans. Recently, Feng and his colleagues reported that *Tubb4b* has a specific role in regulating spermatogonia proliferation and cell cycle using *in vitro* mouse germ stem cell model (Feng et al., 2022), which is consistent with the results shown in this study. To address the role of *Tubb4b* in the later spermatogenic stages *in vivo* would require testis-specific or germ cell-specific KO models of *Tubb4b*.

The molecular functions of TUBA and TUBB in the male germ cells need to be clarified. In general, alpha and beta tubulins form MTs, and these MTs are dynamically regulated to support a wide range of cellular events, including chromosome segregation during mitosis, intracellular transportation of vesicles/organelles (Brouhard and Rice, 2018; Desai and Mitchison, 1997). Germ cells are lost at the gonocytes stage in the sgTuba3a/3b and Tuba3a3b double KO (0% Tuba3 model). At this stage, the gonocytes are known to actively proliferate and relocate near the basement membrane of seminiferous tubules (Nagano et al., 2000). These

steps might be affected in the sgTuba3a/3b and 0% *Tuba3* model, and eventually the gonocytes might have been lost independent of the apoptosis pathway. Although spermatogonia of the 25% *Tuba3* model and sgTubb4b mice could survive and relocate to near the basement membrane, they failed to initiate differentiation to spermatocytes that are in the process of meiosis. Since MTs play critical roles in mitosis and meiosis (Akera, 2021), the initiation step of meiosis might have been inhibited due to insufficient TUBA or TUBB proteins in these cells. Further detailed analysis of spermatogonial cells in these models would reveal the critical functions of MTs in male germ cell development.

Conclusion

Spermatogenesis is the continuous process of spermatozoa production, whereas the mechanism remains poorly elucidated. As an extension of my genetic screening data in Chapter 1, I uncovered the dosage effect of germ cell-specific alpha tubulins, *Tuba3a/3b,* using a newly established *Tuba3a/3b* double KO mouse line. My results indicate that male postnatal germ cells are sensitive to the dosage of the *Tuba3a* and *Tuba3b* genes, and that at least one copy of either *Tuba3a* or *Tuba3b* gene is required for the survival of spermatogonia and 2 copies for the completion of spermatogenesis. I further searched for the partner beta tubulin of TUBA in mouse male germ cells and found that *Tubb4b* is required to differentiate spermatogonia into spermatocytes using the sgTubb4b mouse model (Fig. 33). Since both genes are conserved in humans as *TUBA3C-E* and *TUBB4B* and are highly expressed in testis (Fig. 23, 30B), my experimental evidence may provide significant insights into human reproductive medicine.

Table 8. Sequence information of the primers used for the synthesis of sgRNAs

sgRNA name*	Target intron/exon	Primer/sequence names	Sequence
Tuba3b sgInt1	Intron 1	Target+PAM	AGCTAATTGTCGACATTGTA+TGG
		Tuba3b-sgInt1-F	TAATACGACTCACTATAGAGCTAATTGTCGACATTGTA
		Tuba3b-sgInt1-R	TTCTAGCTCTAAAACTACAATGTCGACAATTAGCT
Tuba3b sgInt4	Intron 4	Target+PAM	TTGGTCGACTCTACTCTTAG+GGG
		Tuba3b-sgInt4-F	TAATACGACTCACTATAGTTGGTCGACTCTACTCTTAG
		Tuba3b-sgInt4-R	TTCTAGCTCTAAAACCTAAGAGTAGAGTCGACCAA
Tubb4b sg1	Exon 1	Target+PAM	CGGCAACCAGATTGGCGCCA+AGG
		Tubb4b-sg1-F	TAATACGACTCACTATAGCGGCAACCAGATTGGCGCCA
		Tubb4b-sgt1-R	TTCTAGCTCTAAAACTGGCGCCAATCTGGTTGCCG
Tubb4b sg4-1	Exon 4	Target+PAM	TATTTACAGCCAGTTTCCGC+AGG
		Tubb4b-sg4-1-F	TAATACGACTCACTATAGTATTTACAGCCAGTTTCCGC
		Tubb4b-sg4-1-R	TTCTAGCTCTAAAACGCGGAAACTGGCTGTAAATA
Tubb4b sg4-2	Exon 4	Target+PAM	ATGGTTCAGGTCACCGTAAG+TGG
		Tubb4b-sg4-2-F	TAATACGACTCACTATAGATGGTTCAGGTCACCGTAAG
		Tubb4b-sg4-2-R	TTCTAGCTCTAAAACCTTACGGTGACCTGAACCAT

*All sgRNAs were produced by GeneArt Precision gRNA synthesis kit.

Table 9. Genotyping PCR primers used in Chapter 2

Target gene	Primer name	Sequence
Tuba3a	Tuba3a-GT-F1	GACAGCTGCTCATGGTATGC
	Tuba3a-GT-R1	AAAGGGTCGTAGGTGATGCA
Tuba3b	Tuba3b-GT-F1	AACTGGGGTGTCTCGGAAAA
	Tuba3b-GT-R1	ACTTGGTGTTGGTCGACTCT
	Tuba3b-GT-F4	TCAAGTCAGCCAGGGAAACA
	Tuba3b-GT-R4	TAAGCTTCGGGGACAGTTCA

Table 10. Establishment of deletion lines

Gene name	Chromosome	Location	Line# (F0#)	Deletion size (bp)	Genotyping primers	PCR product (bp) size	
						WT allele	KO allele
Tuba3a	6	145615963-145621477	3	~1200	Tuba3a-GT-F1xR1	1457	~250
			5	~1200	Tuba3a-GT-F1xR1	1457	~250
Tuba3b	6	125278274-125286042	10	~800	Tuba3b-GT-F1xR1	1761	~900
			11	~300	Tuba3b-GT-F1xR1	1761	~1500
Tuba3b Intron target	6	125278274-125286042	12	~2400	Tuba3b-GT-F4xR4	3003	~590

WT: wild type, KO: knock out

Table 11. Five separate groups of *Tuba3a/3b* KO mice according to *Tuba3* allele number

Gene name	Distinction of five separate groups from *Tuba3a*+/-, *Tuba3b*+/- x *Tuba3a*+/-, *Tuba3b*+/- mating								
	100%	75%		50%			25%		0%
Tuba3a	WT +/+	Het +/-	WT +/+	Het +/-	WT +/+	Null -/-	Het +/-	Null -/-	Null -/-
Tuba3b	WT +/+	WT +/+	Het +/-	Het +/-	Null -/-	WT +/+	Null -/-	Het +/-	Null -/-

Table 12. Sperm status in HTF drop collected from cauda epididymis

Gene dosage of *Tuba3*	Presence (+) or absence (-) of sperm in HTF drop after 1 h inoculation
100%	(+)
75%	(+)
50%	(+)
25%	(-)
0%	(-)

HTF: Human tubal fluid medium

Table 13. List of primary antibodies used in this study

Primary Antibody	Host species	Dilution	Source	Product ID
MVH/DDX4	Rabbit	1:500	Abcam	ab13840
PLZF	Mouse	1:100	Santa Cruz Biotechnology	SC-28319
SOX9	Rabbit	1:1000	Millipore	AB5535
Cleaved Caspase-3	Rabbit	1:200	Cell Signaling Technology	9664
SCP3	Mouse	1:500	Abcam	ab97672

MVH: Mouse Vasa Homolog, DDX4: DEAD-Box Helicase 4, PLZF: Promyelocytic leukemia zinc finger protein, SOX9: SRY-box transcription factor 9, SCP3: Synaptonemal complex protein 3

A

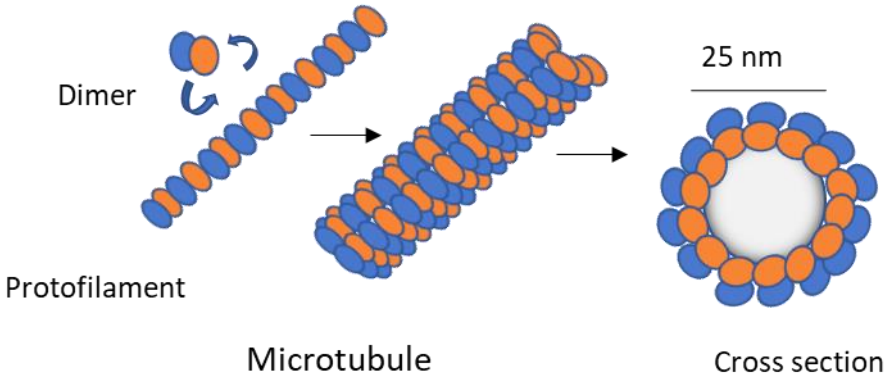

B

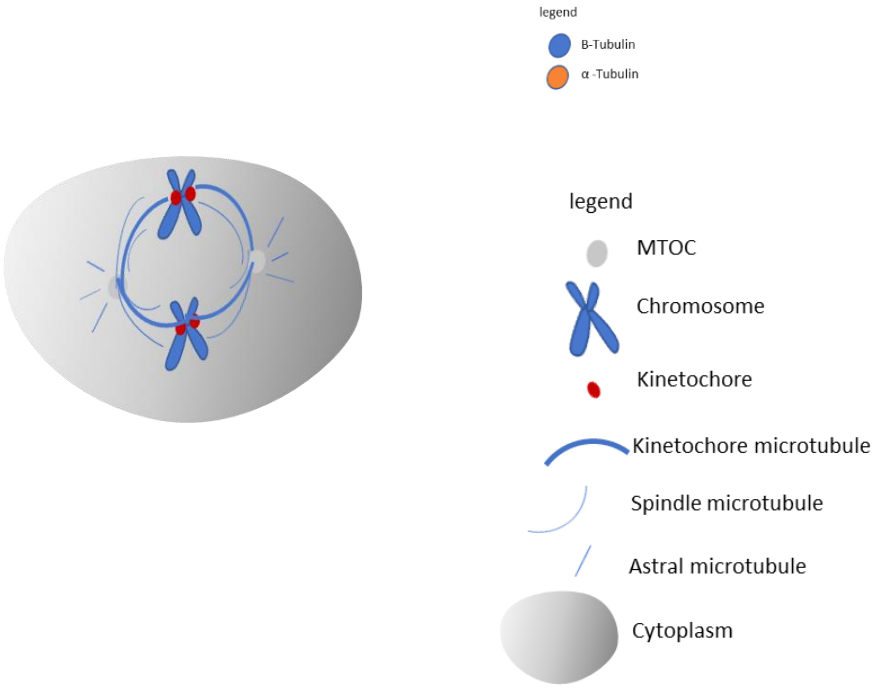

Fig. 19. Structure and organization of microtubules

(A) A single α-tubulin and a β–tubulin form a dimer, and each dimer polymerizes to form a protofilament and 13 protofilaments assemble a hollow tube-like structure known as a microtubule, which has a diameter of 25 nm. (B) Microtubules form dynamic networks in the cytoplasm which are stably anchored at Microtubules Organizing Centers (MTOCs) to support cell division and chromosome segregation. There are different types of microtubules: kinetochore, spindle, and, astral microtubules.

A

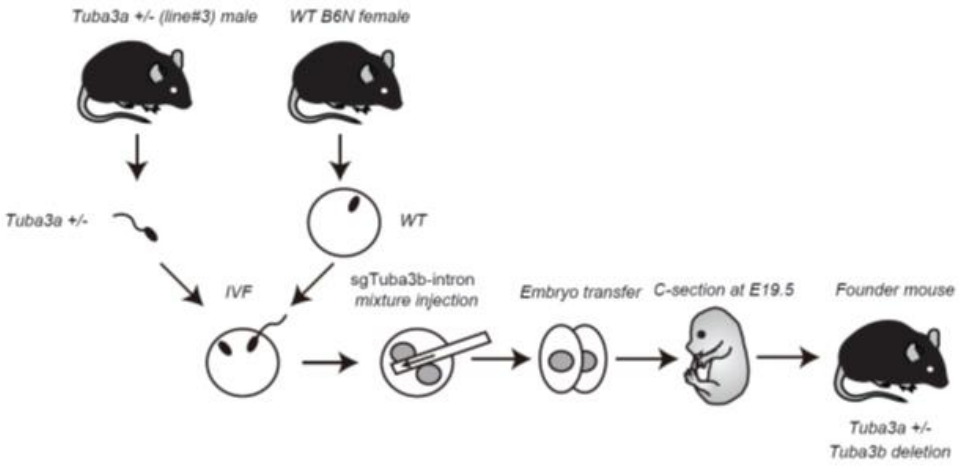
Tuba3a +/- (line#3) male
WT B6N female
Tuba3a +/-
WT
IVF
sgTuba3b-intron
mixture injection
Embryo transfer
C-section at E19.5
Founder mouse
Tuba3a +/-
Tuba3b deletion

B

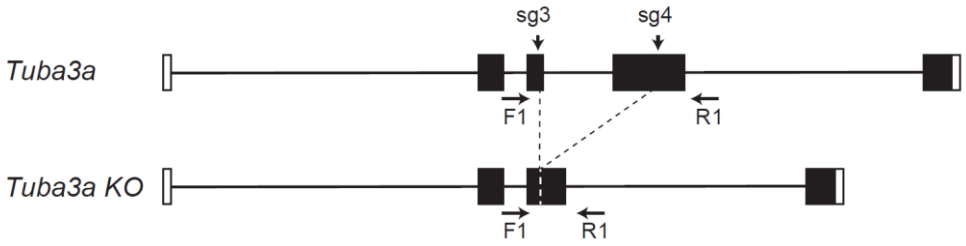
sg3
sg4
Tuba3a
F1
R1
Tuba3a KO
F1
R1

C

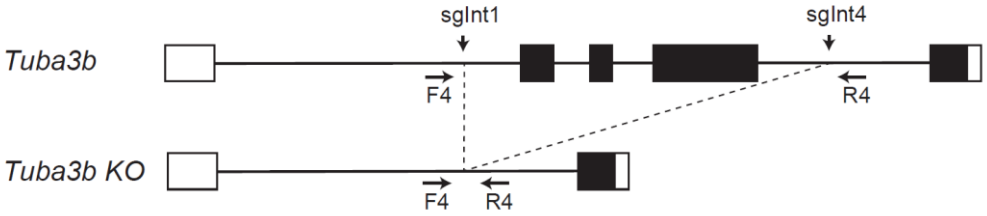
sgInt1
sgInt4
Tuba3b
F4
R4
Tuba3b KO
F4
R4

D

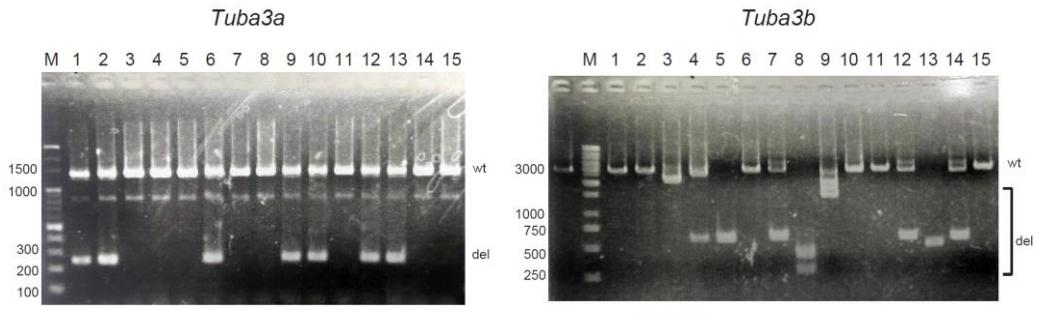
Tuba3a
M 1 2 3 4 5 6 7 8 9 10 11 12 13 14 15
1500
1000
300
200
100
wt
del
Tuba3b
M 1 2 3 4 5 6 7 8 9 10 11 12 13 14 15
3000
1000
750
500
250
wt
del

Fig. 20. Generation of *Tuba3a/3b* KO mouse line

(A) A *Tuba3a* deleted male line (Line#3) was selected to perform IVF with wild-type B6N female mice. CRISPR/RNA mixture containing sgRNAs targeting *Tuba3b* introns was injected into zygotes. Embryos that reached the 2-cell stage were transferred to pseudo-pregnant females of ICR and delivered at E19.5 by C-section. (B) The deletion pattern of *Tuba3a* in Line#3. (C) Two guide RNAs are designed to target introns of *Tuba3b* as intron 1 and intron 4. (D) Selection of pups with double deletion alleles among 15 founder pups, 2 (#12 and 13) possessed deleted alleles for both *Tuba3a* and *Tuba3b*.

wt: wild-type, del: deletion.

A

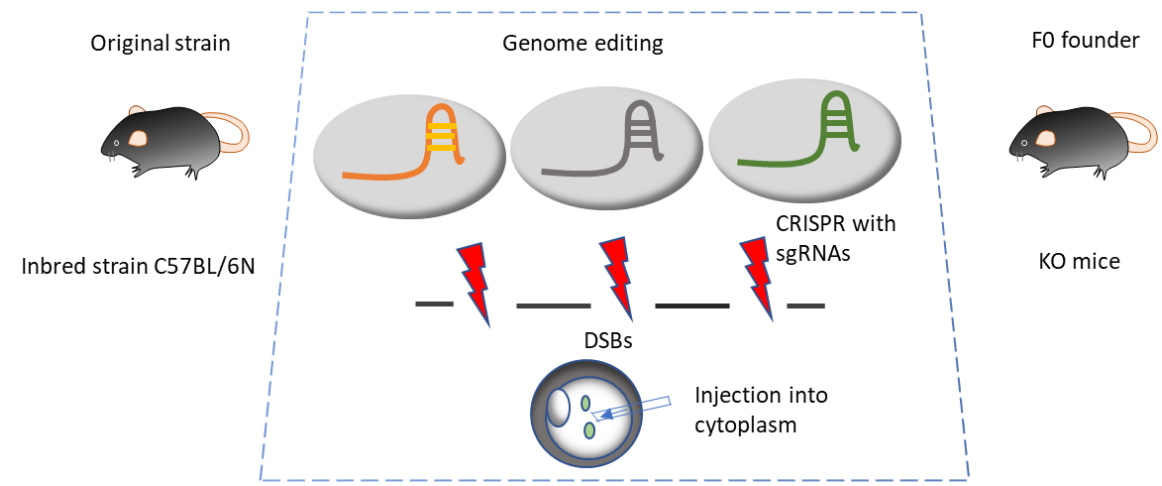
Original strain
Genome editing
F0 founder
Inbred strain C57BL/6N
CRISPR with sgRNAs
KO mice
DSBs
Injection into cytoplasm

B

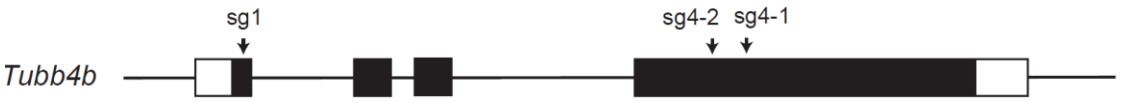
sg1
sg4-2
sg4-1
Tubb4b

C

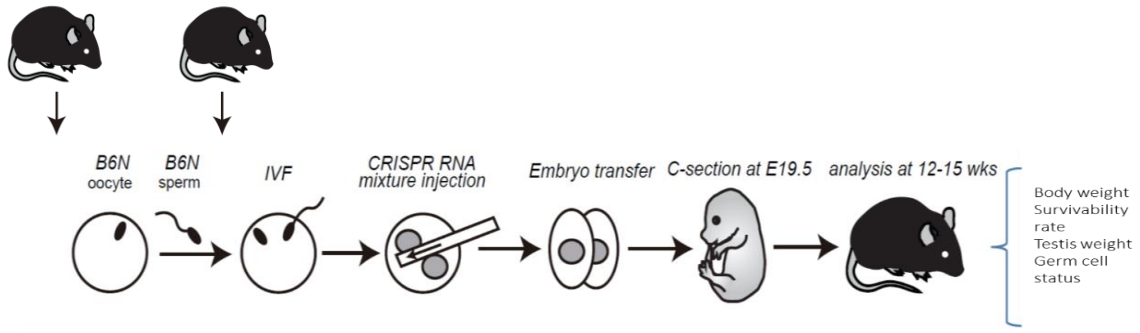
B6N oocyte
B6N sperm
IVF
CRISPR RNA mixture injection
Embryo transfer
C-section at E19.5
analysis at 12-15 wks
Body weight
Survivability rate
Testis weight
Germ cell status

Fig. 21. Generation of *Tubb4b* KO mice

(A) The mixture of three distinct sgRNAs (50 ng/μL each) targeting coding exons and *Cas9* mRNA (100 ng/μL) were injected into B6N inbred zygotes to produce KO founder mice. The individual Cas9/sgRNA complexes generate DSBs in the target regions. (B) Three guide RNAs were designed for *Tubb4b* targeting distinct protein-coding regions of exon 1 and exon 4. (C) B6N oocytes and sperm were *in vitro* fertilized to generate B6N inbred zygotes. The injected embryos that reached the 2-cell stage were transferred to the oviduct of pseudo-pregnant females and finally rescued the pups at E 19.5 by C-section. The phenotypes of founder mice were screened for body weight, survival rate, testis weight, and germ cell status.

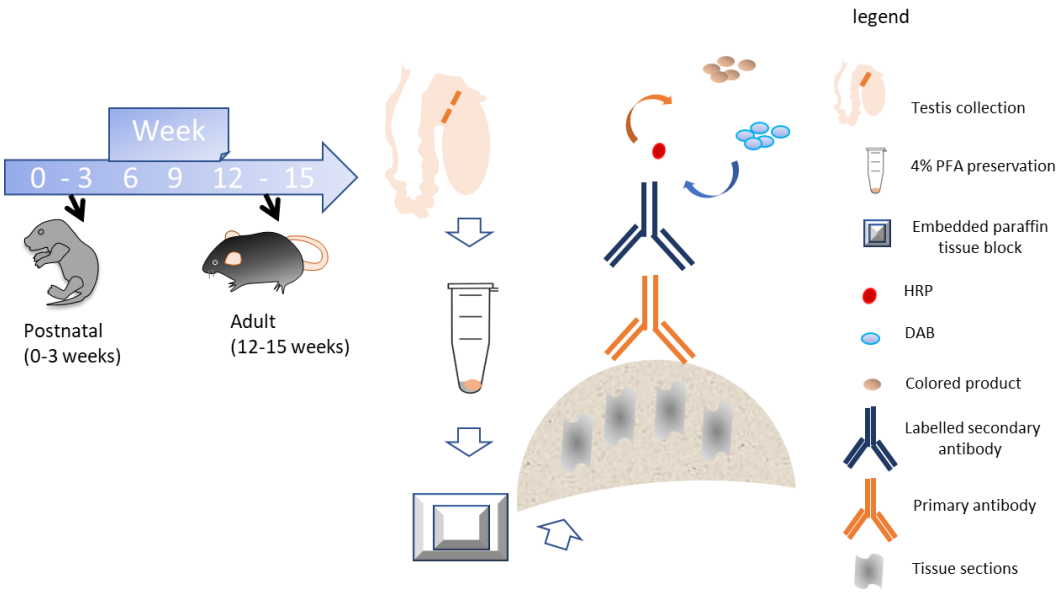

Fig. 22. Lay-out of immunohistochemistry procedure

Testes were collected from postnatal (0-3 weeks) and adult (12-15 weeks) mice and fixed in paraformaldehyde (4% PFA). The fixed testicular samples passed through a series of alcoholic dehydration and performed paraffin embedding to prepare the embedded tissue block and sectioned at 4 µm. The tissue sections (at least four for each sample) were incubated with the primary antibody and biotin-labeled secondary antibodies. The biotin-signal was amplified with horseradish peroxidase (HRP)-containing avidin-biotin complex. Allocation of HRP could be visualized using 3,3′-diaminobenzidine (DAB) as brown-colored products.

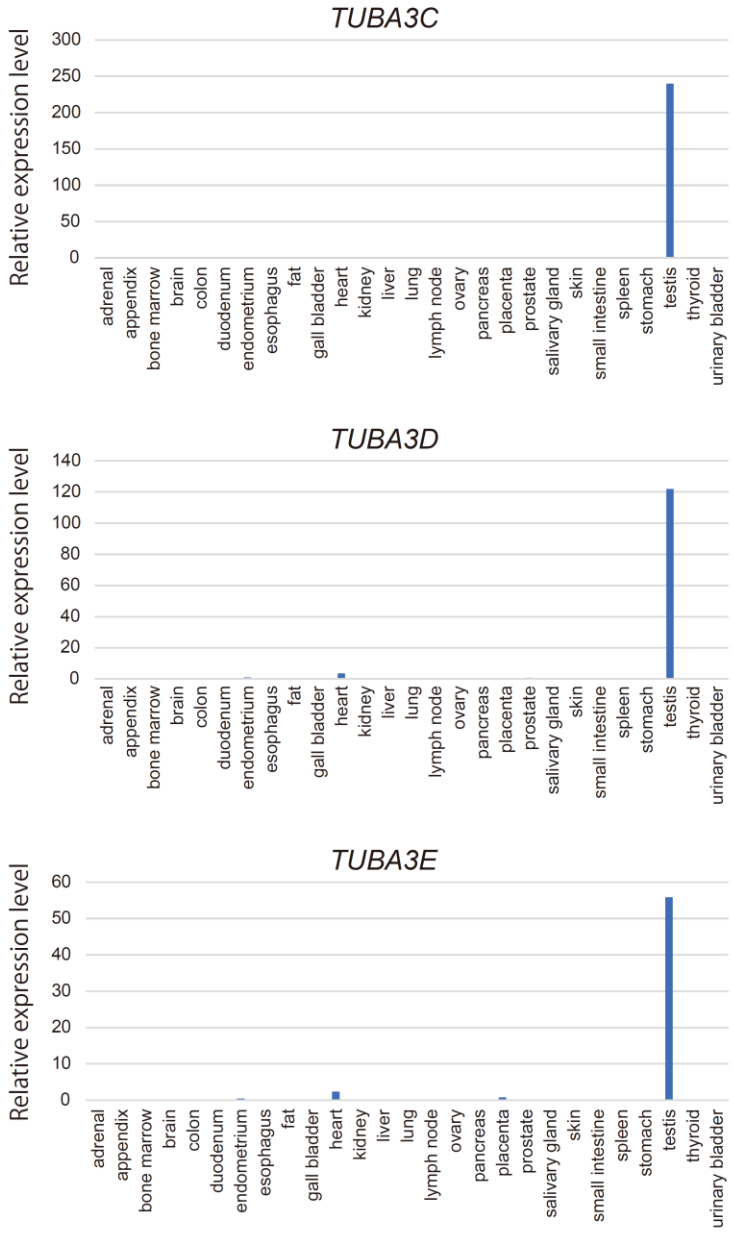

Fig. 23. Gene expression of *TUBA3* genes in human tissues

TUBA3C-E (human homologs of *Tuba3a/3b*) show exclusive testis-specific expression patterns in humans. The expression data were obtained from the National Center for Biotechnology Information (NCBI) database (originally from Fagerberg et al., 2014 [BioProject accession number: PRJEB4337]).

A

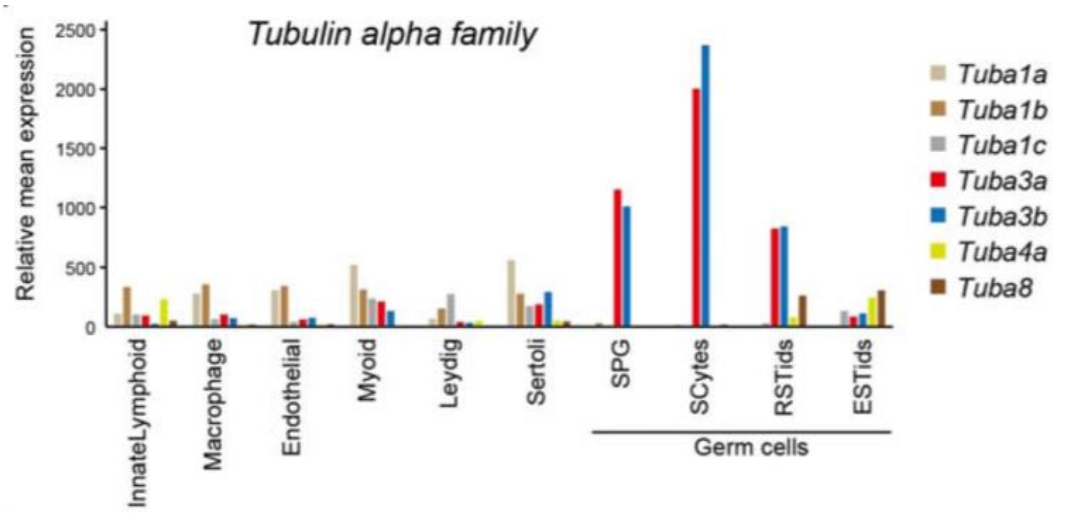
Tubulin alpha family
Relative mean expression
2500
2000
1500
1000
500
0
InnateLymphoid
Macrophage
Endothelial
Myoid
Leydig
Sertoli
SPG
SCytes
RSTids
ESTids
Germ cells
Tuba1a
Tuba1b
Tuba1c
Tuba3a
Tuba3b
Tuba4a
Tuba8

B

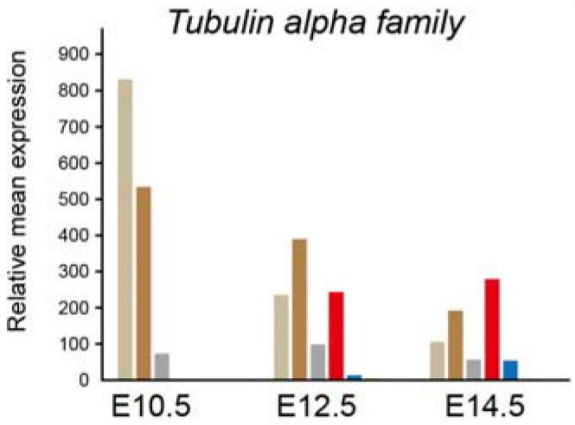
Tubulin alpha family
Relative mean expression
900
800
700
600
500
400
300
200
100
0
E10.5
E12.5
E14.5

C

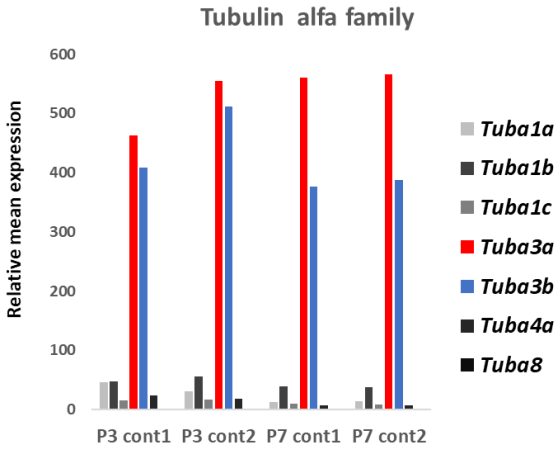
Tubulin alfa family
Relative mean expression
600
500
400
300
200
100
0
P3 cont1
P3 cont2
P7 cont1
P7 cont2
Tuba1a
Tuba1b
Tuba1c
Tuba3a
Tuba3b
Tuba4a
Tuba8

Fig. 24. Expression patterns of tubulin alfa-family genes in mouse male germ line

(A) Bar graphs showing the expression levels of tubulin alpha family genes in multiple cell types of adult mouse testis. Among seven *Tuba* genes of the alfa family, *Tuba3a* and *Tuba3b* were exclusively expressed in germ cells. Single-cell RNA-seq data were obtained from published single-cell RNA-seq datasets (Green et al., 2018) of adult mouse testis. SPG; spermatogonia. SCytes; spermatocytes. RSTids; round spermatids. ESTids; elongated spermatids. (B) Bar diagrams showing the expression levels of tubulin alpha family genes at the embryonic stages (from E12.5 to E14.5). The RNA-seq dataset was obtained from Hill et al., 2018 (GSE76973). E: embryonic. (C) Bar graphs showing the expression levels of Tubulin alpha family genes in male mouse germ cells at P3 and P7. The RNA-seq dataset was obtained from Kuroki et al., 2020 (GSE148053). P: postnatal.

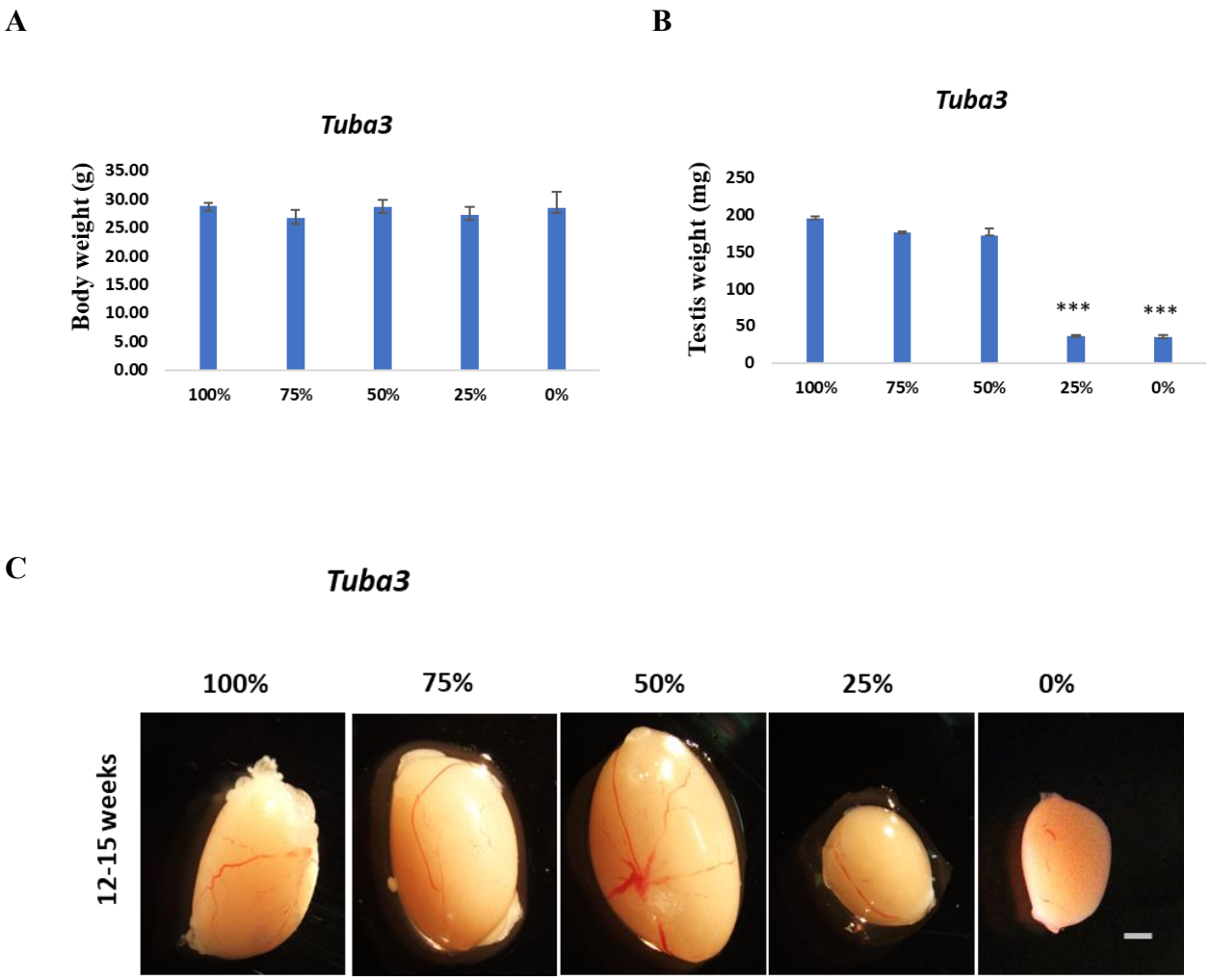

Fig. 25. Dosage effect of *Tuba3* on growth and testicular morphology in adult mice

(A) and (B) Bar graphs showing the body weight (A) and testis weight (B) of adult (12-15 weeks of age) *Tuba3* KO mice with five categorized groups. No significant change was observed in the body weight. The testis weight was significantly reduced in *Tuba3* 25% (*Tuba3a*+/-, *Tuba3b*-/- and *Tuba3a*-/-, *Tuba3b*+/-) and *Tuba3* 0% (*Tuba3a*-/-, *Tuba3b*-/-) groups. *Tuba3* 100% (*Tuba3a*+/+, *Tuba3b*+/+) was used as control. ***$P < 0.001$

(C) Gross morphology of the adult testis. Note that *Tuba3* 25% and *Tuba3* 0% mice had significantly smaller testis in comparison to the control. Scale bar, 1 mm.

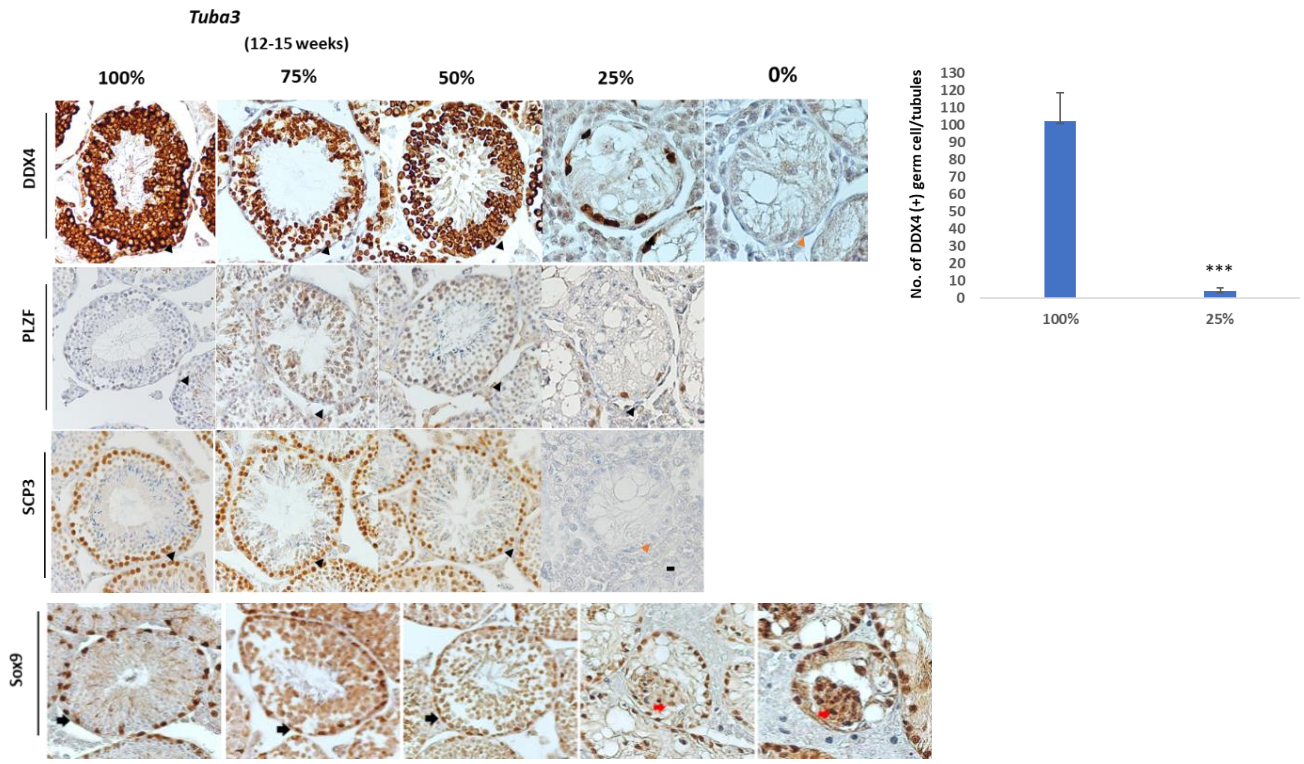

Fig. 26. Immunohistochemical analysis of the testis of different *Tuba3* dosage models in adults

(A) Representative images of adult testis sections immunostained against DDX4, a germ cell-specific marker, PLZF, a spermatogonial marker, SCP3, a meiotic spermatocyte marker, and Sox9, a Sertoli cell marker. Scale bar, 10 μm. (B) Bar graphs showing the number of DDX4 (+) germ cells per tubule. ***$P < 0.001$.

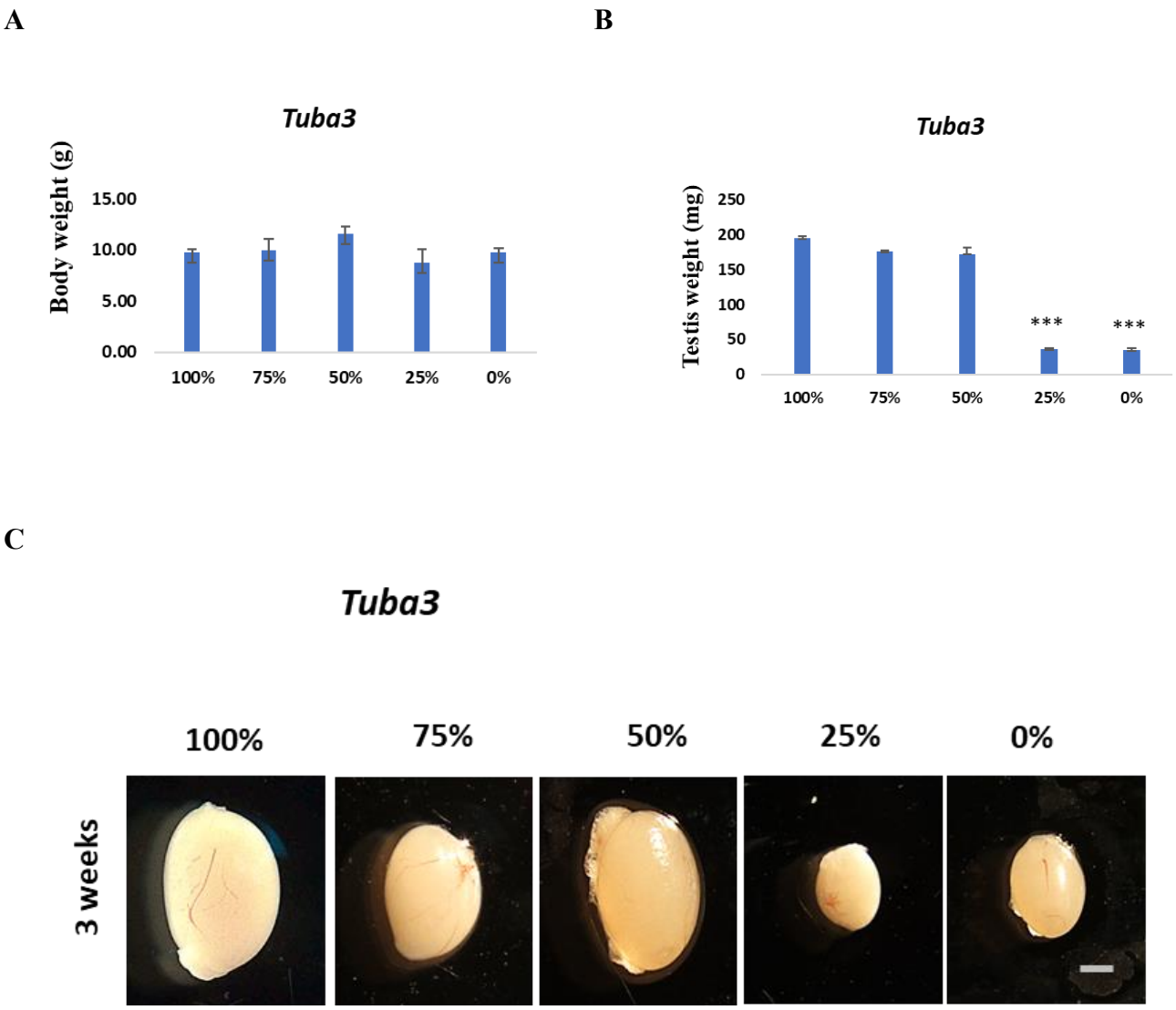

Fig. 27 Dosage effect of *Tuba3* on growth and testicular morphology of mice at the 3 weeks of age

(A) and (B) Bar graphs showing the body weight (A) and testis weight (B) of 3 weeks *Tuba3* KO mice with five categorized groups. *Tuba3* 100% (*Tuba3a*+/+, *Tuba3b*+/+) used as control. ***$P < 0.001$.

(C) Gross morphology of testis at 3 weeks of categorized *Tuba3* KO model mice. Scale bar, 1 mm.

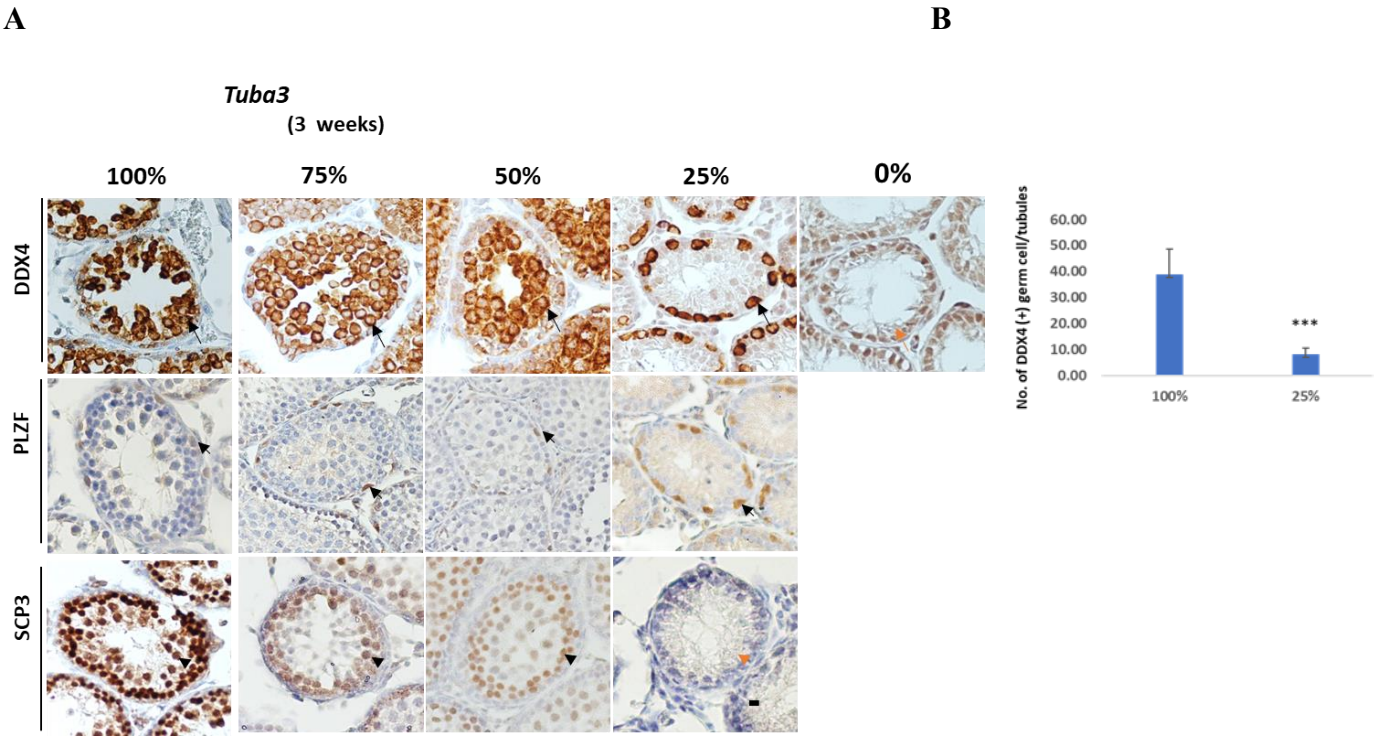

Fig. 28 . Immunohistochemical assay of *Tuba3* KO mouse model at 3 weeks testis

Representative images of adult testis sections immunostained against DDX4, a germ cell-specific marker, PLZF, a spermatogonial marker, SCP3, a meiotic spermatocyte marker, and Sox9, a Sertoli cell marker. Scale bar, 10 μm. (B) Bar graphs showing the number of DDX4(+) germ cells per tubule. ***$P < 0.001$.

A

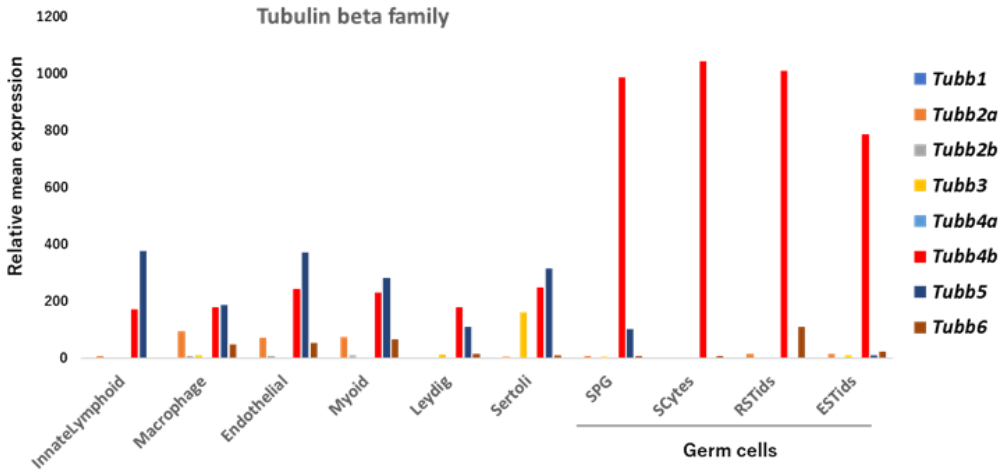

B

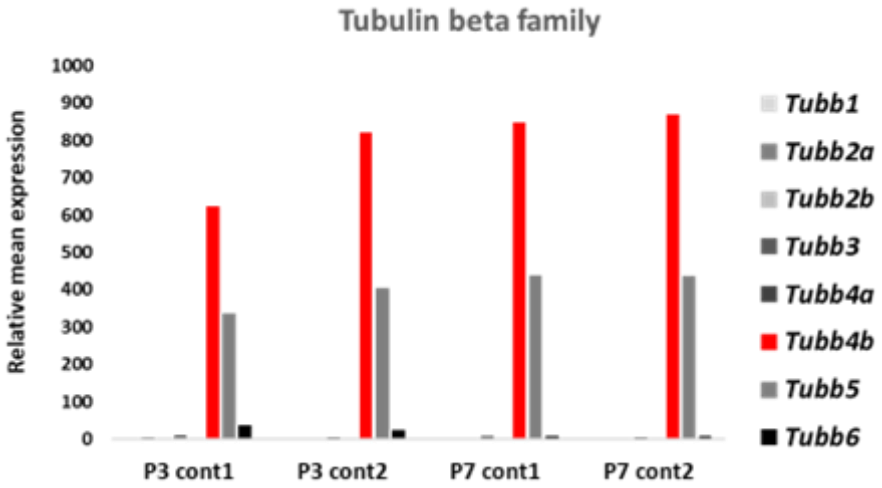

Fig. 29. Expression pattern of tubulin beta-family genes in the male germ line

(A) Bar graphs showing the expression levels of tubulin beta family genes in multiple cell types of adult mouse testis. Among eight *Tubb* family members, *Tubb4b* was exclusively expressed in germ cells. Single-cell RNA-seq data was obtained from Green et al., 2018. SPG; spermatogonia. SCytes; spermatocytes. RSTids; round spermatids. ESTids; elongated spermatids. (B) Bar graphs showing the expression levels of Tubulin beta family genes in male mouse germ cells at P3 and P7. The RNA-seq dataset was obtained from Kuroki et al., 2020 (GSE148053).

A

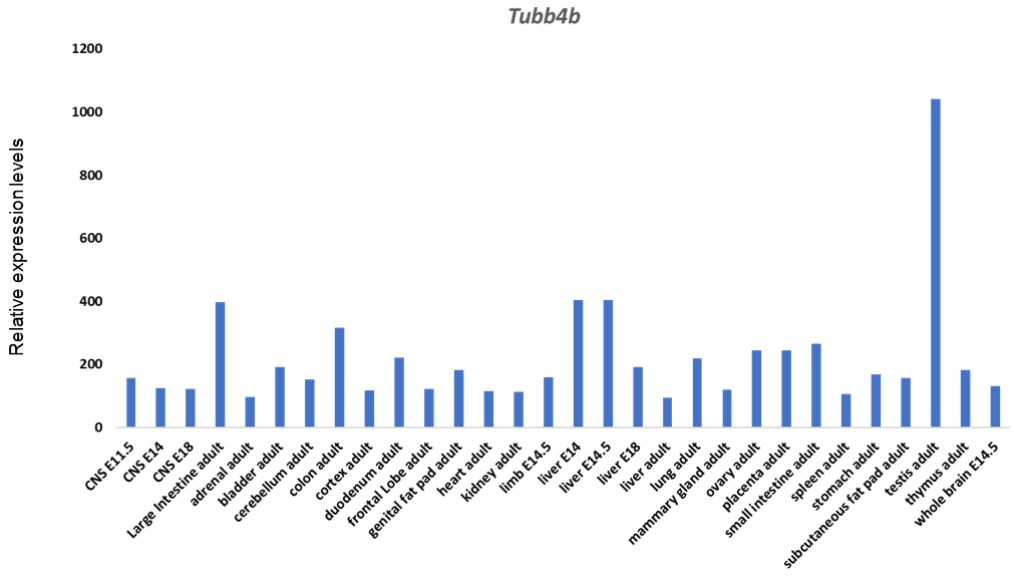

B

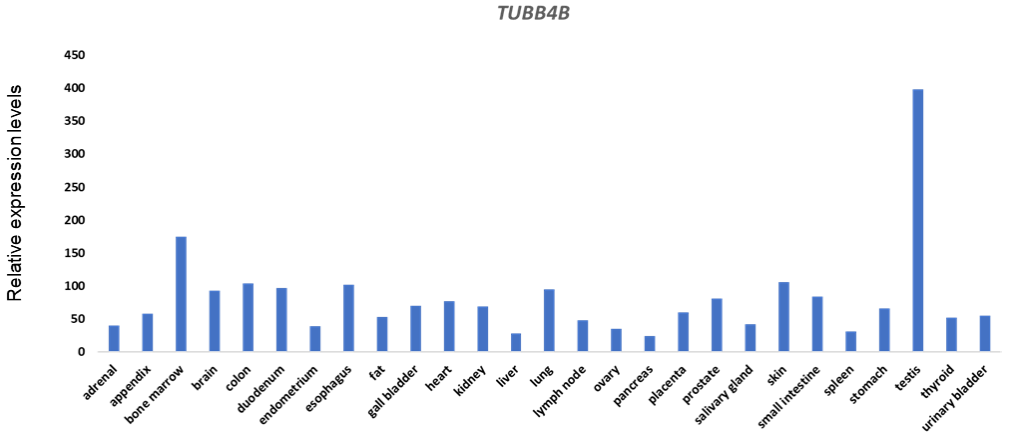

Fig. 30. Expression of mouse *Tubb4b* and human *TUBB4B* in various tissues

(A) Gene expression patterns of *Tubb4b* in various mouse tissues. Mouse *Tubb4b* is relatively highly expressed in the testis. Expression data were obtained from National Center for Biotechnology Information (NCBI, Gene ID: 227613). (B) Gene expression patterns of *TUBB4B* in various human tissues. Human *TUBB4B* was highly expressed in the testis. Expression data were obtained from NCBI (Gene ID: 10383).

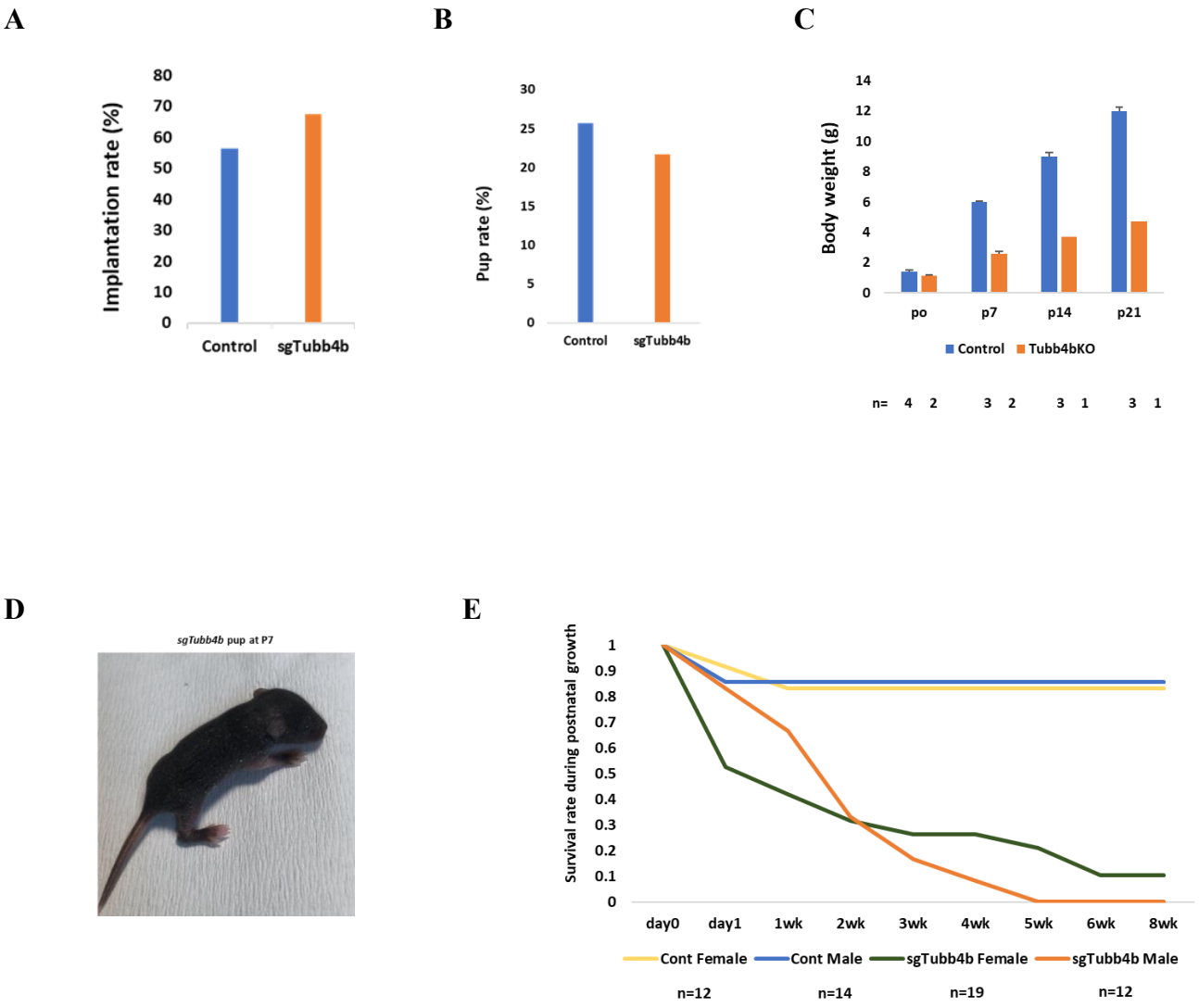

Fig. 31. Growth phenotypes of sgTubb4b mice

The phenotypes of the sgTubb4b founder mice were screened for the indicated parameters. (A) implantation rate. (B) Pup rate. (C) Body weight during the postnatal growth period. (D) The appearance of a survived sgTubb4b pup at P7 with stagnant growth. (E) Survival rate during the postnatal growth period. Note that all sgTubb4b KO male mice died within 5 weeks.

A

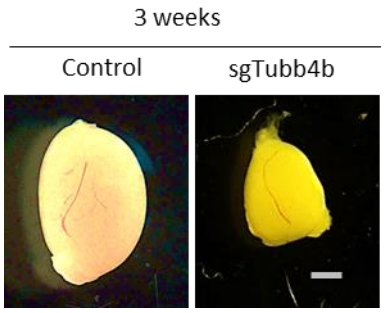
3 weeks
Control
sgTubb4b

B

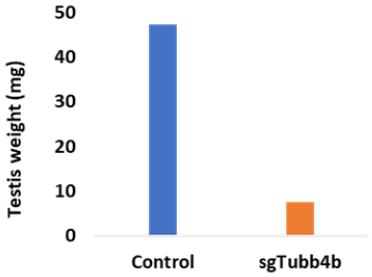
Testis weight (mg)
50
40
30
20
10
0
Control
sgTubb4b

C

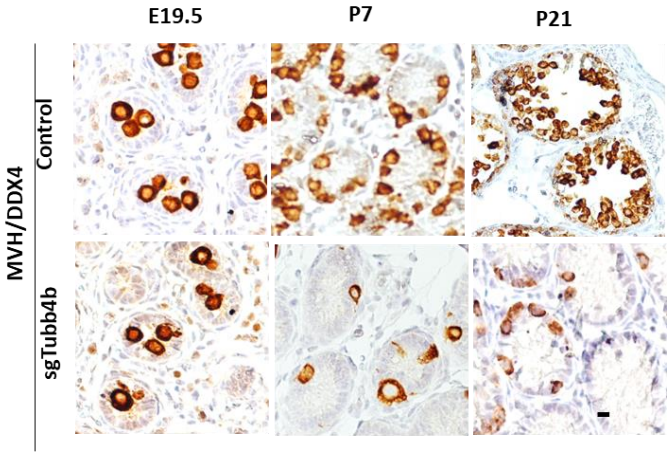
E19.5
P7
P21
MVH/DDX4
Control
sgTubb4b

D

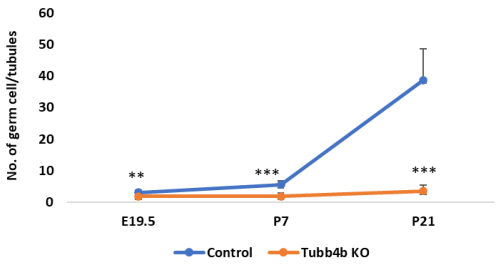
No. of germ cell/tubules
60
50
40
30
20
10
0
**
***
***
E19.5
P7
P21
Control
Tubb4b KO

E

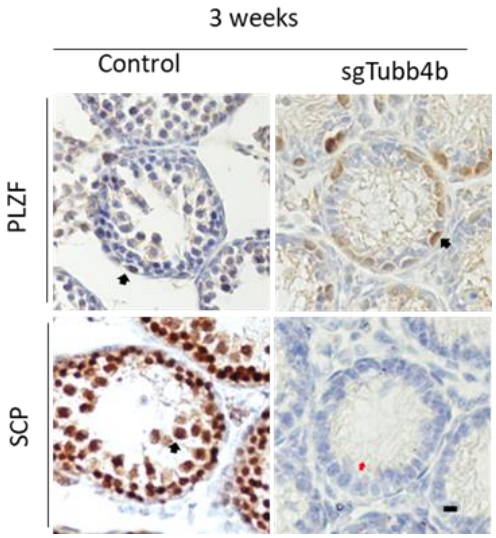
3 weeks
Control
sgTubb4b
PLZF
SCP

F

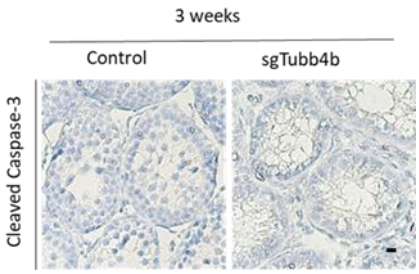
3 weeks
Control
sgTubb4b
Cleaved Caspase-3

Fig. 32. Testicular phenotypes of sgTubb4b founder mice at 3 weeks of age

(A) Gross morphology of testis. Scale bar 1 mm. (B) Bar graphs showing the testis weight at 3 weeks. (C) Representative images of developing testicular sections immunostained against germ cell marker, DDX4. (D) Number of DDX4 (+) germ cells per seminiferous tubule during postnatal stages. (E) Representative images of 3 weeks testis sections immunostained against PLZF (spermatogonia marker) and SCP3 (spermatocyte marker). Scale bar, 10 μm. (F) Representative images of 3 weeks testis sections immunostained against Cleaved Caspase-3 (apoptosis marker). Scale bar, 10 μm.

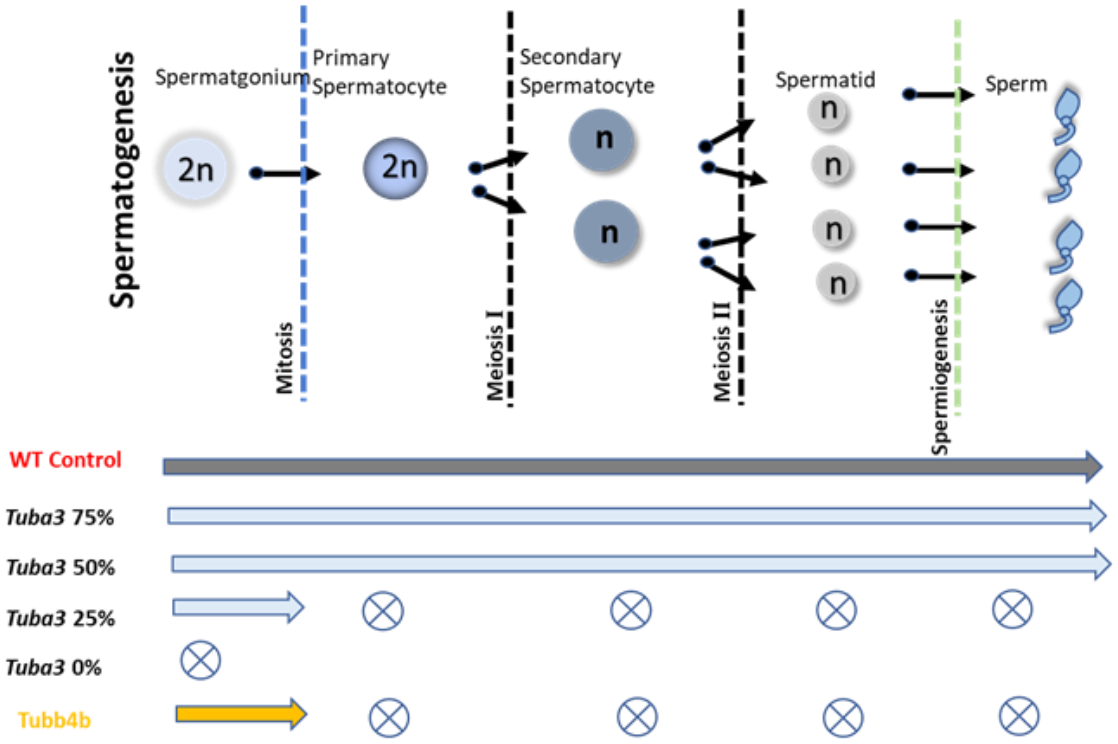

Fig. 33. Dosage-dependent effects of germ cell-specific tubulin genes on germ cell survival and differentiation in mice

Schematic illustration of spermatogenesis and the phenotypes observed in the *Tuba3* KO and *Tubb4b* KO mice in this study. Both *Tuba*3 75% and *Tuba3* 50% models normally completed spermatogenesis as *Tuba3* 100% control. In *Tuba3* 25% testis, although spermatogonia can survive until the adult stages, their differentiation to initiate meiosis was completely blocked. In *Tuba3* 0% model, germ cells including spermatogonia were completely lost. In *Tubb4b* KO mice (sgTubb4b), the differentiation of spermatogonia was completely blocked, similar to *Tuba3* 25% model.

General Discussion

In this study, I selected the novel candidate genes enlisted in the group of SRRGs (Chapter 1) and male germline-specific tubulins (Chapter 2) and conducted phenotypic screening focusing on testicular phenotypes by the Triple CRISPR/Cas9 method. I aimed to figure out the involvement of the selected candidate genes and partly their role in spermatogenesis.

In Chapter 1, I generated individual KO mice of five SRRGS as novel candidate genes (named *Faiml*, *Cox8c*, *Cox7b2*, *Tuba3a/3b,* and *Gm773*) along with reported meiosis essential gene *Majin* as control (Shibuya et al., 2015) by modified Triple CRISPR/Cas9 method. I conducted RT-qPCR analysis of mouse adult tissues and found that the five selected SRRGs were exclusively expressed in testis. The study of adult testis's RNAseq datasets revealed stage-specific expression (pre-, mid-, or post-meiotic expression) in testicular germ cells. Then I examined the testis morphology, histology, and sperm functions in CRISPR- injected KO adult males compared to control B6N mice and revealed that *Cox7b2*, *Gm773*, and *Tuba3a/3b* are required to produce normal spermatozoa. In this experiment, I analyzed the adult testis and observed that *Cox7b2* KO mice had poorly motile and neck-deformed infertile spermatozoa, *Gm773* KO mice produced motile spermatozoa with limited zona penetration abilities, and *Tuba3a/3b* KO mice showed severe testicular hypoplasia with complete absence of germ cells at the early postnatal stages. After that, I started the 2nd experiment try to find out the possible cause(s) of germ cell loss in *Tuba3a/3b* KO mice and the role of TUBA3 proteins on germ cell status.

In Chapter 2, firstly, I established the *Tuba3a/3b* KO mice line according to five different dosage effects as *Tuba3* 100% (used as control), *Tuba3* 75%, *Tuba3* 50%, *Tuba3* 25%, and *Tuba3* 0% respectively. Tubulin is the microtubule's building block, and alpha-tubulin forms a heterodimer with beta-tubulin to assemble the microtubules. Later, based on expression pattern similarity, I also included another novel candidate partner, *Tubb4b*, a member of beta-tubulin family genes, and generated the *Tubb4b* KO mouse by applying the

Triple CRISPR/Cas9 method to focus on the role of this gene on germ cells. Next, I subdivided the *Tuba3a/3b* KO mice line to perform my research study at the two different time manners of young (3 weeks) and adult (12-15 weeks) mice went through screening parameters of examination of gross testis and histology of testis and followed the similar experiment for another novel candidate gene: *Tubb4b.* From these five sub-groups of the *Tuba3a/3b* KO mice line, I conducted the immunostaining of the testis (both 3 weeks and 12-15 weeks) and observed that the germ cells present in both groups of the 75%*Tuba3* model and 50% *Tuba3* model like as control testis (100% *Tuba3*) both in young and adult mice. Whereas a scanty amount of germ cells was noticed in the testicular tubules of the 25% *Tuba3* model and total loss of germ cells in the 0% *Tuba3* model with severe testicular hypoplasia. From this observation, I performed another experiment using some specific germ cell markers to finalize the stuck stage of germ cells and analyzed that all the germ cells remained as spermatogonia without initiation of meiosis in 25% *Tuba3* testis, both in young and adult mice. Specifically, similar phenotypes were recorded for *Tubb4b* KO mice (at three weeks), like 25% *Tuba3* testis as the mitotic arrest of germ cells with severe testicular hypoplasia and undifferentiated spermatogonia stuck at the testicular tubules at three weeks. In *Tubb4b* KO mice pups, I also examined the high mortality rate with low growth rate, and all the pups mainly died within five weeks of being irresponsible with sex. From these findings, I noticed that germ cell survivability requires 25% of TUBA3 proteins but cannot initiate the meiosis for differentiation of spermatogonia and needs 50% TUBA3 proteins as a threshold for the onward initiation of meiosis. I found similar phenotypes for *Tubb4b*, like the 25% *Tuba3* model. Still, another gene of a beta-tubulin family named *Tubb5* also co-expressed with *Tubb4b* as a similar pattern of expression level in the germ cells (Fig. 30A-B). So, double knock-out of *Tubb4b* and *Tubb5* testis might show similar phenotypes of testicular tubules as the 0% *Tuba3* model. But *Tubb5*

is also expressed in other tissues for this; a knock-out approach may be appropriate in this regard.

In summary, this study characterized five novel SRRGS; three genes (*Cox7b2*, *Gm773*, *Tuba3a/3b*) are indispensable at the different time points of spermatogenesis (Chapter 1). This research also figure-out the role of *Tuba3* genes for germ cell survivability and the transition of germ cells from spermatogonia to spermatocyte. A single KO of another candidate partner Tubb4b gene might be hypothesized to play a similar role in a germ cell. Further analyses of KO mice may reveal detailed molecular mechanisms underlying each defective process.

Nowadays, male infertility is a fundamental issue in many fields, including human reproductive medicine, livestock reproduction, and wildlife conservation. From the candidate gene list, *Cox7b2*, *Tuba3a/3b,* and *Tubb4b* are widely conserved in mammals, including humans. Importantly, human homologs of these genes (*COX7B2*, *TUBA3C-E,* and *TUBB4B*) also show exclusive testis-specific expression patterns in humans like those in mice (Fig. 17C, 23, 30B), suggesting that these genes might also play critical roles in male germ cell development in human. It has been estimated that globally infertility affects 8–12% of couples and male factors play a primary or contributing cause in 50% of these couples (Devroey et al., 2009; Evers, 2002; Massart et al., 2012). This study could provide important insights into human reproductive medicine in the field and serve as a spotlight for reproductive treatment, germ cell study, and spermatogenesis. Adaptation of the mouse technique for livestock is progressing, with gradual gains in efficiency. Further work on the roles of genes identified in this study in farm animals may provide a basis to build a reproductive technology that applies to various species.

Acknowledgment

I would like to show my humble gratitude to my previous supervisor Dr. Gen Watanabe and my research supervisor Dr. Shogo Matoba for inviting me Japan and giving me a floor to conduct my research in the renowned lab Bioresource Engineering Division, BRC, RIKEN under the JRA fellowship. I am very grateful to the lab head Dr. Atsuo Ogura and all my lab mates and amicable kindness and support of the lab secretary Ayano Tsukahara.

I would like to express my deep gratitude to my present supervisor Dr. Kentaro Nagaoka for accepting me as a Ph.D. student in the Veterinary Physiology lab of Tokyo University of Agriculture and Technology under his great supervision. I also want to show my deep respect to all the members of my Ph.D. evaluation committee.

I would like to extend my appreciation to the HR section of RIKEN for allowing me to stay in Visitor's Quarter, members of the Tsukuba-Gakuen Hospital for my maternity care during the panic COVID situation and I want to show my heartiest respect to all the members of Tsukuba-Swan nursery since to take care of my two months old boy as a motherly environment otherwise, I could not continue the doctoral tenure.

Finally, I want to show the deep respect to my Allah (God), parents, husband, and my son Sanan Yousuf, without my child's endless sacrifice, I could not carry out my doctoral study. And all my relatives, colleagues and friends for their advice and guidance in the time to encounter the solitary, maternity, and mental pain!

Most Sumona Akter

26, Nov. 2022 (15:00)

References

1. Abbasi F, Miyata H, and Ikawa M. (2018). Revolutionizing male fertility factor research in mice by using the genome editing tool CRISPR/Cas9. Reprod Med Biol. **17**(1): 3–10.
2. Agarwal A, Baskaran S, Parekh N, Cho CL, Henkel R, Vij S, Arafa M, Panner Selvam MK, and Shah R. (2021). Male infertility. Lancet. **397**(10271): 319–333.
3. Akera T. (2021). Tubulin post-translational modifications in meiosis. Cell Dev Biol. **137**: 38–45.
4. Brischigliaro M, and Zeviani M. (2021). Cytochrome c oxidase deficiency. Biochim Biophys Acta Bioenerg. **1862**(1): 148335.
5. Brouhard GJ, and Rice LM. (2018). Microtubule dynamics: An interplay of biochemistry and mechanics. Nat Rev Mol Cell Biol. **19**(7): 451–463.
6. Brower JV, Rodic N, Seki T, Jorgensen M, Fliess N, Yachnis AT, McCarrey JR, Oh SP, and Terada N. (2007). Evolutionarily conserved mammalian adenine nucleotide translocase 4 is essential for spermatogenesis. J Biol Chem. **282**(40): 29658–29666.
7. Chen D, Liu W, Lukianchikov A, Hancock GV, Zimmerman J, Lowe MG, Kim R, Galic Z, Irie N, Surani MA, Jacobsen SE, and Clark AT. (2017). Germline competency of human embryonic stem cells depends on eomesodermin. Biol Reprod. **97**(6): 850–861.
8. Culty M. (2009). Gonocytes, the forgotten cells of the germ cell lineage. Birth Defects Res C Embryo Today. **87**(1): 1–26.

9. Desai A, and Mitchison TJ. (1997). Microtubule polymerization dynamics. Annu Rev Cell Dev Biol. **13**(1): 83–117.

10. Devlin DJ, Nozawa K, Ikawa M, and Matzuk MM. (2020). Knockout of family with sequence similarity 170 member A (Fam170a) causes male subfertility, while Fam170b is dispensable in mice. Biol Reprod. **103**(2): 205–222.

11. Devroey P, Fauser BCJM, and Diedrich K. (2009). Approaches to improve the diagnosis and management of infertility. Hum Reprod Update. **15**(4): 391–408.

12. Dominguez-Brauer C, Thu KL, Mason JM, Blaser H, Bray MR, and Mak TW. (2015). Targeting mitosis in cancer: emerging strategies. Mol Cell. **60**(4): 524–536.

13. Evers JL. (2002). Female subfertility. Lancet. **360**(9327): 151–159.

14. Extavour CG, and Akam M. (2003). Mechanisms of germ cell specification across the metazoans: epigenesis and preformation. Development. **130**(24): 5869–5884.

15. Fagerberg L, Hallström BM, Oksvold P, Kampf C, Djureinovic D, Odeberg J, Habuka M, Tahmasebpoor S, Danielsson A, Edlund K, Asplund A, Sjöstedt E, Lundberg E, Szigyarto CAK, Skogs M, Takanen JO, Berling H, Tegel H, Mulder J, and Uhlén M. (2014). Analysis of the human tissue-specific expression by genome-wide integration of transcriptomics and antibody-based proteomics. Mol Cell Proteomics. **13**(2): 397–406.

16. Fayomi AP, and Orwig KE. (2018). Spermatogonial stem cells and spermatogenesis in mice, monkeys and men. Stem Cell Res. **29**: 207–214.

17. Feng M, Wang K, Fu S, Wei H, Mu X, Li L, and Zhang S. (2022). Tubulin TUBB4B is involved in spermatogonia proliferation and cell cycle processes. Genes. **13**(6):1082

18. Fertuzinhos S, Legué E, Li D, and Liem KF. (2022). A dominant tubulin mutation causes cerebellar neurodegeneration in a genetic model of tubulinopathy. Sci Adv. **8**(7): eabf7262.

19. Fujihara Y, Miyata H, and Ikawa M. (2018). Factors controlling sperm migration through the oviduct revealed by gene-modified mouse models. Exp Anim. **67**(2): 91–104.

20. Fujihara Y, Okabe M, and Ikawa M. (2014). GPI-anchored protein complex, LY6K/TEX101, is required for sperm migration into the oviduct and male fertility in mice. Biol Reprod. **90**(3): 60.

21. Galluzzi L, Vitale I, Aaronson SA, Abrams JM, Adam D, Agostinis P, Alnemri ES, Altucci L, Amelio I, Andrews DW, Annicchiarico-Petruzzelli M, Antonov AV, Arama E, Baehrecke EH, Barlev NA, Bazan NG, Bernassola F, Bertrand MJM, Bianchi K, and Kroemer G. (2018). Molecular mechanisms of cell death: recommendations of the Nomenclature Committee on Cell Death. Cell Death Differ. **25**(3): 486–541.

22. Green CD, Ma Q, Manske GL, Shami AN, Zheng X, Marini S, Moritiz L, Sultan C, Gurczynski SJ, Moore BB, Tallquist MD, Li JZ, and Hammoud SS. (2018). A comprehensive roadmap of murine spermatogenesis defined by single-cell RNA-seq. Dev Cell. **46**(5): 651–667.e10.

23. Griswold MD. (2016). Spermatogenesis: the commitment to meiosis. Physiol Rev. **96**(1): 1–17.

24. Hamer G, Wang H, Bolcun-Filas E, Cooke HJ, Benavente R, and Höög C. (2008). Progression of meiotic recombination requires structural maturation of the central element of the synaptonemal complex. J Cell Sci. **121**(15): 2445–2451.

25. Hancock GV, Wamaitha SE, Peretz L, and Clark AT. (2021). Mammalian primordial germ cell specification. Development, **148**(6): dev189217.

26. Hayashi K, de Sousa Lopes SMC, and Surani MA. (2007). Germ cell specification in mice. Science. **316**(5823): 394–396.

27. Hess RA, Sharpe RM, and Hinton BT. (2021). Estrogens and development of the rete testis, efferent ductules, epididymis and vas deferens. Differentiation. **118**: 41–71.

28. Hill PWS, Leitch HG, Requena CE, Sun Z, Amouroux R, Roman-Trufero M, Borkowska M, Terragni J, Vaisvila R, Linnett S, Bagci H, Dharmalingham G, Haberle V, Lenhard B, Zheng Y, Pradhan S, and Hajkova P. (2018). Epigenetic reprogramming enables the primordial germ cell-to-gonocyte transition. Nature. **555**(7696): 392–396.

29. Hsu PD, Lander ES, and Zhang F. (2014). Development and applications of CRISPR-Cas9 for genome engineering. Cell. **157**(6): 1262–1278.

30. Jeyaraj DA, Grossman G, and Petrusz P. (2003). Dynamics of testicular germ cell apoptosis in normal mice and transgenic mice overexpressing rat androgen-binding protein. Reprod Biol Endocrinol. **1**(1): 48.

31. Johnson AF, Nguyen HT, and Veitia RA. (2019). Causes and effects of haploinsufficiency. Biol Rev Camb Philos Soc. **94**(5): 1774–1785.

32. Kanamori M, Oikawa K, Tanemura K, and Hara K. (2019). Mammalian germ cell migration during development, growth, and homeostasis. Reprod Med Biol. **18**(3): 247–255.

33. Khan M, Jabeen N, Khan T, Hussain HMJ, Ali A, Khan R, Jiang L, Li T, Tao Q, Zhang X, Yin H, Yu C, Jiang X, and Shi Q. (2018). The evolutionarily conserved genes: Tex37, Ccdc73, Prss55 and Nxt2 are dispensable for fertility in mice. Sci Rep. **8**(1): 4975.

34. Kim YG, Cha J, and Chandrasegaran S. (1996). Hybrid restriction enzymes: Zinc finger fusions to Fok I cleavage domain. Proc Natl Acad Sci U S A. **93**(3): 1156–1160.

35. Knossow M, Campanacci V, Khodja LA, and Gigant B. (2020). The mechanism of tubulin assembly into microtubules: insights from structural studies. iScience. **23**(9): 101511.

36. Koonin EV. (2005). Orthologs, paralogs, and evolutionary genomics. Annu Rev Genet. **39**(1): 309–338.

37. Krausz C, and Riera-Escamilla A. (2018). Genetics of male infertility. Nat Rev Urol. **15**(6): 369–384.

38. Kumar DL, and DeFalco T. (2017). Of mice and men: In vivo and in vitro studies of primordial germ cell specification. Semin Reprod Med. **35**(2): 139–146.

39. Kuroki S, Maeda R, Yano M, Kitano S, Miyachi H, Fukuda M, Shinkai Y, and Tachibana M. (2020). H3K9 demethylases JMJD1A and JMJD1B control prospermatogonia to spermatogonia transition in mouse germline. Stem Cell Reports. **15**(2): 424–438.

40. Larasati T, Noda T, Fujihara Y, Shimada K, Tobita T, Yu Z, Matzuk MM, and Ikawa M. (2020). Tmprss12 is required for sperm motility and uterotubal junction migration in mice. Biol Reprod. **103**(2): 254–263.

41. Li M, Huang R, Jiang X, Chen Y, Zhang Z, Zhang X, Liang P, Zhan S, Cao S, Songyang Z, and Huang J. (2015). CRISPR/Cas9 promotes functional study of testis specific X-linked gene in vivo. PLoS One. **10**(11): e0143148.

42. Li W, Guo XJ, Teng F, Hou XJ, Lv Z, Zhou SY, Bi Y, Wan HF, Feng CJ, Yuan Y, Zhao XY, Wang L, Sha JH, and Zhou Q. (2013). Tex101 is essential for male fertility by affecting sperm migration into the oviduct in mice. J Mol Cell Biol. **5**(5): 345–347.

43. Little M, and Seehaus T. (1988). Comparative analysis of tubulin sequences. Comp Biochem Physiol B. **90**(4): 655–670.

44. Luscan R, Mechaussier S, Paul A, Tian G, Gérard X, Defoort-Dellhemmes S, Loundon N, Audo I, Bonnin S, LeGargasson JF, Dumont J, Goudin N, Garfa-Traoré M, Bras M, Pouliet A, Bessières B, Boddaert N, Sahel JA, Lyonnet S, and Perrault I. (2017).

Mutations in TUBB4B cause a distinctive sensorineural disease. Am J Hum Genet. **101**(6): 1006–1012.

45. Ma L, Buchold GM, Greenbaum MP, Roy A, Burns KH, Zhu H, Han DY, Harris RA, Coarfa C, Gunaratne PH, Yan W, and Matzuk MM. (2009). GASZ is essential for male meiosis and suppression of retrotransposon expression in the male germline. PLoS Genet. **5**(9): e1000635.
46. Maasz A, Hadzsiev K, Ripszam R, Zsigmond A, Maka E, Knezy K, Lesch B, Nemeth A, Bene J, Galik B, Gyenesei A, and Melegh B. (2022). TUBB4B gene mutation in Leber phenotype of congenital amaurosis syndrome associated with early-onset deafness. Eur J Med Genet. **65**(4): 104471.
47. Massart A, Lissens W, Tournaye H, and Stouffs K. (2012). Genetic causes of spermatogenic failure. Asian J Androl. **14**(1): 40–48.
48. Matoba S, Nakamuta S, Miura K, Hirose M, Shiura H, Kohda T, Nakamuta N, and Ogura A. (2019). Paternal knockout of Slc38a4/SNAT4 causes placental hypoplasia associated with intrauterine growth restriction in mice. Proc Natl Acad Sci U S A. **116**(42): 21047–21053.
49. Matoba S, Wang H, Jiang L, Lu F, Iwabuchi KA, Wu X, Inoue K, Yang L, Press W, Lee JT, Ogura A, Shen L, and Zhang Y. (2018). Loss of H3K27me3 imprinting in somatic cell nuclear transfer embryos disrupts post-implantation development. Cell Stem Cell. **23**(3): 343-354.e5.
50. Matoba S, and Zhang Y. (2018). Somatic cell nuclear transfer reprogramming: Mechanisms and applications. Cell Stem Cell. **23**(4): 471–485.
51. McLaren A. (2003). Primordial germ cells in the mouse. Dev Biol. **262**(1): 1–15.

52. Miura K, Ogura A, Kobatake K, Honda H, and Kaminuma O. (2021). Progress of genome editing technology and developmental biology useful for radiation research. J Radiat Res. **62**(Suppl 1): i53–i63.

53. Miyata H, Castaneda JM, Fujihara Y, Yu Z, Archambeault DR, Isotani A, Kiyozumi D, Kriseman ML, Mashiko D, Matsumura T, Matzuk RM, Mori M, Noda T, Oji A, Okabe M, Prunskaite-Hyyrylainen R, Ramirez-Solis R, Satouh Y, Zhang Q, and Matzuk MM. (2016). Genome engineering uncovers 54 evolutionarily conserved and testis-enriched genes that are not required for male fertility in mice. Proc Natl Acad Sci U S A. **113**(28): 7704–7710.

54. Nagano R, Tabata S, Nakanishi Y, Ohsako S, Kurohmaru M, and Hayashi Y. (2000). Reproliferation and relocation of mouse male germ cells (gonocytes) during prespermatogenesis. Anat Rec. **258**(2): 210–220.

55. Nguyen DH, Jaszczak RG, and Laird DJ. (2019). Curr Top Dev Biol. **135**: 155–201.

56. Nogales E, Wolf SG, and Downing KH. (1998). Structure of the αβ tubulin dimer by electron crystallography. Nature. **391**(6663): 199–203.

57. Park S, Shimada K, Fujihara Y, Xu Z, Shimada K, Larasati T, Pratiwi P, Matzuk RM, Devlin DJ, Yu Z, Garcia TX, Matzuk MM, and Ikawa M. (2020). CRISPR/Cas9-mediated genome-edited mice reveal 10 testis-enriched genes are dispensable for male fecundity. Biol Reprod. **103**(2): 195–204.

58. Rak M, Bénit P, Chrétien D, Bouchereau J, Schiff M, El-Khoury R, Tzagoloff A, and Rustin P. (2016). Mitochondrial cytochrome c oxidase deficiency. Clin Sci. **130**(6): 393–407.

59. Ravindranath N, Dettin L, Dym M. Mammalian Testes: Structure and Function. 2003; pp. 1–19. In: Introduction to Mammalian Reproduction, 1st ed. (D. R. P. Tulsiani ed.) Springer, Boston, MA.

60. R Core Team. R: A Language and Environment for Statistical Computing. (2015).
61. Saitou M. (2009). Specification of the germ cell lineage in mice. Front Biosci. **14**(3): 1068–1087.
62. Saitou M, and Yamaji M. (2012). Primordial germ cells in mice. Cold Spring Harb Perspect Biol. **4**(11): a008375.
63. Sander JD, and Joung JK. (2014). CRISPR-Cas systems for genome editing, regulation and targeting. Nat Biotechnol. **32**(4): 347–355.
64. Schultz N, Hamra FK, and Garbers DL. (2003). A multitude of genes expressed solely in meiotic or postmeiotic spermatogenic cells offers a myriad of contraceptive targets. Proc Natl Acad Sci U S A. **100**(21): 12201–12206.
65. Shamshirgaran Y, Liu J, Sumer H, Verma PJ, and Taheri-Ghahfarokhi A. (2022). Tools for efficient genome editing; ZFN, TALEN, and CRISPR. Methods Mol Biol. **2495**: 29–46.
66. Shamsi MB, Kumar K, and Dada R. (2011). Genetic and epigenetic factors: Role in male infertility. Indian J Urol. **27**(1): 110–120.
67. Shibuya H, Hernández-Hernández A, Morimoto A, Negishi L, Höög C, and Watanabe Y. (2015). MAJIN links telomeric DNA to the nuclear membrane by exchanging telomere cap. Cell. **163**(5): 1252–1266.
68. Shimada K, Park S, Miyata H, Yu Z, Morohoshi A, Oura S, Matzuk MM, and Ikawa M. (2021). ARMC12 regulates spatiotemporal mitochondrial dynamics during spermiogenesis and is required for male fertility. Proc Natl Acad Sci U S A. **118**(6): e2018355118.
69. Snell WJ, and White JM. (1996). The molecules of mammalian fertilization. Cell. **85**(5): 629–637.

70. Sommer D, Peters AE, Baumgart AK, and Beyer M. (2015). TALEN-mediated genome engineering to generate targeted mice. Chromosome Res. **23**(1): 43–55.

71. Soper SFC, van der Heijden GW, Hardiman TC, Goodheart M, Martin SL, de Boer P, and Bortvin A. (2008). Mouse Maelstrom, a component of nuage, is essential for spermatogenesis and transposon repression in meiosis. Dev Cell. **15**(2): 285–297.

72. Stukenborg JB, Kjartansdóttir KR, Reda A, Colon E, Albersmeier JP, and Söder O. (2014). Male germ cell development in humans. Horm Res Paediatr. **81**(1): 2–12.

73. Sun J, Lu Y, Nozawa K, Xu Z, Morohoshi A, Castaneda JM, Noda T, Miyata H, Abbasi F, Shawki HH, Takahashi S, Devlin DJ, Yu Z, Matzuk RM, Garcia TX, Matzuk MM, and Ikawa M. (2020). CRISPR/Cas9-based genome editing in mice uncovers 13 testis- or epididymis-enriched genes individually dispensable for male reproduction. Biol Reprod. **103**(2): 183–194.

74. Sunagawa GA, Sumiyama K, Ukai-Tadenuma M, Perrin D, Fujishima H, Ukai H, Nishimura O, Shi S, Ohno R, Narumi R, Shimizu Y, Tone D, Ode KL, Kuraku S, and Ueda HR. (2016). Mammalian reverse genetics without crossing reveals Nr3a as a short-sleeper gene. Cell Rep. **14**(3): 662–677.

75. Susaki EA, Ukai H, and Ueda HR. (2017). Next-generation mammalian genetics toward organism-level systems biology. NPJ Syst Biol Appl. **3**:15.

76. Tanaka A, Suzuki K, Nagayoshi M, Tanaka A, Takemoto Y, Watanabe S, Takeda S, Irahara M, Kuji N, Yamagata Z, and Yanagimachi, R. (2018). Ninety babies born after round spermatid injection into oocytes: Survey of their development from fertilization to 2 years of age. Fertil Steril. **110**(3): 443–451.

77. Ti SC. (2022). Reconstituting microtubules: A decades-long effort from building block identification to the generation of recombinant α/β-tubulin. Front Cell Dev Biol. **10**: 861648.

78. Toyooka Y, Tsunekawa N, Takahashi Y, Matsui Y, Satoh M, and Noce T. (2000). Expression and intracellular localization of mouse Vasa-homologue protein during germ cell development. Mech Dev. **93**(1-2): 139–149.

79. Urnov FD, Rebar EJ, Holmes MC, Zhang HS, and Gregory PD. (2010). Genome editing with engineered zinc finger nucleases. Nat Rev Genet. **11**(9): 636–646.

80. Wang H, Yang H, Shivalila CS, Dawlaty MM, Cheng AW, Zhang F, and Jaenisch R. (2013). One-Step generation of mice carrying mutations in multiple genes by CRISPR/Cas-mediated genome engineering. Cell. **153**(4): 910–918.

81. Wassarman PM. (1987). The biology and chemistry of fertilization. Science. **235**(4788): 553–560.

82. Wassarman PM. (1999). Mammalian fertilization: molecular aspects of gamete adhesion, exocytosis, and fusion. Cell. **96**(2): 175–183.

83. Yanagimachi R. (2005). Intracytoplasmic injection of spermatozoa and spermatogenic cells: Its biology and applications in humans and animals. Reprod Biomed Online. **10**(2): 247–288.